

EXPANSIVE MINERAL GROWTH AND CONCRETE DETERIORATION

Final Report
For Iowa DOT Project HR-384

Sponsored by the Iowa Department of Transportation
Project Development Division and
the Iowa Highway Research Board

Robert D. Cody, Paul G. Spry,
Anita M. Cody and Hyomin Lee
Department of Geological and Atmospheric Sciences
Iowa State University
Ames, IA 50011

September 1997

EXPANSIVE MINERAL GROWTH AND CONCRETE DETERIORATION

**Final Report
September 1997**

Iowa DOT HR-384

**Submitted to the Project Development Division
of the Iowa Department of Transportation
and
The Iowa Highway Research Board**

**Robert D. Cody, Paul G. Spry,
Anita M. Cody, and Hyomin Lee
Department of Geological and Atmospheric Sciences
Iowa State University
Ames, IA 50011**

DISCLAIMER

The contents of this report do not represent a warranty on the products used on behalf of the State of Iowa, Iowa State University, Iowa Department of Transportation, Highway Research Board, or the authors. The opinions, findings, and conclusions expressed in this publication are those of the authors and not necessarily those of the Highway Division or Project Development Division of the Iowa Department of Transportation. The responsibility for the use of information in this report remains with the user. This report is for information purposes and is made available with the understanding that it will not be cited without the permission of the authors.

The calcium magnesium acetate compounds used in this work should not be confused with commercially available calcium magnesium acetate deicer trade name Cryotech CMA®. Cryotech CMA® has different chemical properties than the test material and was not part of this study.

TABLE OF CONTENTS

	Page No.
ABSTRACT	xi
INTRODUCTION AND PROBLEM STATEMENT	1
RESEARCH OBJECTIVES	2
PART I. EXPANSIVE MINERALS FEATURES OF IOWA HIGHWAY CONCRETES	
METHODS OF STUDY	4
COLLECTION OF HIGHWAY CONCRETE SAMPLES	4
GENERAL PROCEDURES AND INSTRUMENTATION	4
CHARACTERISTICS OF IOWA HIGHWAY CONCRETE SAMPLES	5
DURABLE AND NON-DURABLE CONCRETES	5
DOLOMITE COARSE AGGREGATE CHARACTERISTICS	6
Crystallinity and Crystal Size	6
Reaction Rim Development	6
Chemical Composition	8
Pyrite Inclusions	8
FINE AGGREGATE CHARACTERISTICS	10
CEMENT PASTE CHARACTERISTICS	11
Chemical Composition of Cement Paste	11
Air-Entrainment Voids	14
RESULTS AND DISCUSSION	14
INTRODUCTION	14
BRUCITE, $Mg(OH)_2$, OCCURRENCE IN IOWA CONCRETES	15
Forms and Distribution	15
Brucite Formation in Iowa Concrettes	17
Mechanisms of Brucite Formation in Iowa Concrettes	19
ETTRINGITE, $3CaO \cdot Al_2O_3 \cdot 3CaSO_4 \cdot 32H_2O$, OCCURRENCES IN IOWA CONCRETES	20
Forms and Distribution	20
Relationship of Ettringite to Pyrite Inclusions	22
Oxidation of Pyrite	22
Spatial Relationships of Pyrite and Ettringite.	24

	Page No.
Mechanisms of Ettringite Formation	25
Importance of Sulfur and Water	25
Sulfur from Cement Blend	26
Sulfur from Pyrite	26
Sulfur from Deicer Applications	27
Ettringite-Forming Reactions	28
Specific Mechanisms in Iowa Highway Concretes	32
EXPANSIVE MECHANISMS AND IOWA CONCRETE DETERIORATION	33
CEMENT-AGGREGATE EXPANSIVE REACTIONS	33
Alkali-Carbonate Reactions	34
Alkali-Silica Reactions	34
Alkali-Silicate Reactions	35
EXPANSION DUE TO BRUCITE GROWTH	35
Expansion Mechanisms	35
Brucite-Induced Expansion in Iowa Concrete	36
EXPANSION DUE TO ETTRINGITE FORMATION	38
Expansion Mechanisms	38
Ettringite Expansion in Iowa Concretes	40
 PART II. EXPERIMENTAL DETERIORATION OF IOWA HIGHWAY CONCRETE 	
PURPOSE OF EXPERIMENTS	45
EXPERIMENTAL METHODS	45
Wet/Dry (W/D) Experiments	45
Freeze/Thaw (F/T) Experiments	46
RESULTS	47
RELATIVE AGGRESSIVENESS OF SALT SOLUTIONS	47
Calcium Magnesium Acetate	47
Sodium Sulfate	50
Magnesium Chloride	50
Calcium Chloride	50
Sodium Chloride and Water	50

	Page No.
EFFECTS ON CONCRETE SAMPLES	51
Secondary Mineral Formation	51
Effects of Water	53
Effects of Calcium Chloride Solutions	53
Effects of Magnesium Chloride Solutions	55
Effects of Sodium Chloride Solutions	56
Effects of Sodium Sulfate (Na ₂ SO ₄) Solutions	59
Effects of Calcium Magnesium Acetate (CMA) Solutions	60
Effects of Magnesium Acetate Solutions	63
Effects of Calcium Acetate Solutions	63

PART III. SUMMARY AND RECOMMENDATIONS

SUMMARY OF PART I. EXPANSIVE MINERAL FEATURES OF IOWA CONCRETES	65
SUMMARY OF PART II. EXPERIMENTAL DETERIORATION OF IOWA CONCRETES	68
RECOMMENDATIONS	70
ACKNOWLEDGMENTS	72
REFERENCES	73

TABLES

Table I. Concrete Core Locations and Other Data Iowa Highway Concretes	9
Table II. Chemical Composition of Dolomite Aggregate.	12
Table III. Characteristics of Portland Cement Used for Iowa Highway Concretes	13
Table IV-A. Sulfur Content (wt. %) in Cement Paste, Dolomite Aggregate, and Maximum Calculated SO ₃ Content (wt. %) of Cement Paste, Samples A to F.	29
Table IV-B. Sulfur Content (wt. %) in Cement Paste, Dolomite Aggregate, and Maximum Calculated SO ₃ Content (wt. %) of Paste, Samples G, G-1 to G-4.	30
Table V-A. Summary of Observations of Brucite in Iowa Concretes.	42
Table V-B. Summary of Observations of Ettringite in Iowa Concretes.	43
Table VI. Secondary Minerals in Solutions and on Concrete Surfaces	52

TEXT FIGURES

Fig. T1. Stability diagram for selected iron minerals at 25°C and $\Sigma\text{Fe}=10^{-4}$, $\Sigma\text{S}=10^2$, and $\Sigma\text{Ca}=10^4$ mole/liter.	23
Fig. T2. Wet/dry and freeze/thaw cycling experiments.	48
Fig. T3a. Experimental deterioration of concrete using freeze-thaw conditions for 15 cycles.	49
Fig. T3b. Experimental deterioration of concrete using wet/dry conditions for 15 cycles.	49
Fig. T4. Expansive white chert with secondary mineral formation.	51

Appendix I.**PLATES AND FIGURES.****Expansive Growth in Iowa Highway Concrete Samples****PLATES**

I-A. Light micrograph showing typical characteristics of reactive dolomite aggregate (Crawford-Lee quarry; US 30).	89
I-B. Light micrograph showing typical characteristics of non-reactive dolomite aggregate (Sundheim quarry; US 20).	89
II-A. Light micrograph of unoxidized pyrite inclusions in dolomite aggregate.	93
II-B. Light micrograph of oxidized pyrite inclusions in dolomite aggregate.	93
III-A. Light micrograph showing a typical occurrence of fine aggregate in Iowa highway concrete.	97
III-B. Light micrograph showing microcracks in quartz fine aggregate, US 20 highway.	97

FIGURES

Fig. 1. SEM micrograph and EDAX maps of Crawford Lee quarry concretes from US 30.	101
Fig. 2. SEM micrograph and EDAX area maps of Nelson quarry concretes from US 63.	103
Fig. 3. SEM micrograph and EDAX area maps of Paralta quarry concrete from IA 13.	105
Fig. 4. SEM micrograph and EDAX maps of Crawford Lee quarry concretes from IA 21.	107
Fig. 5. SEM micrograph and EDAX area maps of Dotzler quarry concrete from IA 9.	109
Fig. 6. SEM micrograph and EDAX area maps of Sundheim quarry concrete from US 20.	111

	Page No.
Fig. 7. SEM micrograph and EDAX element maps showing the oxidation of large pyrite inclusions in dolomite aggregate from Portland West quarry, I 35.	113
Fig. 8. SEM micrograph and EDAX area maps of Crawford Lee quarry concrete from IA 100.	115
Fig. 9. SEM micrograph and EDAX area maps showing brucite occurrence in the dolomite aggregate and cement paste.	117
Fig. 10. SEM micrograph and EDAX area maps showing the brucite and ettringite formation in the unaltered cement paste.	119
Fig. 11. SEM micrograph and EDAX element maps of ettringite in paste from US 63.	121
Fig. 12. SEM micrograph and EDAX area maps showing void-fill ettringite in cement paste.	123
Fig. 13. SEM micrographs showing both void-rim and void-fill types of ettringite in cement paste.	125
Fig. 14. SEM micrograph and EDAX area maps showing ettringite in pre-existing cracks.	127
Fig. 15. High magnification SEM micrograph and EDAX area maps showing lack of ettringite in microcracks	129
Fig. 16. SEM micrograph and EDAX area maps showing abundant ettringite close to coarse aggregate containing oxidized pyrite inclusions.	131
Fig. 17. High magnification SEM micrograph and EDAX area maps showing small ettringite deposits around aluminate particles in cement matrix.	133

Appendix II.
PLATES AND FIGURES.
Experimentally Altered Iowa Highway Concrete Samples

PLATES

IV-A. Light micrograph showing experimentally-induced deterioration after wet/dry cycling in CaCl_2 , Nelson quarry concrete from US 63.	137
IV-B. Light micrograph showing experimentally-induced deterioration after freeze/thaw cycling in MgCl_2 , Nelson quarry concrete from US 63.	137
V-A. Light micrograph showing experimentally induced-deterioration after wet/dry cycling in CMA, Nelson quarry concrete from US 63.	141
V-B. Light micrograph showing secondary mineral growth after freeze/thaw cycling in CMA of Sundheim quarry concrete from US 20.	141
VI-A. Light micrograph showing the crack-filling minerals after wet/dry cycling in CMA of Sundheim quarry concrete from US 20.	145
VI-B. Light micrograph showing experimentally-induced deterioration after wet/dry cycling in Na_2SO_4 . of Sundheim quarry concrete from US 20.	145

FIGURES

Fig. 18. SEM micrograph and EDAX area maps showing results of freeze/thaw cycling in H ₂ O of Nelson quarry concrete from US 63.	149
Fig. 19. SEM micrograph and EDAX area maps showing experimentally-induced deterioration after wet/dry cycling in CaCl ₂ of Nelson quarry concrete, US 63.	151
Fig. 20. SEM micrograph and EDAX element maps showing an enlarged area of Fig. 19.	153
Fig. 21. SEM micrograph and EDAX area map showing experimentally-induced alteration of Sundheim quarry concrete from US 20 after wet/dry cycling in CaCl ₂ .	155
Fig. 22. SEM micrograph and EDAX area maps showing experimentally-induced deterioration of Nelson quarry concrete from US 63 after freeze/thaw cycling in MgCl ₂ .	157
Fig. 23. SEM micrograph and EDAX element maps showing the aggregate-paste interface in Nelson quarry concrete from US 63 after wet/dry cycling in MgCl ₂ .	159
Fig. 24. SEM micrograph and EDAX area maps showing cement paste deterioration after wet/dry cycling in MgCl ₂ of Nelson quarry concrete from US 63.	161
Fig. 25. High magnification SEM and EDAX maps showing MSH features in cement paste.	163
Fig. 26. EDAX point analysis of magnesium silicate hydrate (MSH) shown in Fig 25.	165
Fig. 27. SEM micrograph and EDAX area maps showing the deposition of secondary minerals on the surface of concrete after wet/dry cycling in MgCl ₂ of Portland West quarry concrete, I 35.	167
Fig. 28. EDAX point analysis of void-filling matter shown in Fig. 24.	169
Fig. 29. SEM micrograph and EDAX area maps showing Nelson quarry concrete from US 63 after wet/dry cycling in NaCl.	171
Fig. 30. High magnification SEM micrograph and EDAX area maps of area shown in Fig. 28.	173
Fig. 31. EDAX point analyses of void-filling minerals shown in Fig. 30.	175
Fig. 32. SEM micrograph and EDAX area maps showing deterioration in Sundheim quarry concrete from US 20 after wet/dry cycling in Na ₂ SO ₄ .	177
Fig. 33. SEM micrograph and EDAX area maps showing deterioration in Sundheim quarry concrete from US 20 after freeze/thaw cycling in Na ₂ SO ₄ .	179
Fig. 34. High magnification SEM micrograph and EDAX area maps showing deterioration in Sundheim quarry concrete from US 20 after wet/dry cycling in Na ₂ SO ₄ .	181
Fig. 35. EDAX area maps showing effects on Sundheim quarry concrete from US 20 after wet/dry cycling in Na ₂ SO ₄ .	183

	Page No.
Fig. 36. SEM micrograph and EDAX area maps showing experimentally-induced deterioration of Nelson quarry concrete from US63 after wet/dry cycling in CMA.	185
Fig. 37. SEM micrograph and EDAX maps showing secondary mineral growth in Sundheim quarry concrete from US20 after freeze/thaw cycling in CMA.	187
Fig. 38. SEM micrograph and EDAX element maps showing the growth of brucite and calcite in Nelson quarry concrete from US63 after wet/dry cycling in CMA.	189
Fig. 39. EDAX element maps of the same area shown in Plate VI-A showing crack-filling minerals that formed after wet/dry cycling in CMA.	191
Fig. 40. High magnification SEM and EDAX maps showing part of the area of Fig. 36.	193
Fig. 41. EDAX point analysis of void-filling minerals shown in Fig. 40.	195
Fig. 42. SEM micrograph and EDAX area maps showing experimentally-induced deterioration of Sundheim quarry concrete from US 20 after wet/dry cycling in magnesium acetate.	
Fig. 43. SEM micrograph and EDAX area maps showing the growth of brucite in voids of durable Sundheim quarry concrete (US 20) after freeze/thaw cycling in magnesium acetate.	197
Fig. 44. SEM micrograph and EDAX area maps showing results of wet/dry cycling in calcium acetate, Sundheim quarry concrete from US 20.	199

ABSTRACT

for the final report on HR 384:

Iowa Concrete Deterioration and Expansive Mineral Growth

by

Robert D. Cody

Paul G. Spry

Anita M. Cody

Hyomin Lee

A significant question is what role does newly-formed expansive mineral growth play in the premature deterioration of concrete? These minerals formed in cement paste as a result of chemical reactions involving cement and coarse/fine aggregate. Petrographic observations and SEM/EDAX analysis were conducted in order to determine chemical and mineralogical changes in the aggregate and cement paste of samples taken from Iowa concrete highways that showed premature deterioration. Mechanisms involved in deterioration were investigated.

Ettringite, $3\text{CaO} \cdot \text{Al}_2\text{O}_3 \cdot 3\text{CaSO}_4 \cdot 32\text{H}_2\text{O}$, completely fills many small voids and occurs as rims lining the margin of larger voids. Microscopic ettringite is common disseminated throughout the paste in many samples. Severe cracking of cement paste causing premature deterioration is often closely associated with ettringite locations, and strongly suggests that ettringite contributed to deterioration. Pyrite, FeS_2 , is commonly present in coarse/fine aggregates, and its oxidation products is observed in many concrete samples. Pyrite oxidation provides sulfate ions for ettringite formation. The oxidation of pyrite in aggregate particles appears to be affected by several factors such as aggregate type, aggregate reactivity, and pyrite size and location. Ettringite is most common in poorly performing concretes.

Brucite, $\text{Mg}(\text{OH})_2$, is another potentially expansive mineral that forms in cement paste of concretes containing reactive dolomite aggregate as a result of partial dedolomitization of the aggregate. No cracking was observed to be spatially associated with brucite, but most brucite was microscopic in size and widely disseminated in the cement paste of less durable concretes. Expansion stresses associated with its growth at innumerable microlocations may be relieved by cracking at weaker locations in the concrete.

A second objective was to investigate whether deicer solutions exacerbate the formation of expansive minerals and concrete deterioration. Each deicer salt causes characteristic concrete deterioration by altering dedolomitization rims at the coarse-aggregate paste interface, altering cement paste and/or formation of new minerals. Magnesium in deicer solutions causes the most severe paste deterioration by forming non-cementitious magnesium silicate hydrate and brucite. Chloride in deicer solutions promotes decalcification of paste and alters ettringite to chloroaluminate. CMA and Mg-acetate produces the most deleterious effects on concrete, with Ca-acetate being much less severe.

INTRODUCTION AND PROBLEM STATEMENT

Considerable progress has been made in reducing premature failure of highway concrete, but several problem areas remain. A highly significant problem is the importance of expansion resulting from newly-formed minerals in concrete. Iowa highways constructed of concrete containing carbonate rock coarse aggregate from certain quarries sometimes have service lives of less than 10 years. Two important secondary minerals, brucite and ettringite, are often implicated in premature deterioration, and the cause of deterioration is often attributed to expansion and cracking related to their growth. Brucite, $\text{Mg}(\text{OH})_2$, precipitation in concrete produced by magnesium released from the dolomite coarse aggregate and/or from other sources may be a cause of reduced concrete service life, but the specific mechanisms and the importance of expansion in the deterioration of concrete by brucite growth are still controversial. The other potentially important deleterious mineral is ettringite, $3\text{CaO}\cdot\text{Al}_2\text{O}_3\cdot 3\text{CaSO}_4\cdot 32\text{H}_2\text{O}$ or $\text{Ca}_6\text{Al}_2(\text{SO}_4)_3(\text{OH})_{12}\cdot 26\text{H}_2\text{O}$, which may also produce harmful expansion. Primary ettringite which grows when concrete is still plastic, easily pushes other materials aside and is not harmful. However ettringite may also form long after concrete has hardened. This later-stage material is usually referred to as delayed ettringite, and many researchers have concluded its growth produces damaging expansive pressures. Delayed ettringite

formation is especially enhanced by the availability of sulfur because its other components, calcium, aluminum, and water are abundant in Portland cement concrete. Sulfur can be derived from gypsum added to the concrete to delay setting, from sulfate-containing ground or surface waters that can enter the concrete, or from the oxidation of sulfide minerals that occur in coarse and fine aggregate to soluble sulfate. The current report investigates the role that these and other potentially expansive minerals have in premature deterioration of Iowa highway concretes.

RESEARCH OBJECTIVES

The major objective of this research was to determine the role of expansive mineral growth in premature deterioration of Iowa highway concrete. This research objective was accomplished by:

- (A) Determining the abundance, spatial location, and characteristics of potentially expansive minerals in older Iowa highway concrete.
- (B) Determining chemical and physical changes that have occurred in this concrete as a result of new mineral growth.
- (C) Identifying specific mechanisms involved in the formation of these minerals.
- (D) Determining the mechanisms that cause cracking of concrete and whether they involve expansive mineral growth.

Another important objective was to investigate the effect of various deicer solutions on the formation of expansive minerals and concrete deterioration. This objective was accomplished by conducting laboratory experiments designed to determine the relative aggressiveness of different currently used or potentially useful deicers on existing Iowa

highway concrete deterioration. A previous study by Cody et al. (1996) focused on the effects that NaCl, CaCl₂, and MgCl₂ had on gross concrete deterioration and Mg migration from dolomite coarse aggregate. The current investigation analyzed in detail the effects that those salts, calcium magnesium acetate (CMA), and sodium sulfate have on the formation of expansive minerals and concrete deterioration.

This report will be presented in two parts: expansive mineral growth in Iowa highway concrete, and experimental study of deterioration by secondary mineral growth in Iowa highway concrete.

**PART I. EXPANSIVE MINERALS FEATURES
OF IOWA HIGHWAY CONCRETES**

METHODS OF STUDY

COLLECTION OF HIGHWAY CONCRETE SAMPLES

Seven core samples (A to G) with different aggregate sources and different service records were obtained from seven different Iowa highways by personnel of the Iowa Department of Transportation (Table I). Selection of the core samples was on the basis of premature deterioration of the highways which Iowa DOT personnel believed probably was due to adverse reactions between coarse aggregate and cement paste. Coarse aggregates used in these concretes were from Portland West, Crawford-Lee, Dotzler, Nelson, and Sundheim quarries. Concrete containing Sundheim coarse aggregate was included as an example of concretes containing high performance aggregate. In addition to these seven samples, four concretes cores (Gan-1, 2, 3, and 4) previously investigated for dedolomitization reactions in an earlier Iowa DOT contract (HR-355) were included in the current investigation (Table I). Coarse aggregate for these four concretes were obtained from the Sundheim, Paralta, Garrison, and Smith quarries.

GENERAL PROCEDURES AND INSTRUMENTATION

Each of the four-inch diameter concrete highway cores obtained from the Iowa DOT were cut into small rectangular blocks, approximately 2cm x 2cm x 4cm. Polished thin-sections were made from blocks from the top (1" from top of the road surface) and bottom (1" from the bottom) portions of each core. Petrographic analyses of thin-sections

were conducted with both transmitted and reflected light utilizing a standard petrographic polarizing microscope. Petrographic examination was used to identify specific areas to be studied by scanning electron microscope, and to supplement observations of features difficult to observe with scanning electron microscopy such as color changes on coarse aggregate margins.

An Hitachi S 2460 reduced-vacuum scanning electron microscope was used in this study. Back-scattered images were taken and energy dispersive analytical x-ray (EDAX) area mapping was performed for Si, Al, K, Na, O, Ca, Mg, S, Cl, and Fe. EDAX point analyses were obtained at high magnification for qualitative mineral identification. An accelerating voltage of 15 kV was generally used for imaging whereas EDAX point analyses were obtained at 20 kV.

CHARACTERISTICS OF IOWA HIGHWAY CONCRETE SAMPLES

DURABLE AND NON-DURABLE CONCRETES

The majority of our core samples were concretes constructed with dolomite coarse aggregate. Previous research classified these Iowa highway concretes into two groups, durable and non-durable concretes, based on their service records (Cody et al. 1994; Gan et al. 1996). The term “durable concrete” was used for the highway concretes which had extended service lives of > 40 years before significant deterioration, and “non-durable concrete” was used for concretes with service lives of < 16 years. These terms have no necessary correspondence with ASTM-defined durability.

DOLOMITE COARSE AGGREGATE CHARACTERISTICS

Crystallinity and Crystal Size

For the purpose of this study, dolomite coarse aggregate used in Iowa highway construction will be discussed as "reactive and non-reactive" dolomite aggregate, which can be distinguished by petrographic and SEM observation. There are marked differences in crystal size and crystallinity between reactive and non-reactive aggregate (Hadley 1964b; Lemish et al. 1958; Tang et al. 1989; Cody et al. 1994; Deng et al. 1994; Gan et al. 1996). Reactive dolomite aggregate consists of mostly fine-grained, poorly-crystallized dolomite crystals with many small void spaces between loosely intergrown crystals (Plate I-A). Non-reactive dolomite aggregate typically consists of coarse-grained, well-crystallized dolomite crystals which are tightly intergrown and contain few voids (Plate I-B). The dolomite crystal size criterion, reported by Cody et al. (1994) and Gan et al. (1996), for distinguishing reactive from non-reactive aggregate is approximately 50-70 μm maximum diameter.

Reaction Rim Development

When reactive dolomite coarse aggregate is used in Iowa highway construction, reaction between the aggregate particles and the cement paste can produce a series of reaction zones or rims in both. Five reaction zones at the dolomite-paste interface were identified by Cody et al. (1994) and Gan et al. (1996): an unaltered dolomite aggregate interior (Zone A), two reaction rims on the margin of dolomite aggregate (an inner dark dolomite rim, Zone B, and an outer light-colored dolomite rim, Zone C), a light-colored paste rim (Zone D), and unaltered cement (Zone E). Boundaries between these zones are

generally gradational. In Zone B, abundant inter-crystalline voids are developed as a result of the dissolution of dolomite crystals by dedolomitization reactions. Finely-crystalline calcite crystals occur as thin linings at the edges of dolomite crystals in this zone. Zone C is marked by calcite accumulation in which finely-crystalline calcite fills inter-crystalline voids. Zone D is in the cement paste adjacent to reactive dolomite aggregate and is a dense calcite accumulation zone produced by dedolomitization of dolomite and concomitant carbonation of portlandite. The presence or the thickness of these rims and the spatial distribution of the zones is related to the aggregate reactivity and is not always identical within different parts of the same concrete sample. Interfaces can be classified according to the following scheme (Cody et al. 1994; Gan et al. 1996): the Type I interface represents the most complete interface in which all reaction rims occur (A+B+C+D+E) (Plate I-A; Figs. 1, 2, 3). In many case, Zone B is present throughout the dolomite aggregate particle and results from pervasive dedolomitization (Fig. 4). The Type II interface includes patterns in which Zone C, the light-colored dolomite rim, is absent (Fig. 5) or Zone B is missing. It is the most common type of interface. Type III interfaces have no reaction rims visible in either dolomite aggregate or paste (Plate I-B; Fig. 6).

Types I and II interfaces typically occur at the reactive dolomite aggregate-paste interfaces whereas Type III interface is an indication of the lack of reactivity between dolomite aggregate and paste interface.

Chemical Composition

Bulk chemical analyses of Iowa highway dolomite coarse aggregates were provided by the Iowa DOT (Table II), and show that dolomite aggregates in durable and non-durable concretes have no significant differences in chemical composition. Analyses indicate that all the dolomite aggregates contain approximately 20 wt % MgO and 30 wt % CaO, which is close to the theoretical composition of dolomite, 21.86 wt. % and 30.41 wt. %. This conclusion is supported by microprobe analyses (Cody et al. 1994). The SiO₂, Al₂O₃ and K₂O contents show positive correlations among each other to indicate the presence of clay minerals as impurities.

Pyrite Inclusions

Sulfide minerals are often present in many geologic materials including limestone and dolomite rock. When rocks containing sulfur-bearing minerals are used for aggregate in concrete construction, they can serve as a potential sources of sulfate which causes deterioration (Oberste-Padtburg et al. 1984; Salomon et al. 1992; Chinchon et al. 1995; Casanova 1996). Of these sulfide minerals, pyrite (FeS₂) and pyrrotite (Fe_{1-x} S) are the most common in carbonate rocks. Dolomite and limestone aggregates used in Iowa highway concretes frequently contain pyrite. Large quantities of magnesium sulfate efflorescence have been noted on the surfaces of several pyritic dolomites used in Iowa concrete (Dubberke personal communication, 1996), thus demonstrating that the pyrite has oxidized to produce sulfate and that this type of rock may contain large amount of

Table I. Concrete Core Locations and Other Data for Iowa Highway Concretes.

Sample No.	Core Location	Year*	Coarse Aggregate Source	Portland Cement
A	I-35, Cerro Gordo Co.	1974	Portland West quarry, Shellock Fm.	Northwestern I
B	US 30, Linn Co.	1981	Crawford Lee quarry, Spring Grove Member, Wapsipinicon Fm.	Lehigh I
C	IA 9, Howard Co.	1974	Dotzler quarry, Spillville Fm.	Lehigh I
D	IA 21, Iowa Co.	1982	Crawford Lee quarry, Spring Grove Member, Wapsipinicon Fm.	Martin Marietta (?)
E	US 63, Howard Co.	1971	Nelson quarry, Cedar Valley Fm.	Dewey I
F	US 20, Dubuque Co.	1988	Sundheim quarry, Hopkinton Fm	Davenport I
G	IA 100, Linn Co.	1989	Crawford Lee quarry, Spring Grove Member, Wapsipinicon Fm.	Continental III
Gan-1	US 63, Tama Co.	1972	Smith quarry, Coralville Member, Cedar Valley Fm.	Lehigh I
Gan-2	US 151, Linn Co.	1947	Paralta quarry, Otis Member, Wapsipinicon Fm.	Mixed (Medusa, Lehigh, Dewey, Atlas, Alpha)
Gan-3	US 218, Benton Co.	1971	Garrison quarry, Coralville Member, Cedar Valley Fm.	Davenport I
Gan-4	US 20, Dubuque Co.	1988	Sundheim quarry, Hopkinton Fm.	Davenport I

*year the highway was constructed.

soluble magnesium. Presumably, the soluble magnesium was derived by dedolomitization reactions. Aggregate composed of dolomite containing oxidized pyrite may reduce concrete service life because sulfate has been known for many years to damage concrete.

Pyrrhotite is less common than pyrite in dolomite whereas chalcopyrite (CuFeS_2) is generally rare. The sulfur content of dolomite aggregates from different quarries is shown in Table II. Small pyrite inclusions ($< 10 \mu\text{m}$) are primarily disseminated within dolomite and limestone aggregates (Plate II-A) whereas larger pyrite crystals ($> 50 \mu\text{m}$) are present in some dolomite aggregates (Fig. 7). In several aggregates, pyrite in dolomite aggregate is either partially or completely oxidized to goethite ($\text{FeO}(\text{OH})$) (Plate II-B; Fig. 7).

FINE AGGREGATE CHARACTERISTICS

In Iowa highway concretes, about 25 to 35 vol. % of the concrete consists of fine aggregate ($< 2.5 \text{ mm}$). Examination of petrographic thin-sections of samples shows that the fine aggregates of studied samples consist chiefly of quartz, with minor amounts of orthoclase feldspar, clay minerals, ferromagnesian minerals such as biotite and amphibole, goethite, and limonite. Quartz is a major constituent and is present as discrete detrital grains, although it also occurs as fragments of quartz-bearing rocks. Detrital quartz is rounded to sub-angular (Plate III-A).

Strained quartz, indicated by undulatory extinction, is often present (Plate III-A, B). This type of quartz is reactive and often is involved in alkali-silica reactions (Smith et al. 1992; Grattan-Bellow 1992) which produce expansive silica gel responsible for cracking of quartz grains and/or cement paste. Smith et al. (1992) suggested that the reactivity of undulatory quartz is a function of undulatory extinction angle, texture, and grain size. Petrographic observation of thin-sections shows that quartz grains in most samples are generally unaltered from their original state (Plate III-A), but some grains

appear to have undergone cracking (Plate III-B). Microcracks in places occur in the paste adjacent to quartz grains. These cracks may be caused by expansion resulting from the alkali-silica reaction, but there is little evidence of significant amounts of silica gel adjacent to quartz grains or in micro-cracks associated with them.

Other silicate minerals are predominately feldspars that include plagioclase, orthoclase and microcline. Potassium- and sodium-rich clay minerals commonly occur as well. Adjacent to some clay minerals, minor cracking of aggregate and paste is observed in a few samples. Minor amounts of hematite and goethite are present as discrete detrital grains in the fine aggregate. Aggregate particles containing a matrix of pyrite that is partially oxidized to goethite were observed in many samples.

CEMENT PASTE CHARACTERISTICS

Chemical Composition of Cement Paste

Five different types of Portland cement were used in the construction of the Iowa highway concretes studied here (Table I). All of the cements are type I except for one type II used in the construction of IA 100. Bulk chemical analyses of the cements were obtained by the Iowa DOT, and the average, standard deviation, maximum and minimum values of duplicate analyses are listed in Table III. In this table, *Potential Compound Composition* refers to the maximum compound composition allowable by ASTM C150 calculations based on the chemical composition of the cement. MgO contents of concrete should be limited to 4~5 wt. % because an excess causes formation of the mineral

Table II. Chemical Composition of Dolomite Aggregate.

Aggregate Source	MgO	CaO	SiO ₂	Al ₂ O ₃	K ₂ O	P ₂ O ₅	MnO	S	FeO*	TiO ₂	CO ₃	Total
Portland West	16.47	32.58	4.40	1.11	0.56	0.01	0.02	0.30	0.44	0.06	43.52	99.49
Crawford, Lee	18.47	32.88	0.82	0.15	0.05	0.01	0.04	0.34	0.51	0.01	45.94	99.23
Nelson	17.00	33.97	2.19	0.40	0.18	0.02	0.02	0.26	0.33	0.02	45.19	99.57
Dotzler	20.30	29.67	2.69	0.59	0.25	0.03	0.01	0.30	0.27	0.04	45.42	99.57
Sundheim	20.11	30.41	2.56	0.49	0.20	0.01	0.02	0.03	0.15	0.03	45.82	99.84
Smith	18.24	32.71	1.74	0.40	0.14	0.02	0.00	0.35	0.34	0.02	45.59	99.56
Paralta	22.01	29.47	0.59	0.11	0.06	0.01	0.03	0.04	0.23	0.01	47.15	99.72
Garrison	18.38	32.13	1.57	0.36	0.13	0.01	0.03	0.66	0.62	0.01	45.28	99.19

Iowa DOT chemical analysis data, average

* FeO is converted from Fe₂O₃

periclase (MgO) which may expand by a slow hydration reaction to brucite, Mg(OH)₂, (Taylor 1990) and result in concrete damage. The content of MgO in the Portland cement of Table III varies from 2.35 % to 3.38 wt. %, which is within suggested limits of MgO content. The SO₃ content should be limited to 2.5 ~ 4 wt. %, because excess can cause expansion by the formation of delayed ettringite (Taylor 1990). The SO₃ content in the Portland cements of Table III are all within this limit. Type I cement contains 2.71 % to 3.16 wt. % whereas type III cement has a somewhat higher content of 3.57 wt. % SO₃. Alkalis (K₂O and Na₂O) are also important constituents of Portland cement because they can create deleterious alkali aggregate reactions. In Portland cement, alkali contents are limited to 0.6 wt. % equivalent Na₂O (Na₂O equivalent = Na₂O + K₂O, Taylor 1990). The contents in Portland cements listed fall into this limit except Davenport (type I) which is slightly over this limit (0.66 % equivalent Na₂O).

Table III. Composition of Portland Cement Used for Iowa Highway Concretes.

Name of Portland Cement		Chemical Composition, %						Na ₂ O equiv.	Loss of Ignition, %	Insoluble Residue, %	Total	Potential Compound Composition, %			
		SiO ₂	Al ₂ O ₃	Fe ₂ O ₃	CaO	MgO	SO ₃					C ₃ S	C ₂ S	C ₃ A	C ₄ AF
Davenport	Avg.	21.22	4.50	2.81	63.23	3.17	2.71	0.66	1.03	0.29	99.87	54.22	19.92	7.15	8.56
	S. Dev.	1.23	0.39	0.39	1.17	0.50	0.24	0.12	0.31	0.20					
	Max.	24.76	6.65	4.14	65.45	4.65	3.4	0.94	2.07	1.28					
	Min.	17.09	2.92	2.16	55.1	1.57	1.97	0.37	0.44	0.02					
Continental	Avg.	21.24	4.75	2.24	63.95	3.40	2.94	0.33	1.37	0.21	100.54	55.47	19.05	8.78	6.83
	S. Dev.	1.15	0.62	0.53	1.10	0.67	0.34	0.21	3.53	0.16					
	Max.	24.24	6.14	3.39	67.61	5.12	4.23	0.83	31.01	0.92					
	Min.	19.07	2.58	1.3	61.34	2.01	2.44	0.01	0.44	0					
Continental III	Avg.	20.67	4.98	1.37	63.96	3.38	3.57	0.09	1.27	0.23	99.52	57.73	15.70	10.87	4.17
	S. Dev.	0.33	0.14	0.01	0.36	0.17	0.17	0.02	0.11	0.10					
	Max.	20.94	5.14	1.39	64.30	3.52	3.71	0.12	1.38	0.35					
	Min.	20.27	4.82	1.36	63.47	3.14	3.33	0.07	1.13	0.12					
Lehigh	Avg.	21.19	4.95	2.36	63.89	2.62	3.16	0.56	0.98	0.29	100.23	53.45	20.43	9.12	7.17
	S. Dev.	1.36	0.36	0.21	1.39	0.55	0.23	0.12	0.35	0.36					
	Max.	25.57	6.09	3.37	67.18	4.72	3.78	0.82	1.81	2.66					
	Min.	18.05	3.36	2.03	60.37	0.95	2.22	0.40	0.17	0.03					
Northwestern	Avg.	21.65	4.94	2.04	64.11	2.35	2.97	0.47	1.06	0.26	100.02	51.89	22.93	9.62	6.21
	S. Dev.	1.59	0.31	0.46	1.15	0.71	0.28	0.14	0.33	0.13					
	Max.	24.53	5.51	3.1	67.44	4.22	3.67	0.81	2.15	0.69					
	Min.	18.68	3.78	1.55	62.05	1.15	2.05	0.21	0.4	0.03					

Air-Entrainment Voids

The Iowa highway concretes studied here contain very similar amounts of entrained air (6 % \pm 1 ½ vol. %). Air-entrainment voids appear to be uniformly distributed over all of the core surfaces. Microscopic thin-section observation shows that air entrainment voids are spherical, and that the air entrainment void diameters vary from several tens of microns to several millimeters. Sample F (US 20) and G (IA 100) contain class C fly ash which occurs as tiny spherical grains. White mineral deposition in the entrainment voids is often observed in core samples. No significant large-scale cracks were seen in the core samples.

RESULTS AND DISCUSSION

INTRODUCTION

Abundant brucite and ettringite were observed in most of the highway concretes studied, and large amounts of calcite mineralization occurred in the outer regions of partially dedolomitized dolomite aggregate rims. Ettringite was the most abundant mineral, followed by calcite, and then by brucite. These minerals were the only potentially expansive substances identified by petrographic microscope and electron imaging methods. Gypsum was not detected in significant amounts in any samples.

BRUCITE, Mg(OH)₂, OCCURRENCE IN IOWA CONCRETES

Brucite crystals are very difficult to identify petrographically because of their small size and optical character which is similar to that of calcite and dolomite. EDAX area mapping at high-magnification and EDAX point analysis methods are more useful in identifying brucite crystals. The exact location of brucite in the paste and aggregate can be determined by comparing element maps with back-scattered images. The morphology and characteristic occurrences of individual brucite crystals are easily observed at high magnification, but such observations may lead to a false impression about the distribution patterns in the cement paste. When supplemented with careful examination at low-magnification, however, the characteristics of crystal growth and distribution patterns are more clearly discernible.

Forms and Distribution

The abundance and size of brucite crystals in the Iowa concretes studied are closely related to the reactivity of dolomite aggregate. In Iowa concrete highways, US 30, IA 9, IA 21, US 23, IA 100, US 63, US 151, and US 218, which contain reactive dolomite aggregate, abundant brucite is commonly found in the cement paste near dolomite aggregate - cement paste interfaces (Figs. 1 - 5). In highway concrete containing non-reactive dolomite aggregate (I 35 and US 20) (Fig. 6) and limestone aggregate (IA 100) (Fig. 8), much less abundant and typically smaller brucite crystals are observed. Low-magnification EDAX element analysis clearly showed the distribution pattern of brucite

crystals precipitated in the cement paste, but was incapable of identifying brucite formation in aggregate interiors because brucite could not be distinguished from dolomite. With high-magnification observations (Fig. 9), brucite in the reaction rims of cement paste and aggregate can be identified.

Relatively large brucite crystals are frequently found in the cement paste of many samples (Fig. 9), whereas brucite in dolomite aggregate is identified by the location of extremely fine, disseminated white spots visible in corresponding Mg - O element maps. The very small grain size and widespread dissemination indicate that most of the brucite in dolomite aggregate interiors may exist as microcrystalline coatings associated with newly-formed finely crystalline calcite on the surface of dolomite crystals. In the cement paste, brucite typically occurs as larger irregular nodules, and is generally not associated with air-entertainment voids or other obvious open spaces (Fig. 10). Some of the disseminated Mg in the cement paste may be associated with magnesium silicate hydrate (MSH).

Small, < 20 μ m diameter, euhedral to subhedral, brucite crystals often occur in the calcite matrix in the reaction Zone D of the cement paste (Fig. 9). There is no obvious spatial association of brucite with cracks in either cement paste or aggregate (Figs. 9, 10). In many locations, more brucite is present in the unaltered paste (Zone E) than in the light-colored cement paste zone (Zone D) adjacent to reactive dolomite aggregate particles. This suggests that a significant quantity of magnesium migrates considerable distances from dedolimitizing dolomite coarse aggregate sources into the cement paste before precipitation (Figs. 1 - 5). If Mg were less mobile, brucite should be more

common in dolomite rim zones or in Zone D cement. It is also possible that brucite forms in the unaltered paste because the paste is richer in hydroxide ions than the bleached, altered paste zone or the dolomite rim zones.

Brucite Formation in Iowa Concrete

The greater abundance of brucite, $\text{Mg}(\text{OH})_2$, in Iowa concretes containing reactive dolomite aggregates than in those with non-reactive dolomite is strong evidence that brucite is a by-product of the release of magnesium ions by dedolomitization of dolomite, $\text{CaMg}(\text{CO}_3)_2$:

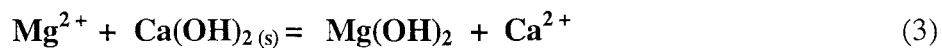


where M represents alkali substances (mainly Na or K). Other sources of magnesium for brucite could be deicer salts which contain small amounts of Mg-salts, Mg-rich clay minerals in carbonate aggregate, and the magnesium in cement clinker. Consideration of the effects in Iowa concrete of these non-dolomitic Mg-sources on brucite formation is beyond the scope of this report except to point out a potential significance of widely disseminated microscopic brucite without any spatial relationship to reactive coarse aggregate in some samples. This brucite occurrence suggests that it results from a more pervasive source of Mg^{2+} than partially dedolomitized coarse aggregate. Deicer applications could provide such a source.

In concrete, the alkali carbonate produced by reaction (1) reacts with portlandite, $\text{Ca}(\text{OH})_2$ in Portland cement and regenerates alkali :



Magnesium ions released by dedolomitization produce brucite crystals that form in three different stages. In the first or earliest stage, brucite crystals in voids or interstitial spaces in the dolomite aggregate appears to rapidly precipitate on dolomite surfaces. These crystals must have formed quickly after Mg^{2+} release because brucite has an extremely low solubility and is observed to precipitate rapidly. In the second stage, brucite precipitated in interstitial pores in the cement paste as pore solutions in this material slowly became supersaturated during progressive migration of magnesium ions away from dolomite aggregate sources. Finally, and perhaps simultaneous with the second stage, crystal surface-induced (topochemical) brucite formed by a reaction between magnesium ions in pore solution and portlandite in the cement paste (Oberste-Padtburg 1985; Tumidajski and Chan 1986) . Unlike in the previous stages which involve precipitation from supersaturated solutions, this reaction was topochemical in nature:



According to Cohen (1983a), a topochemical reaction is defined as “ a reaction between a solid particle and a surrounding solution in which the hydration product is formed on the surface of the particle”.

Mechanisms of Brucite Formation in Iowa Concrete

Examination of EDAX area maps of many samples shows that brucite growth in dolomite coarse aggregate rim areas is restricted. Considerably less brucite is formed in Zone B and Zone C compared with the amount of newly-formed calcite precipitated in these zones, and this is especially evident in Zone C where dense accumulations of calcite occur in interstitial spaces in the dolomite coarse aggregate. Stoichiometric considerations of Eqs. (1) and (2) predict that twice as much calcite as brucite should form via a combination of the two reactions. This prediction is not fulfilled because the observed volume of newly-formed calcite is much greater than twice that of brucite.

We conclude, therefore, that direct precipitation of brucite in areas of dedolomitization seems to rarely occur in actual conditions. The dense accumulation of finely crystalline calcite and the near absence of brucite in aggregate reaction zones close to magnesium sources indicates that the calcite precipitation, reaction (2) is much faster than the dedolomitization reaction (1). Magnesium ions appear to typically migrate considerable distances into the cement paste before brucite forms. Most of the brucite occurs in otherwise unaltered cement paste, outside of the cement reaction zone (Zone D) adjacent to dolomite aggregate particles, and at some distances from dolomite sources.

The precipitation of calcite as a result of reaction (2) causes pH increases, regeneration of OH^- , and a decrease in CO_3^{2-} in pore solutions. These changes enhance dedolomitization and portlandite dissolution in the cement paste near reactive aggregate particles. Because brucite precipitation in concrete typically seems to be retarded, further

migration of magnesium ions from their sources into the cement paste occurs where brucite forms either by direct precipitation in voids or by reaction with hydroxyl ions (OH⁻) on the surface of portlandite.

We conclude that more brucite formed by topochemical reactions between magnesium ions and portlandite in the cement matrix rather than by direct precipitation in void because the common irregular-shaped nodular brucite has no clear relationship to pre-existing voids in cement paste. This would also explain the lack of brucite in altered cement paste (reaction Zone D). In this reaction zone, topochemical reactions between dissolved magnesium and hydroxyl ions on portlandite surfaces is limited because portlandite is depleted during its transformation to calcite via reaction (2). Magnesium ions released by dissolution of dolomite when acid is generated during pyrite oxidation may also contribute to the formation of brucite. This mechanism will be briefly discussed in the section on ettringite formation.

ETTRINGITE, $3\text{CaO}\cdot\text{Al}_2\text{O}_3\cdot3\text{CaSO}_4\cdot32\text{H}_2\text{O}$, OCCURRENCE

IN IOWA CONCRETES

Forms and Distribution

In our Iowa highway concrete samples, ettringite chiefly occurs in air-entrainment void spaces where it grows as needle-like crystals projecting from the void walls (Fig. 11). It occurs in two forms in these air-entrainment voids. The first type is void-fill ettringite in which the mineral completely fills air-entrainment voids that are usually less than about 100 μm in diameter (Figs. 12, 13). Abundant cracks, which are irregular and

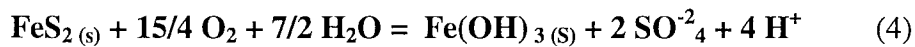
very disruptive, occur in the ettringite fills. The second type is void-rim ettringite that occurs as rims of ettringite lining the margin of voids. This type usually formed in air-entrainment voids of diameter greater than about 100 μm (Fig. 13). Large radially-oriented cracks are prominent throughout the ettringite rims. Some of the cracks in both void-fill and void-rim ettringite continue into the cement paste.

The two types of ettringite depend on a relation between the amount of ettringite-forming pore solutions and the size of void spaces. The void-rim type represents an early stage in delayed ettringite formation. It is transformed into the void-fill type by further crystal growth provided that enough crystal precipitating pore solutions pass through the voids. The vast majority of ettringite crystals occur in air-entrainment voids, but minor amounts of ettringite also fill microscopic interstitial pores in the cement paste (Fig. 10).

Interstitial cement pore space filled by ettringite was observed in high magnification back-scattered SEM images (Figs. 10, 13). Rarely, ettringite also occurred in cracks as shown in Figure 14. These cracks formed along the boundary between quartz fine aggregate particles and cement paste, and appear to result from alkali-silica reaction-induced expansion. Under high-magnification, detailed observations of paste micro-cracks that extend from ettringite-filled voids reveal that ettringite does not occur in them (Figs. 13, 15). This observation provides strong evidence that the micro-cracks developed after ettringite formation.

Relationship of Ettringite to Pyrite Inclusions

Oxidation of Pyrite. Sulfate is a necessary component for the formation of ettringite in the cement paste, so that oxidation of sulfide minerals in concrete coarse and fine aggregate may promote delayed ettringite formation. The oxidation of pyrite is a complex process involving a number of reactants and products under varying oxygen fugacities and pH's. However, the major reactions involved in pyrite oxidation under alkaline concrete-forming conditions are:



Ferrihydrite



Goethite



Hematite

Volume changes for the reactions are +3.05, -3.12, and -8.81 cm³/mole sulfide respectively for reaction (4), (5), and (6), and have been referred to as “primary expansion” due to pyrite oxidation (Casanova and Aguado, 1996). A stability diagram for pyrite (FeS₂), siderite (Fe(CO₃)), ferrihydrite (Fe(OH)₃), calcite (CaCO₃), and gibbsite (Al(OH)₃) and aqueous species is presented in Figure T1. As shown in the diagram, ferrihydrite is the predominant pyrite oxidation product under alkaline conditions in

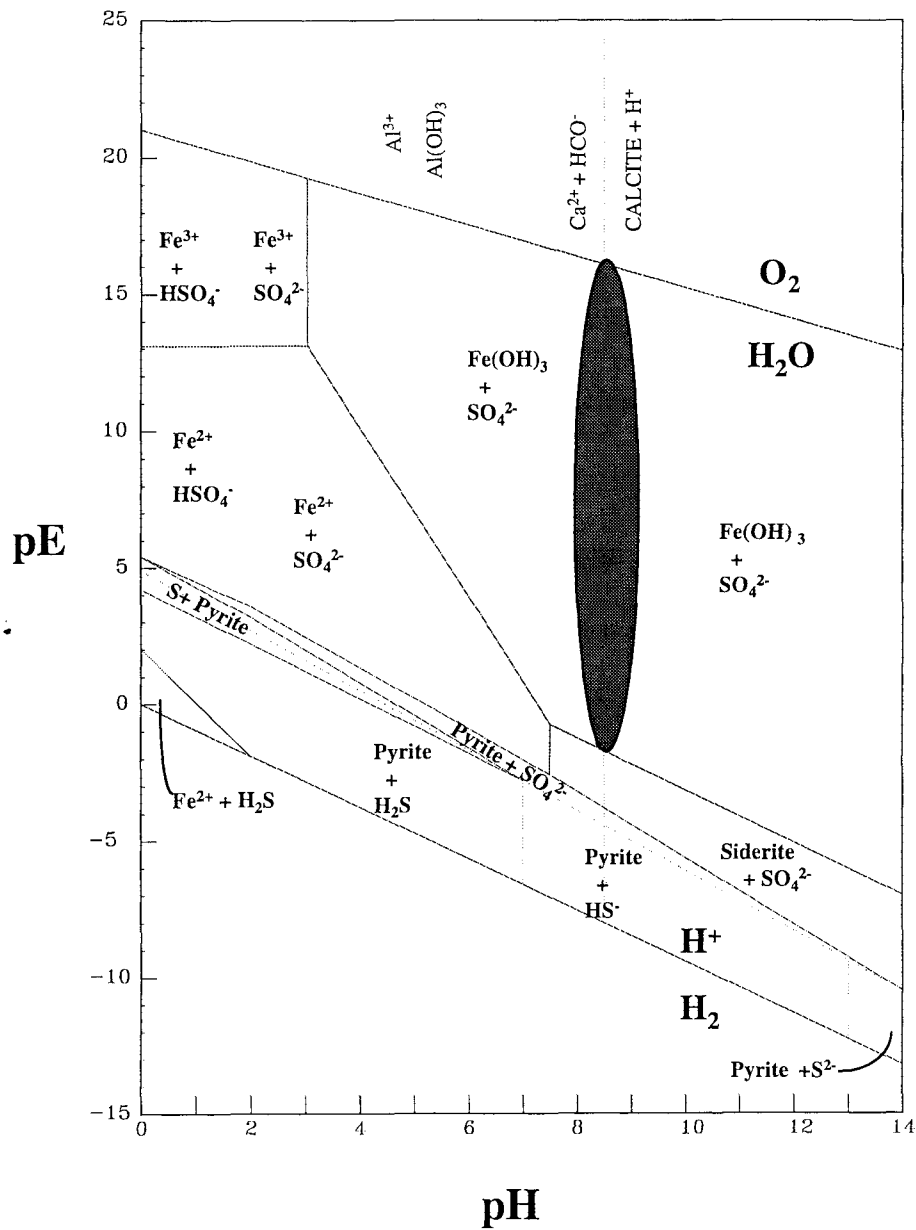


Fig. T1. A stability diagram for selected iron minerals at 25°C and $\Sigma\text{Fe}=10^{-4}$, $\Sigma\text{S}=10^{-2}$, $\Sigma\text{Ca}=10^{-4}$ mole/liter and $\text{PCO}_2=10^{3.5}$ bar. The shaded area indicates the probable pE - pH values associated with calcite dissolution in pore waters (after Chinchon et al. 1995)

concrete. Ferrihydrite may subsequently transform into goethite by dehydration: $Fe(OH)_3(s) = FeOOH(s) + H_2O$, and further dehydration could produce the hematite: $2FeO(OH)(s) = Fe_2O_3(s) + H_2O$. Dehydration to hematite seems unlikely to occur in highway concrete because this reaction requires low moisture, and water is generally retained in concrete (Casanova and Aguado 1996). Reactions (4) and (5) are probably predominant in highway concretes. Evidence of pyrite oxidation in cement samples is suggested by the presence of iron oxides, usually goethite, replacing pre-existing pyrite (pseudomorphs of goethite after pyrite).

As a result of pyrite oxidation, acid generation may result in relatively low local micro-environmental pH surrounding the oxidation products. Typically in concrete, and always in dolomite or limestone aggregates, however, pore solutions are saturated with carbonate. Under these conditions, hydrogen ions generated by pyrite oxidation are neutralized by combining with CO_3^{2-} to form bicarbonate (HCO_3^-), and the pH should remain essentially constant by balancing acid generation and acid consumption except for very short time intervals or under unusual local conditions (Nicholson et al. 1988).

Spatial Relationships of Pyrite and Ettringite. In general, relatively abundant ettringite occurs in the cement paste near dolomite aggregates that contain a considerable amount of oxidized pyrite inclusions (Figs. 1, 2, 4, 5, 16). The abundance of ettringite appears to be closely associated with the amount of pyrite oxidation as evidenced by the quantities of goethite and/or ferrihydrite. The oxidation of pyrite is affected by carbonate coarse aggregate properties and by the location of pyrite in these aggregates. Crystal size, the degree of crystallinity and porosity, and aggregate reactivity are important in affecting

pyrite oxidation. Pyrite inclusions located in open spaces such as interstitial pores or intercrystalline boundaries typically are well-oxidized, as is shown by abundant iron oxide replacements of original pyrite, because oxidizing solutions can more easily move thorough these open spaces and make contact with pyrite (Plate II-B). Pyrite enclosed within large, well-crystallized dolomite crystals is not typically oxidized because pyrite has little chance to be exposed to oxidizing solutions (Plate II-A).

The volume and amount of void spaces in dolomite coarse aggregate also varies with aggregate type. More open spaces occur in fine-grained, poorly-crystallized aggregate, whereas they rarely occur in coarse-grained, well-crystallized aggregate. The finer-grained, poorly crystallized dolomite is more amenable to dedolomitization than the coarser-grained, well-crystallized dolomite, and this reaction produces secondary void spaces, especially in Zone B. Pyrite in Zone B of reactive dolomite coarse aggregate is most often exposed to oxidizing pore solutions and, consequently, is more oxidized compared to that in non-reactive dolomites.

In places, ettringite is found in the cement paste rim (Zone D) near reactive dolomite aggregate that contains well-oxidized pyrite inclusions. In general, however, less abundant ettringite occurs in this zone compared to that outside of the light-colored paste alteration zone (Fig. 1 - 5).

Mechanisms of Ettringite Formation

Importance of Sulfur and Water. Sulfate is a necessary component for the formation of ettringite in concrete, and it can be derived either from internal or external

sources (Wolter 1996). Internal sources of sulfate are the sulfate or sulfide components of cement, coarse and fine aggregate, pozzolans and admixtures in concrete. External sources include natural or polluted ground water, and soils with high sulfate content (Pettifer and Nixon 1980; Al-Amoudi et al. 1992) and sulfate-rich acid rain. For highway concrete, other potential sulfate sources are sulfur dioxide from the combustion of motor fuels and the sulfate impurities of deicing salt (Pitt et al. 1987).

Water is also an important factor in the formation of ettringite since it is essential to the reactions between soluble sulfate ions derived from internal or external sources and the cement components. In addition, ettringite requires abundant water for its formation because it is a highly hydrated mineral.

• **Sulfur from Cement Blend.** We evaluated the potentially significant internal sources of sulfur for ettringite formation in Iowa highway concretes which include the amount of sulfur in the Portland cement blends used for the highways, and sulfide mineral concentration and locations in fine and coarse aggregate. External sources of sulfur are not considered in this first section of the report.

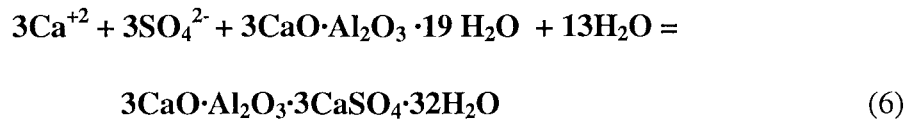
Portland cement blends used in the studied highway concretes contain relatively uniform SO_3 contents which vary between 2.71 to 3.57 wt. % (Table 3), and are well within the range of 2.5 ~ 4.0 wt. % considered necessary to prohibit secondary ettringite formation in concrete (Taylor 1990).

Sulfur from Pyrite. The maximum sulfate contributed by the oxidation of pyrite in dolomite coarse aggregate can be roughly estimated based on the sulfur content in the aggregate and on the mixing specifications for concrete under following assumptions: (1) all

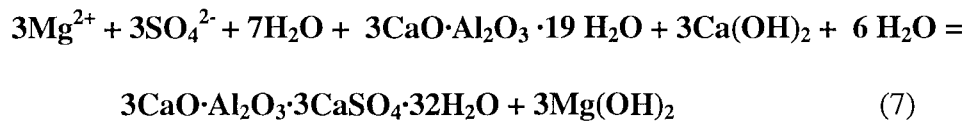
sulfur in coarse aggregate exists as pyrite, (2) all pyrite inclusions are oxidized, (3) the average mixing specification (coarse aggregate is 40 wt. % of total concrete; fine aggregate is 40 wt. %; the water/cement ratio is 0.45), and (4) all pyritic SO_4^{2-} migrates from aggregate to cement. The estimated SO_3 (wt. % of cement) which can be derived from the oxidation of pyrite inclusions in coarse dolomite aggregate is listed for each sample in Tables IV-A, B, column 7, and the potential total available SO_3 for ettringite formation is listed in the last column. As given in the table for example, calculations show that 0.3 wt. % of sulfur content in the coarse dolomite aggregate can result in the addition of up to 2.61 wt % of SO_3 in cement paste of Iowa highway IA35. Because all concrete samples contain both unoxidized and oxidized pyrite, ettringite formation will be less than the calculated maximum.

Sulfur from Deicer Applications. Petrographic observations indicate that much ettringite is rather uniformly disseminated through cement pastes of the older highways studied here (I 35, IA 9, US 63, US 151 and US 218). Some of this ettringite may result from long-term deicer applications on these older highways. According to Pitt et al. (1987), rock salt (NaCl) applied as a deicer on Iowa highways contains up to 4 wt. % sulfate impurities such as gypsum and magnesium sulfate. These minerals dissolve and their ions migrate downward into the concrete where they may react with hydrous tricalcium aluminate (C_3A) in the paste to form ettringite. Deicer sulfate impurities probably significantly contributed to the formation of ettringite in Iowa highway concretes.

Ettringite-Forming Reactions. Sulfate ions released by pyrite oxidation or other sources may exist with dissolved magnesium released during dedolomitization, reaction (1), or with dissolved calcium released by reaction (3). These ions can migrate outward into the cement paste and react with cement paste components such as C₃A and calcium hydroxide (CH) to form ettringite by reaction (6), or ettringite and brucite by reaction (7):



and



Other minerals including gypsum could precipitate as intermediate phases, but no gypsum was observed in the EDAX element maps of any concrete sample. The lack of gypsum suggests that conditions in Iowa highway concrete are not favorable for its formation. Although both of the above reactions involve solid C₃A and CH, two possible reaction mechanisms have been suggested for the reactions between ions in pore solutions and these cement paste components. The proposed reactions are: (1) *topochemical* (Chatterji and Jeffery 1963; Cohen 1983a) and (2) *through solution* (Chatterji 1976; Metha 1976a, b, c; Deng and Tang 1994; Fu and Beaudoin 1995, 1996). Topochemical reactions have already been discussed. Monteriro (1985) defined the “through solution” mechanism as “the cement compounds dissolve to produce ions in solution that

Table IV-A. Sulfur Content (wt. %) in Cement Paste, Dolomite Aggregate, and Maximum Calculated SO₃ Content (wt. %) of Cement Paste, Samples A to F.

	Aggregate Source	Type of Cement		SO ₃ Content In Cement (wt. %)	S Content in Dolomite Aggregate (wt. %)	Potential Pyritic SO ₃ (wt. %) in Cement*	Potential Total SO ₃ (wt. %) in Cement**
A (IA 35)	Portland West	North-western I	Mean	2.97	0.3	2.61	5.58
			STD	0.28	0.129	1.12	1.40
			Max.	3.67	0.537	4.50	8.17
			Min.	2.05	0.072	0.60	2.65
B (US 30)	Crawford Lee	Lehigh I	Mean	3.16	0.335	3.21	6.37
			STD	0.23	0.116	1.11	1.34
			Max.	3.78	0.516	4.95	8.73
			Min.	2.22	0.242	2.32	4.54
C (IA 9)	Dotzler	Lehigh I	Mean	3.16	0.304	2.92	6.08
			STD	0.23	0.05	0.8	1.03
			Max.	3.78	0.398	3.82	7.60
			Min.	2.22	0.225	2.16	4.38
D (IA 21)	Crawford Lee	Martin Marietta	Mean	NA	0.335	3.21	NA
			STD	NA	0.116	1.11	NA
			Max.	NA	0.516	4.95	NA
			Min.	NA	0.242	2.32	NA
E (US 63)	Nelson	Dewey I	Mean	NA	0.257	2.60	NA
			STD	NA	0.189	1.81	NA
			Max.	NA	0.684	6.56	NA
			Min.	NA	0.06	0.58	NA
F (US 20)	Sundheim	Davenport I	Mean	2.71	0.026	0.21	2.92
			STD	0.24	0.003	0.03	0.27
			Max.	3.4	0.022	0.25	3.65
			Min.	1.97	0.003	0.04	2.01

* This value represents the total wt. % of pyritic sulfur that could accumulate in the cement paste phase given assumptions in text..

** This value is the sum of the SO₃ Content in Cement (wt. %) (column 5) plus the Potential Pyritic SO₃ (wt. %) in Cement (column 7).

Table IV-B. Sulfur Content (wt. %) in Cement Paste, Dolomite Aggregate, and Maximum Calculated SO₃ Content (wt. %) of Cement Paste, Samples G to G-4.

	Aggregate Source	Type of Cement		SO ₃ Content in Cement (wt. %)	S Content in Dolomite Aggregate (wt. %)	Potential Pyritic SO ₃ (wt. %) in Cement*	Potential Total SO ₃ (wt. %) in Cement**
G (IA 100)	Crawford Lee	Continental III	Mean	3.57	0.335	3.21	6.78
			STD	0.17	0.116	1.11	1.28
			Max.	3.71	0.516	4.95	8.66
			Min.	3.33	0.242	2.32	5.65
Gan-1 (US 63)	Smith	Lehigh I	Mean	3.16	0.337	3.23	6.39
			STD	0.23	0.131	1.26	1.49
			Max.	3.78	0.493	0.47	4.25
			Min.	2.22	0.174	1.67	3.89
Gan-2 (US 151)	Paralta	Mixed	Mean	NA	0.037	0.35	NA
			STD		0.0043	0.04	Na
			Max.		0.041	0.39	Na
			Min.		0.028	0.27	Na
Gan-3 (US 218)	Garrison	Davenport I	Mean	2.71	0.54	5.18	7.89
			STD	0.24	0.136	1.30	2.54
			Max.	3.4	0.884	8.48	11.88
			Min.	1.97	0.398	3.82	5.79
Gan-4 (US 20)	Sundheim	Davenport I	Mean	2.71	0.026	0.21	2.92
			STD	0.24	0.003	0.03	0.27
			Max.	3.4	0.022	0.25	3.65
			Min.	1.97	0.003	0.04	2.01

* This value represents the total wt. % of pyritic sulfur that could accumulate in the cement paste phase given assumptions in text..

** This value is the sum of the SO₃ Content in Cement (wt. %) (column 5) plus the Potential Pyritic SO₃ (wt. %) in Cement (column 7).

will recombine to form hydration products which subsequently precipitate out from supersaturated solution”, i.e. direct precipitation from solution.

Hansen (1976) concluded that ettringite formed by a topochemical reaction because tricalcium aluminate does not dissolve in an aqueous medium. He proposed that ettringite forms radially around residual topochemically-reacting C_3A particles (Cohen 1983a; Older and Yan 1994). If the ettringite-forming reaction is topochemical, then there should be a definite relationship between the crystal structures of the reacting particles and that of ettringite (Metha 1976 a, b; Older and Yan 1994). Because of large difference in crystal structures of ettringite (trigonal) and anhydrous calcium aluminate (C_3A ; cubic) or sulfoaluminate (C_4A_3S), however, the topochemical reaction is considered by many workers to be kinetically difficult at normal temperatures (Metha, 1983; Deng and Tang, 1994).

Metha (1976a) believed that the formation of ettringite on the surfaces of reacting particles and its random deposition in other locations is an indication of a “through solution mechanism” for precipitation rather than a topochemical one. Deng and Tang (1994) assumed that the bonds of Ca-O and Al-O of aluminate are broken when polar H_2O molecules and/or OH^- ions interact with aluminate particles and, eventually, Ca^{2+} and $Al(OH)_4^-$ ions form in pore solutions. As a result of reactions between these ions and SO_4^{2-} ions in solution, ettringite preferentially precipitates in open spaces such as voids and cracks as needle-like (acicular) crystals whenever pore solutions are critically supersaturated (Day 1992; Metha 1976a; Fu et al. 1995; Fu and Beaudoin 1995, 1996).

Fu and Beaudoin (1995, 1996) concluded that ettringite crystallization rates are controlled by the degree of supersaturation required to form ettringite critical-size nuclei.

Specific Mechanisms in Iowa Concretes. Ettringite in Iowa highway concretes mainly grew in air entrainment voids, interstitial pore spaces, and pre-existing cracks which are not closely associated with aluminate particles. Occasionally it occurs in cracks between cement paste and coarse or fine aggregate. The characteristic occurrence of ettringite in open spaces without association with C_3A or CH reacting particle locations indicate that a solution precipitation rather than a topochemical reaction was involved in its formation. In rare instances, ettringite (5-10 μ m size) was observed under high-magnification, in association with aluminate particles that appear to be partly consumed by ettringite (Figs. 12, 17). This type of ettringite appears to have formed by a topochemical reaction. The acicular habit of ettringite in entrainment voids is another indication of solution-precipitation reaction for its formation (Fig. 11) since it is generally accepted that crystals precipitating from supersaturated solutions are often elongate along their principal crystallographic axis (Metha 1976b).

Freeze-thaw conditions may also enhance ettringite formation. Day (1992) proposed that freezing of capillary pore solutions in highway concrete plays a significant role in ettringite formation in larger voids. He concluded that pore solutions can be expelled from capillaries into larger voids, where conditions are favorable to larger ettringite crystals, during freezing of the concrete pore solutions. Day (1992) also pointed out that a reduction in $Ca(OH)_2$ concentrations in solution results in an increase in ettringite solubility. In Iowa highway concrete, the formation of calcite in reaction zones

of the cement paste locally depletes $\text{Ca}(\text{OH})_2$, and may result in ettringite dissolution. This may partly explain the near absence of ettringite in cement phase reaction rims (Zone D).

The larger accumulation of ettringite in older concretes compared to younger concretes may be related to the amount of deicer applied during winter months. Older highways have received more deicer applications over their many years of use than younger highways. An example of this is the abundant ettringite in concrete of US 218 which was constructed using Paralta dolomite aggregate that contained very low amounts of S (0.04 wt. %). The sulfur generated from the combustion of motor fuels may have also contributed to ettringite formation in older highway deterioration, but its significance is unclear.

EXPANSIVE MECHANISMS AND IOWA CONCRETE DETERIORATION

CEMENT-AGGREGATE EXPANSIVE REACTIONS

Publications on concrete deterioration abound with conclusions that the growth of expansive substances is responsible for much of the premature deterioration of concretes. The following section will present an overview of some of these studies, and our interpretations on the role of expansive mineral growth in Iowa concrete deterioration.

Premature deterioration of Iowa highway concrete may be caused by various types of chemical reactions between aggregate and cement paste which are grouped into a

general term *alkali-aggregate reaction* (AAR). The highly alkaline environment (pH 11-12) of Portland cement induces reactions between coarse/fine aggregate particles of concrete and the Portland cement paste. Three major types of these alkali-aggregate reactions have been reported (Gillott 1975; Tang 1992; Rogers 1993; West 1996) : (1) alkali-carbonate reaction (ACR), (2) alkali-silica reaction (ASR), and (3) alkali-silicate reaction.

Alkali-Carbonate Reactions

Among these reactions, ACR seems to be the most significant for Iowa highway concretes because carbonate rocks are chiefly used in their construction (Lemish et al. 1958; Bisque and Lemish 1958; Cody et al. 1994; Gan et al. 1996). Since 1957, when alkali-carbonate reaction was first discovered in Canada, the deterioration of concrete by ACR has been reported by many researchers (Bisque and Lemish 1958; Hadley 1961, 1964a, b; Swenson and Gillott 1960, 1964, 1967; Lemish and Moore 1964; Gillott 1964, 1975; Mather 1964; Poole 1981; Tang et al. 1986, 1989, 1994; Deng et al. 1993; Rogers 1993; Milanesi and Batic 1994;). The alkali-carbonate reaction is characterized by dedolomitization of dolomitic limestones, calcitic limestones, and dolomite rocks (Gillott and Swenson 1969; Gan et al. 1996).

Alkali-Silica Reactions

Alkali-silica reaction (ASR) is the reaction between silica aggregates and hydroxides in concrete. ASR is documented by the presence of alkali-silica gel in voids,

cracks, and aggregate reaction rims (British Cement Association 1993; West 1996). Damage of concrete is caused by excessive expansion and resultant cracking. Alkali-silica gel has the property of absorbing water and consequently expanding. Opal, chalcedony, cristobalite, tridymite, and strained quartz are typical reactive constituents of ASR.

Alkali-Silicate Reactions

The alkali-silicate reaction is a variant on alkali-silica reactions in which the typical reactive component in the aggregate phases is not free silica but silica from phyllosilicates (Rogers 1993; West 1996). This reaction is characterized by a slow or late-stage expansion (Rogers 1993; Tang 1992; Mu 1996). Schlorholtz and Amenson (1995) reported that certain shale particles used as fine aggregate for constructing Iowa highway concretes (US 20 and I 35) are subject to this type of reaction.

EXPANSION DUE TO BRUCITE GROWTH

Expansion Mechanisms

It is generally accepted that alkali-carbonate reactions such as dedolomitization of dolomite coarse aggregate causes major concrete deterioration by expansion, but the mechanism of expansion is not agreed upon. Although we previously concluded (Cody et al. 1994; Gan et al. 1996) that brucite growth resulting from dedolomitization of dolomite coarse aggregate produced expansion and cracking, our current research proves that the

relationships between brucite growth and concrete deterioration is more complex than previously believed.

Many studies concluded that brucite growth is at least partly responsible for expansion and concrete deterioration. Durand et al. (1992) experimentally observed that alkali-aggregate reactions generate expansion with stresses of 4.4 MPa. Tang et al. (1991) and Deng and Tang (1993) calculated the amount of expansion based on the solid volume changes associated with dedolomitization by using molar volume data of dolomite, calcite, brucite, portlandite which are 64.34, 36.93, 24.63 and 33.06 cm³/mol, respectively (Deng and Tang 1993). Their calculations showed that the dolomitization reactions (1) and (2) result in a net 7.5 % volume increase. However, Deng and Tang (1993) calculated that newly formed calcite/ brucite crystalline masses have a 25.95 % porosity under an assumption of tight-packing of equant spheres of brucite and calcite particles in restricted spaces. When porosity is included, a volume increase of 36.5 % results from the combined reactions (1) and (2). They concluded that this volume increase in the restricted spaces of reaction rims causes cracking because of internal stresses (Diab and Prin 1992; Durand et al. 1992; Deng and Tang 1993). Additional details on the causes of brucite expansion are presented in Cody et al. (1994) and Gan et al. (1996).

Brucite-Induced Expansion in Iowa Concretes

Our current SEM study reveals that significant amounts of brucite occur in the light-colored cement paste reaction rim and in dolomite aggregate reaction rims in

concretes constructed with reactive coarse aggregate, but that more secondary calcite than brucite forms in these regions. In Iowa highway concrete samples, however, macro- or micro-cracking is not closely associated spatially with aggregate reaction rims (i. e., cracks only rarely occur at or parallel to aggregate-paste interfaces where dedolomitization occurred).

Abundant relatively coarse, euhedral to irregular shaped, brucite crystals occur in reactive aggregate concrete in the less altered cement matrix outside of Zone D (Fig. 10). Our study, however, found no evidence for significant volume increases associated with brucite. These crystals result from either topochemical replacement of portlandite crystals (reaction 3) or from direct precipitation of brucite in microscopic interface voids. Our observations best support topochemical reactions with resultant volume decreases for microscopic brucite formation. If direct precipitation took place, we should expect a volume increase with expansion cracking associated with the formation of brucite crystals (Tang et al. 1991; Deng and Tang 1993). If topochemical replacement of portlandite with brucite occurred, there should be a 25 % volume decrease which should cause void space generation in areas of cement associated with brucite crystals and a lack of expansion cracking. As shown in the SEM micrograph (Fig. 10), open spaces are indeed associated with irregular-shaped brucite masses in the cement matrix, and no observable cracking is spatially associated with the brucite.

Our observations that cracking is not spatially related to brucite locations are not conclusive evidence against brucite-induced expansion because concretes containing abundant brucite also exhibit significant micro-cracking and occasionally larger cracks. If

brucite formation causes expansion and cracking in Iowa concretes, then we have demonstrated that cracking must result from generalized stresses built up within macroscopic concrete masses, and these stresses are relieved by cracking along weak directions and zones rather than in close proximity to brucite crystals.

EXPANSION DUE TO ETTRINGITE FORMATION

Expansion Mechanisms

The formation of ettringite is widely believed to cause expansion of cement and crack deterioration of concrete. Numerous studies have been conducted to identify the mechanism of ettringite formation and presumed expansion (Metha 1969, 1973; Metha and Hu 1978; Ogawa and Roy 1981, a, b, c; Metha and Wang 1982; Cohen 1983a, b; Cohen et al. 1985; Piasta and Hebda 1991; Bonen and Cohen 1992; Ping and Beaudoin 1992; Shayan and Quick 1992; Scrivener and Taylor 1993; Deng and Tang 1994; Glasser et al. 1995; Diamond 1996; Fu and Beaudoin 1996; Kelham 1996; Shayan and Ivanusec 1996). There is no doubt about the occurrence of delayed ettringite in severely deteriorated concrete, but the mechanism of expansion remains controversial (Mather 1984). Two principal hypotheses of ettringite-related expansion mechanisms have been proposed: (1) the crystal growth theory and (2) the swelling theory. These theories are discussed in detail by Cohen (1983b) and Diamond (1996). Cohen (1983a) suggested a model of expansion by crystal growth, that is, expansion is caused by the longitudinal growth of ettringite crystals formed on the surface of Al-bearing particles. According to this model, expansion is caused by crystalline pressures exerted against the surrounding

matrix when crystal sizes become greater than thickness of solution films from which they are crystallizing. Consequently large crystals will be more expansive than small ones. Ping and Beaudoin (1992) pointed out that two conditions are necessary to build crystallization pressure: (a) “confined crystal growth of the solid product” and (b) “activity product of reactants in the pore solution is greater than the solubility product of solid product under atmospheric pressure”. Diamond (1996) supports this hypothesis and presents a thermodynamic argument for ettringite crystal growth pressures.

Metha (1973), on the basis of his experiments, suggested an alternative hypothesis for expansion. According to the studies of Metha and his colleagues (Metha and Hu, 1978; Metha and Wang, 1982), expansion is caused by water adsorption on the negatively charged surfaces of ettringite. Expansion of ettringite by this mechanism appears to be closely related to the morphology, size, and rate of ettringite formation. The finely-crystalline ettringite of colloidal size causes significant expansion because its immense surface areas can adsorb large quantities of water on a weight basis. Large elongate ettringite crystals do not cause significant expansion because of their small specific surface areas cannot adsorb much water.

In contrast to the above two hypotheses which propose that ettringite itself is involved in expansion-related concrete damage, another hypothesis proposes that ettringite growth is only indirectly responsible for expansion and cracking (Diamond 1996). Ettringite growth typically involves loss of air-entrainment void space by crystal filling. According to Diamond (1996), the filling of air-entrainment voids by ettringite may cause loss of void effectiveness in preventing freeze damage to concrete during

freezing/ thawing. If freezing solutions are denied access to air-entrainment and other voids because of filling or sealing by ettringite, then ice expansion will cause cracking.

It has been proposed that ettringite crystals formed in open space cannot cause expansion, and only the growth of ettringite in confined space can cause severe expansion. However, many recent researchers (Shayan and Quick 1992; Scrivener and Taylor 1993; Deng and Tang 1994; Glasser et al. 1995; Diamond 1996; Fu and Beaudoin 1996) showed that open space ettringite growth can also cause expansion. Shayan and Ivanusec (1996) suggested that void-lining ettringite in open spaces may develop fine micro-cracks during dry intervals and crystallization pressure can develop during precipitation of additional ettringite when liquid fills micro-cracks under moist conditions.

Ettringite-Induced Expansion in Iowa Concretes

Abundant ettringite crystallized in the interstitial pore spaces, pre-existing cracks, and air-entrainment voids in Iowa highway concrete. This characteristic occurrence of ettringite in pre-existing open spaces without association with reacting particle locations indicates that direct precipitation (“through solution”) is the major reaction mechanism involved in its formation. Topochemical reactions may be partially responsible for extremely small ettringite crystals disseminated within the cement paste.

Our SEM analysis revealed that the cracks are spatially associated with both void-fill and void-rim type ettringite. These expansion cracks originate from ettringite within entrainment voids and extend into the cement paste. The fact that ettringite does not fill

these paste cracks indicates that the cracks are fairly recent and developed after ettringite formation. Although ettringite can easily be observed in large open spaces in the cement paste using SEM/ petrographic microscope, ettringite probably also fills microscopic interstitial pore spaces in the cement paste before it fills large open spaces. Direct evidence for this was not obtained, nevertheless, because tiny pore-space ettringite is difficult to identify with EDAX. Assuming that ettringite fills sub-microscopic interstitial pore spaces in the cement paste, the expansion mechanism of ettringite causing the deterioration of Iowa highway concretes can be suggested as follows: (i) expansion pressures develop because of volume increases during growth of ettringite which completely fills microscopic interstitial voids and small air-entrainment voids. These pressures result from either crystal growth or water absorption, (ii) void-fill and void-rim ettringite in larger interstitial pores and entrainment voids causes loss of void effectiveness in preventing freezing damage when the concrete is water saturated.

Table V-A. Summary of Observations of Brucite in Iowa Concretes.

No.	Highway & Quarry	Year Built	Aggregate Type	Aggregate Crystal. & Size	Aggregate React.	Reaction Rims	Brucite	Calcite Aggr. Rim	Paste Rim
A	I 35, Portland West	1975	Dolomite	WC, CG	Non-reactive	A+E <i>or</i> A+D+E	+	-	+
B	US. 30 Crawford-Lee	1981	Dolomite	PC, FG	Reactive	A+B+C+D+E <i>or</i> A+B+D+E	++	++	+++
			Limestone	WC~PC, CG~FG	Non-reactive	No reaction rims	+	-	-
C	IA 9, Dotzler	1974	Dolomite	PC, FG	Reactive	A+B+D+E <i>or</i> A+B+C+D+E	+++	+	++
D	IA 21, Crawford-Lee	1982	Dolomite	PC, FG	Reactive	A+B+C+D+E, A+B+C+D+E, <i>or</i> A+B+C+(D)+E	++	++	++
			Limestone	WC~PC, CG~FG	Non-reactive	No reaction rims	+	-	-
E	US 63, Nelson	1971	Dolomite	PC, FG	Reactive	A+B+C+D+E	+++	++	+++
F	US 20, Sundheim	1988	Dolomite	WC, CG	Non-reactive	A+E <i>or</i> A+D+E	+	-	+
G	IA 100 Crawford-Lee	1989	Limestone	WC, CG	Non-reactive	No reaction rims	+	-	+
Gan-1	US 63, Smith	1972	Dolomite	PC, FG	Reactive	A+B+D+E <i>or</i> A+B+C+D+E	+++	++	+++
Gan-2	US 151 Paralta	1947	Dolomite	PC, FG	Reactive	A+B+C+D+E <i>or</i> A+B+D+E	+++	++	+++
Gan-3	US 218 Garrison	1971	Limestone	PC, FG	Non-reactive	-	+	-	+
			+ Dolomite	PC, FG	Reactive	A+B+D+E	++	+	++
Gan-4	US 20, Sundheim	1988	Dolomite	WC, CG	Non-reactive	A+E <i>or</i> A+C+E	+	-	+

WC = Well-crystallized; PC = Poorly-crystallized; CG = Coarse-grained; FG = Fine-grained.

A, B, C, D, E refer reaction rims and refer to Appendix II for characteristics of each rim.

+: Rare, ++ Common, +++: Abundant.

Table V-B, Summary of Observations of Ettringite in Iowa Concretes.

No.	Highway & Quarry	Year Built	Aggregate Type	Pyrite in aggr. (Est, vol. %)	Oxidation	Ettringite	Cracks
A	I 35, Portland West	1975	Dolomite	2~3 %	L	++	++
B	US. 30 Crawford-Lee	1981	Dolomite & Limestone	< 3 %	M S	+++	++
C	IA 9, Dotzler	1974	Dolomite	2~3 %	M	+++	++
D	IA 21, Crawford-Lee	1982	Dolomite & Limestone	< 3 %	L S	++	++
E	US 63, Nelson	1971	Dolomite	< 2 %	M	+++	+++
F	US 20, Sundheim	1988	Dolomite	<< 1%	S	+	+
G	IA 100 Crawford-Lee	1989	Limestone	< 1%	S	+	++
Gan-1	US 63, Smith	1972	Dolomite	2~3 %	M	++	++
Gan-2	US 151 Paralta	1947	Dolomite	<< 1%	M	++	++
Gan-3	US 218 Garrison	1971	Limestone & Dolomite	3~4 %	S M	++	++
Gan-4	US 20, Sundheim	1988	Dolomite	<< 1%	S	+	+

L = Large percentage of pyrite is oxidized (> 50 %); M = Moderate (15~50 %);

S = Small (< 15 %).

+ = Small amount of air entrainment voids (~200µm) are filled with ettringite (< 15 %);

++ = Moderate amount filled (15% - 50%);

+++ = Abundant filling (> 50%).

PART II. EXPERIMENTAL DETERIORATION OF IOWA HIGHWAY CONCRETE

PURPOSE OF EXPERIMENTS

In a previous project, Iowa DOT HR-355, we studied the effect that NaCl, CaCl₂, and MgCl₂ had on the gross deterioration of concretes from Iowa highways and on Mg migration from dolomite coarse aggregate. In this project, we did a more detailed study on the effects of NaCl, CaCl₂, MgCl₂, Na₂SO₄, CMA, Ca-acetate, and Mg-acetate on the deterioration of concrete during less severe freeze/thaw (F/T) and wet/dry (W/D) conditions. Special attention was paid to the secondary minerals that were formed and the mineral changes that might occur as a direct result of deicer application or exposure to sulfate-bearing ground water. Because the acetates are less detrimental to the environment and to steel reinforcement in concrete, the effects of three acetates were examined to determine if one was less detrimental to concrete than the others. The possibility of using Iowa corn byproducts to produce acetate was a further incentive for the latter study.

EXPERIMENTAL METHODS

Small 3 cm x 1.5 cm x 1.5 cm blocks weighing between 7 g and 11 g were cut from the seven highway cores examined in the first section of this report. Two blocks from each core were immersed in 200 ml of solution and sealed in cleaned polymethylpentene containers that were stored for 132 hours at 58°C in a constant temperature chamber. The solutions used were 0.75 M CaCl₂·2H₂O, MgCl₂·6H₂O, NaCl, CMA based on a molar ratio of 3:7, i.e. 3[Ca(CH₃COO)₂·H₂O] : 7[Mg(CH₃COO)₂·4H₂O], Na₂SO₄, Ca(CH₃COO)₂·H₂O, Mg(CH₃COO)₂·4H₂O, and distilled water. All solutions contained 0.01% sodium azide to control bacterial growth. The chloride solutions in these experiments were identical to the less-concentrated solutions used in our previous

experiments. Chloride experiments were repeated to obtain freshly-treated concrete and thin-sections that had not been stored in dry conditions for several years. The chloride treatments were run simultaneously with the other salts in order to compare the relative aggressiveness of each.

Wet/Dry (W/D) Experiments

After being immersed in 58°C solutions for 132 hours, blocks were removed from the solutions, dried 58°C (\approx 135°F) for 24 hours, air cooled to 25°C, returned to their immersion solutions at 25°C, and again stored at 58°C for 132 hours.

Freeze/Thaw (F/T) Experiments

Samples removed from the 58°C solutions after 132 hours were air cooled to 25°C and stored for 24 hours in a freezer at -4°C (25°F). The blocks were air warmed to 25°C, returned to their respective solutions at 25°C, and stored at 58°C for 132 hours.

Cycling was continued until the blocks exhibited cracking or crumbling. Blocks with aggregate from the Sundheim quarry, Highway US 20 (Sample F) were removed for sectioning after 28 cycles. Concrete highways made with Sundheim coarse aggregate have service lives of 40 years and are considered to be durable concretes without aggregate-related problems (Gan et al. 1996). It seemed reasonable that in this concrete, the effects of deicing salts could be isolated from other variables.

After 42 cycles, remaining blocks from samples A (Portland West, Highway I 35), B (Crawford-Lee, Highway US 30), and E (Nelson, Highway IA 64) were removed for thin-sectioning and examination with light and scanning electron microscopes. All remaining experiments were discontinued after 50 cycles.

RESULTS

RELATIVE AGGRESSIVENESS OF SALT SOLUTIONS

The relative aggressiveness of 0.75 M solutions of the different salts toward concrete is compared in Figure T2, Wet/Dry and Freeze/Thaw Cycling Experiments, and Figure T3. White-filled bars in Figure T2 denote experiments that were terminated because of visually-detected deterioration. Dark-filled bars show experiments that were terminated for sectioning, even though they might have showed no visual deterioration. The two vertical lines labeled 'Th. Sect.' indicate that experiments were stopped at that time (dark bars) and thin sections were made from the samples.

In experimentally treated concretes, identical terminology used in the first section of this report for alteration zones of dolomite coarse aggregate and cement paste will be used with the subscript 'e' indicating that these are the zones observed after experiments. Thus, Ae = dolomite aggregate interior after experiments; Be = dark dolomite rim after experiments; Ce = light-colored dolomite rim after experiments; De = light-colored cement rim after experiments; Ee = Cement paste interior after experiments.

Calcium Magnesium Acetate

As shown in Figures T3a and T3b, it is apparent that CMA caused the most aggressive degradation of concrete in both W/D and F/T experiments. All CMA-treated samples showed deterioration by 15 cycles. Wet/dry cycle degradation was the worst, producing brown color, crumbling, failure of the paste-coarse aggregate boundary, and the general appearance of paste dissolution.

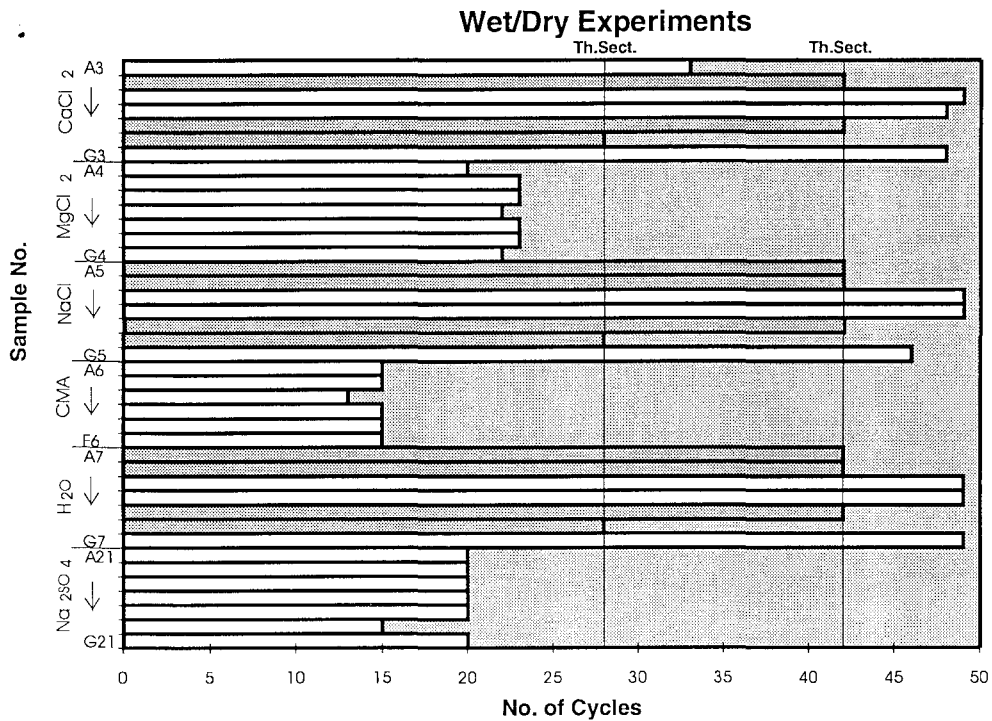
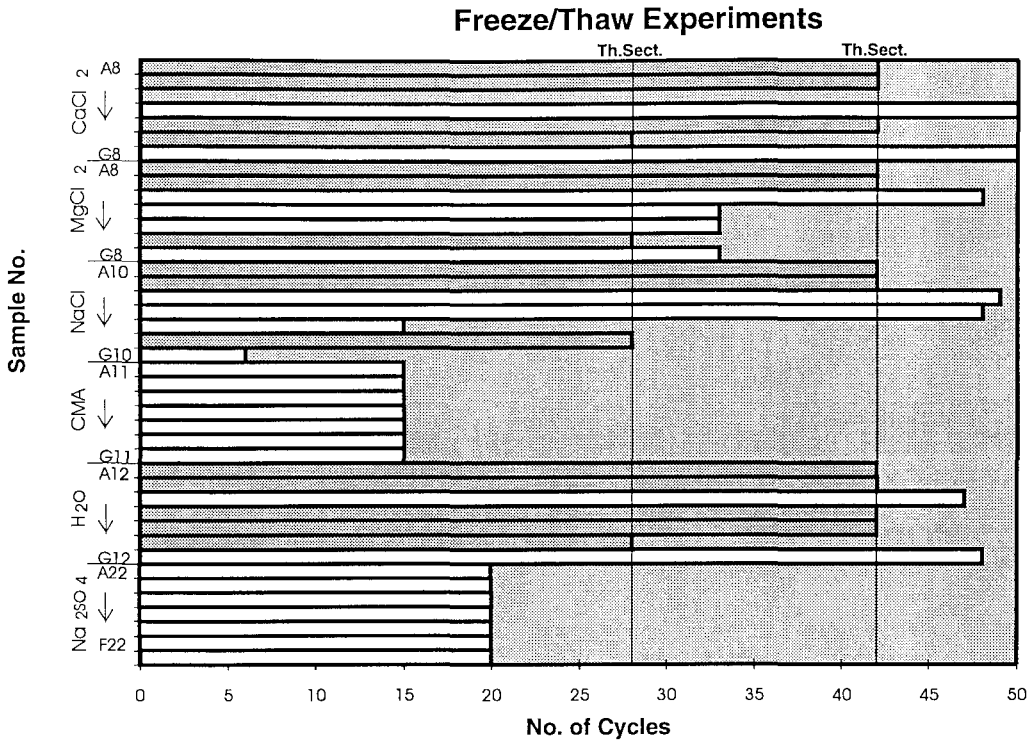


Fig. T2. Wet/dry and freeze/thaw cycling experiments. The dark bars represent experiments that were terminated early in order to make thin sections or for other reasons. Light bars represent experiments that were terminated because of significant sample deterioration. Th. Sec. = thin sections.

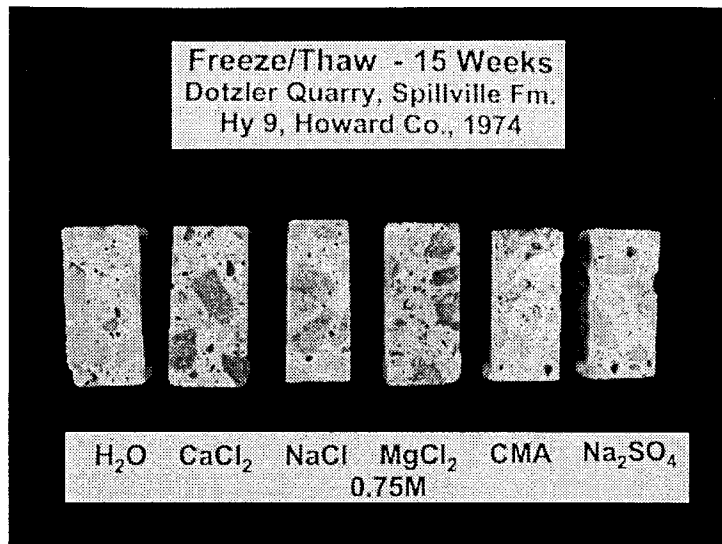


Fig. T3a. Experimental deterioration of concrete using freeze-thaw conditions for 15 cycles. Note that using the relatively dilute solutions with freeze/thaw cycling produces almost no visible damage to the concrete samples.

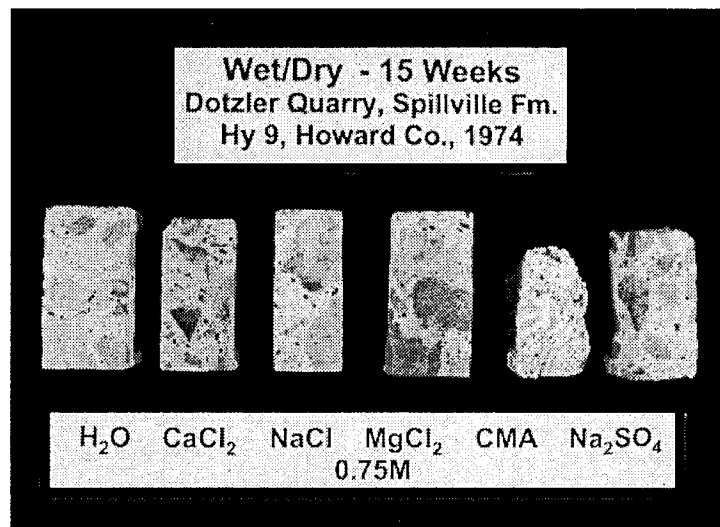


Fig. T3b. Experimental deterioration of concrete using wet/dry cycling for 15 cycles. Damage is especially noticeable with sodium sulfate and calcium magnesium acetate (CMA).

Sodium Sulfate

This salt was next in severity, with all W/D and F/T experiments discontinued after 20 cycles. Large random cracks in the paste and degradation of the paste-coarse aggregate boundary were evident.

Magnesium Chloride

Wet/dry experiments were ended after 23 cycles, but freeze/thaw experiments lasted 33 cycles for half the blocks, the full 50 cycles in one block, and 42 cycles in two sampled blocks. The longevity of these blocks is attributed to the formation of a thick 'protective coat' on the concrete surfaces, which will be discussed later. Beneath the white protective coat was brown-colored, crumbled paste with random fractures.

Calcium Chloride

In W/D experiments, treated blocks endured an average of 45 cycles (range 33-49). Blocks lasted 50 cycles in F/T experiments where a shiny, blue-gray 'protective coat' on the concrete surfaces was formed. The cement paste was darker after both treatments.

Sodium Chloride and Water

Sodium chloride and distilled water were least destructive, giving similar durability in W/D experiments, but NaCl was more deleterious in F/T experiments. NaCl-treated blocks showed surface roughening (dissolution), edge crumbling, and a thin gray-white surface coat. NaCl crust on the surface of some blocks was thicker over fine aggregate quartz grains which were micro-cracked, indicating that the micro-cracks served as channels for fluid movement. Water-treated (F/T) blocks developed mild edge crumbling that left fine aggregate pieces in relief.

EFFECTS ON CONCRETE SAMPLES

Secondary Mineral Formation

In several samples, it was immediately obvious that white grains in the fine aggregate used in roads with Crawford-Lee quarry coarse aggregate expanded excessively when exposed to NaCl, CaCl₂, and MgCl₂ deicers (Fig T3). The mineral was identified by x-ray diffraction analysis with Ni-filtered CuK α radiation and found to be composed of α -quartz, thus indicating chert. X-ray diffraction analysis of the secondary expansive white mineral accumulations formed by solution reactions showed that α -quartz and calcite were the major minerals.

Crystals that precipitated in the saline immersion liquids and on the walls of containers were also analyzed by x-ray diffraction. Visually-detected surface coats of secondary minerals from blocks treated with CaCl₂, NaCl, and MgCl₂ were removed with care taken not to include underlying concrete. X-ray diffraction analyses detected the minerals shown in Table VI.

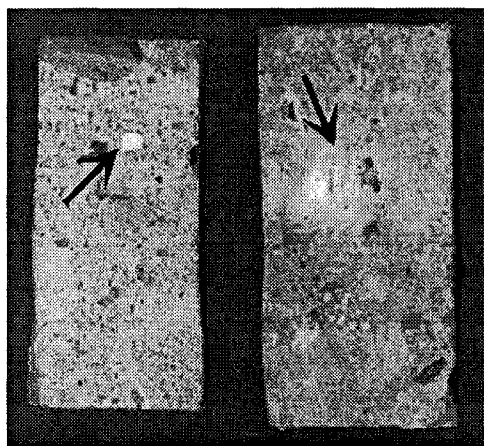


Fig. T4. Expansive white chert with secondary mineral formation. The photograph on the left shows pre-experiment white chert, and that on the right shows a similar chert particle after reaction during wet/dry cycling with NaCl.

The presence of calcite in solution was attributed to atmospheric carbonation of calcium leached from the concrete or added as a reagent. Formation of brucite, $Mg(OH)_2$, in magnesium-rich solutions indicated that the leached component was a hydroxide from the cement paste.

The formation of a protective mineral coat on a concrete test specimen is not unusual. Locher (1969) found that sodium bicarbonate formed a calcite coat that decreased the severity of damage from magnesium sulfate attack. Neville (1969) also observed that weak solutions of magnesium sulfate produced a white coating of magnesite ($MgCO_3$) and/or calcite that reduced the permeability of concrete test samples and decreased the rate of further reaction. He also found that if the protective coat was ruptured, corrosion would continue as before, and he believed that in real structures where stress and varied conditions exist, the protection offered by such coatings would be decreased.

Table VI. Secondary Minerals in Solutions and on Concrete Surfaces.

Solutions	Crystals in Solution	Crystals on Concrete Surfaces
Water	calcite	no coating
$CaCl_2$	calcite + minor brucite	aragonite + brucite + gypsum (tr.)
$NaCl$	calcite	calcite + halite
$MgCl_2$	brucite + minor calcite	brucite + $Mg_2(OH)_3Cl \cdot 3H_2O$ + calcite
CMA	brucite + minor calcite	no coating (sample dissolution)
Na_2SO_4	calcite	no coating (sample dissolution)

Effects of Water

In our previous experiments (Cody et al. 1994) samples were cycled in water 16 times in W/D and F/T conditions. From visual observation of concrete specimens, no exterior changes were noticed and no coarse aggregate or paste changes were detected. In the present work, samples were cycled 49 times under the same conditions. The edges of the blocks in W/D experiments were roughened. Calcite formed in the storage solutions indicating that Ca(OH)_2 was leached from the cement paste. Blocks from F/T experiments exhibited fine cracks on the bottom surfaces that they rested upon during freezing. In untreated samples, SEM and EDAX showed that ettringite had formed in the voids during previous road conditions. It probably caused greater destruction in F/T experiments than in W/D by impeding ice expansion. There was no evidence of secondary minerals or chemical reactions caused by experimental conditions, although SEM and petrographic analyses did reveal that pre-treatment reaction rims appeared slightly broadened in some samples (Fig. 18).

Effects of Calcium Chloride Solutions

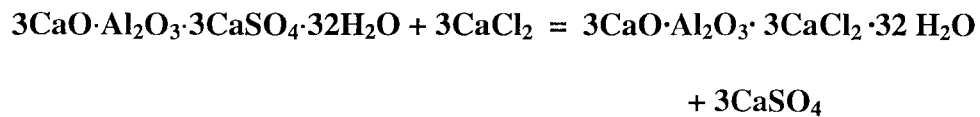
In nondurable concrete, reaction rims observed after wet/dry and freeze/thaw conditions (Plate IV-A) appear similar to the original reaction rim patterns seen in untreated concrete, but significant difference occurs in the light-colored dolomite aggregate rim Zone Ce. The EDAX element maps (Figs. 19, 20) show a decrease in Ca and a significant concentration of Mg in rim Zone Ce. In pre-experiment rims considerable volumes of calcite existed without significant quantities of brucite, but in the post-experiment rims abundant brucite and less calcite were observed. The observed

decrease in calcite is supported by microprobe analyses (Cody et al. 1994). The dark dolomite rim, Zone Be, and the light-colored cement rim, Zone De, remained essentially the same as they were in untreated samples. In durable concrete with non-reactive dolomite aggregate, no new reaction rims occurred after wet/dry and freeze/thaw cycles in calcium chloride (Fig. 21).

Critical changes occurred in the cement paste of both durable and non-durable concrete. In light microscope views, the cement paste (Zone Ee) is observed to be significantly discolored (Plate IV-A). EDAX element maps (Figs. 19, 21) show that a significant concentration of Cl occurs at the corresponding area. This may be due to the formation of calcium chloride hydrate phases ($3\text{CaO}\cdot\text{CaCl}_2\cdot 12\text{H}_2\text{O}$; $\text{CaO}\cdot\text{CaCl}_2\cdot 2\text{H}_2\text{O}$), to adsorption of Cl ion by the CSH (calcium silicate hydrate) phase, or to the release of iron from calcium alumino ferrite hydrate. Kosmatka and Panarese (1988) attribute most color effects in concrete to this component. Exact mechanisms of this discoloration, however, are still unclear.

It is well known that chloroaluminate (Freidel's salt = monochloroaluminate, $\text{CaO}\cdot\text{Al}_2\text{O}_3\cdot \text{CaCl}_2\cdot 10\text{H}_2\text{O}$ + trichloroaluminate $3\text{CaO}\cdot\text{Al}_2\text{O}_3\cdot 3\text{CaCl}_2\cdot 32\text{H}_2\text{O}$) forms from reaction between the chloride solution and C_3A (Ramchandran et al. 1976; Chatterji 1978; Berntsson and Chandra 1982; Ftikos and Parissakis 1985; Worthington et al. 1988; Day 1992; Bonen and Sarkar 1994; Kurdowski et al. 1994). The EDAX element maps show that chloroaluminate formed in the air entrainment voids after wet/dry and freeze/thaw cycles in CaCl_2 (Fig. 20). Ettringite was observed in the air entrainment voids of untreated concrete from the same highway concrete sample, but it is rarely found in the CaCl_2 -treated samples, and only in small amounts associated with chloroaluminate.

According to Day (1992), chloroaluminate is more stable than ettringite in the presence of chloride solution, especially, at elevated temperature. The absence of ettringite and the formation of chloroaluminate in CaCl₂-treated concrete suggests that the chloroaluminate was formed by the transformation of pre-existing Ca sulfoaluminate (ettringite) to calcium chloroaluminate. This transformation produces a substitution of Cl⁻ ions for SO₄²⁻ ions in the ettringite chemical formula:



The chloroaluminate formed in CaCl₂-treated concrete is possibly the tri-chloroaluminate which has the same structure as ettringite (Day 1992). The trace of gypsum detected in the surface coat of the sample block may be the result of sulfate released during ettringite conversion. Brucite in cement paste appears to be stable in CaCl₂ treated concrete. No other newly formed minerals were observed in either cement paste or air entrainment voids.

Effects of Magnesium Chloride Solutions

The exterior of concrete blocks treated with 0.75 M MgCl₂ solutions exhibited a 'protective coat' that x-ray diffraction analysis showed to consist of three substances - brucite, Mg₂(OH)₃Cl · 3H₂O, and calcite. Brucite was also found in solutions. The x-ray diffraction analyses showed no evidence of the magnesite (MgCO₃) coating that Neville (1969) found in his magnesium chloride-treated samples.

In MgCl₂-treated samples, distinctive reaction rims were formed at the margins of reactive dolomite aggregate (Plate IV-B). A significant amount of brucite formed in the

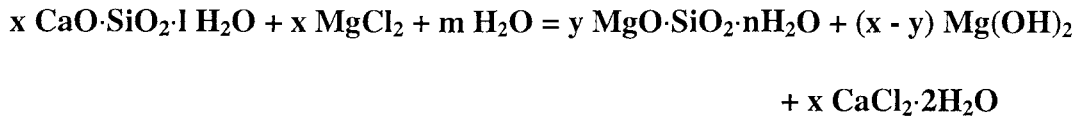
outer light-colored dolomite rim, a feature not seen in the rims of untreated dolomite (Fig. 22, cf Fig. 2). This change occurred in both wet/dry and freeze/thaw conditions, and is very similar to the development of brucite observed in the CaCl_2 -treated concrete (cf. Fig. 19). In samples with reactive dolomite aggregate that did not previously contain a light-colored dolomite rim, the reaction rims remained identical to those in untreated concrete (Fig. 23). New brucite precipitation was superimposed on the original light-colored rims as a result of MgCl_2 treatment. In concrete containing non-reactive dolomite aggregate, there was no evidence of new or enhanced reaction rims on dolomite aggregate.

Brucite was also formed in air entrainment voids and in the interface between the fine aggregate and cement paste (Figs. 22, 23) where it destroyed the integrity of the paste - fine aggregate interface and caused 'popping out' of quartz grains when thin sections were made. Calcite formed in association with brucite at the inner and outer margins of void-rim brucite in the air entrainment voids (Figs. 22, 23).

Critical deterioration of the cement paste of MgCl_2 -treated concrete was due to the formation of non-cementitious magnesium silicate hydrate, MSH. When MSH formed in the cement paste, many cracks resulted (Figs. 24, 25). Point analyses of MSH showed wide compositional variation from place to place depending upon the degree of alteration. In areas where the cement paste was subject to a high degree of alteration, the calcium silicate hydrate, CSH, almost completely changed to MSH as indicated by EDAX point analyses (Fig. 26). Only negligible amounts of Ca were detected. In general, paste in contact with brucite was significantly altered to MSH.

Formation of MSH resulted from reaction between magnesium ions and the CSH phase of the cement, with replacement of CSH by MSH. Using a modification of

Bonen's (1992) equation, the general reaction for the formation of MSH from CSH in Mg-chloride solution can be written as follows:



$$\text{where } l + m = n + 3x - y$$

This reaction is known to involve shrinkage because the magnesium is smaller than the calcium ion, and the volume of the product (MSH) is less than the volume of CSH. Abundant shrinkage cracks, therefore, developed in the MSH phase (Figs. 24, 25). From this reaction, displaced Ca^{2+} leaches out into cement paste because CaCl_2 is highly soluble and can form portlandite (Ca(OH)_2), or calcite/aragonite (CaCO_3). Calcite associated with brucite in air voids or in cracks in some samples supports this concept. Needles of calcium carbonate and brucite precipitated on the surface of a MgCl_2 -treated sample (Fig. 27).

The light-colored cement rim, Zone De, does not show secondary calcification or other mineralization (Figs. 22, 23). The deleterious effects of MgCl_2 occur in both durable and non-durable concretes treated in wet/dry and freeze/thaw conditions.

EDAX element maps and point analyses show that air voids in cement that is highly altered to MSH are filled with new material rich in Mg, Al, Cl, and (Si), but air voids in slightly altered paste are filled with another type of material, which is rich in Ca, Mg, Al, S, with minor amounts of Si and Cl (Figs 24, 25, 28). This observations suggests that ettringite was altered to a chloroaluminate phase. It is not clear whether the Mg associated with ettringite indicates that it altered to a new magnesium-rich mineral, or

that brucite grew on the surface of ettringite (or chloroaluminite) or in cracks associated with them.

Effects of Sodium Chloride Solutions

After NaCl treatment in wet/dry and freeze/thaw experiments, no “new” rims or rim changes are visible in either dolomite aggregate or cement paste non-durable concrete (Fig. 29). No reaction rims were observed in durable concrete.

Void-filling ettringite was altered to the chloroaluminate phase, Friedel's salt, in the most severe case, but, in most cases, chloroaluminate formed interior to ettringite that was in contact with the cement paste of the void margin. Sodium chloride solutions are known to leach portlandite from concrete and to make the mortar porous and more susceptible to further damage (Heffman 1984). Soluble portlandite can react with atmospheric CO₂ to form the calcite that we observed in solution, or it can react with NaCl according to the equation: $2\text{NaCl} + \text{Ca}(\text{OH})_2 = 2\text{NaOH} + \text{CaCl}_2$. The CaCl₂ produced in the reaction can then react with calcium aluminates to form the chloroaluminate Friedel's salt.

Heller and Ben Yair (1966) found chloroaluminate on the surface of relatively new mortar samples treated with CaCl₂ solutions. We found no evidence of Friedel's salt on the concrete surfaces, but we did observe it associated with ettringite in the interior of our NaCl-treated, aged concrete samples removed from Iowa highways (Fig. 30). Chlorides are thought to solubilize the sulfaluminate, ettringite, and to be deposited as calcium chloroaluminate (Neville 1969) or to cause a replacement reaction in which the

sulfate of ettringite is replaced by chloride with the formation of structurally similar trichloroaluminate (Day 1992) (Figs. 30, 31).

Brucite in the cement paste appears to be stable in NaCl-treated concrete. No other newly-formed minerals were observed in cement paste or in the air entrainment voids.

Effects of Sodium Sulfate (Na_2SO_4) Solutions

Sodium sulfate was the second most aggressive solution tested. Experiments were terminated after 20 cycles because large cracks formed in both W/D and F/T samples. Those in W/D treatment were larger and more numerous.

Abundant ettringite formed in the air entrainment voids of non-durable concrete that had only small amounts of ettringite before sulfate treatment (Figs. 32, 33). More abundant ettringite appeared to form in wet/dry conditions than in freeze/thaw. The physical appearance and the in-void occurrence of ettringite were identical to that formed in untreated concrete during highway use. Void-rim or void-fill types of ettringite occurred in many air-entrainment voids, but not in the air voids of the light-colored cement paste rim (Zone De) where calcite had precipitated. No significant amount of gypsum was found in the air voids after sulfate treatment. Ettringite was observed in small interstitial pores in the cement phase in some areas, and in the boundaries between fine aggregate and cement paste (Fig. 34). High magnification EDAX element maps show that much of the ettringite that had formed in Na_2SO_4 - treated samples contains

appreciable Si, indicating that some Si probably substitutes for Al in the ettringite to form thaumasite* .

Petrographic microscope examination revealed that the cement paste was discolored by sodium sulfate treatment. This discoloration may result from decalcification of CSH and precipitation of calcite. Reaction rims of nondurable concrete aggregate survived sodium sulfate treatment without change. The severe cracking of sodium sulfate-treated concretes under both W/D and F/T conditions was mainly caused by ettringite growth-induced expansion pressures.

Effects of Calcium Magnesium Acetate (CMA) solutions

In the initial experiments performed for this research, CMA-treated samples were fairly decomposed after 15 cycles. The severity of paste breakdown made thin sectioning difficult. CMA experiments were therefore rerun for only 12 cycles, and samples were compared with those treated in 12 cycles with magnesium acetate and calcium acetate.

* Ettringite has a composition $\{Ca_6[Al(OH)_6]_2 \cdot 24H_2O\}(SO_4)_3 \cdot 2H_2O$ which is based on two columns of $[Ca_3[Al(OH)_6] \cdot 12H_2O]^{3+}$. The SO_4^{2-} ions and remaining water molecules are linked between these positively charged columns (Day 1992, Taylor 1990). A wide variety of ions can replace Al^{3+} and or SO_4^{2-} . EDAX point analyses revealed that ettringite in both untreated and treated Iowa highway concretes contains Si partially substituting for Al (Fig. 11, 35), but the relative content of silicon varies in samples. This indicates that the replacement of Al by Si occurred in Iowa highway concrete.

Because a considerable amount of CO_3^{2-} is released during dedolomitization, thaumasite ($\{[Ca_6(Si)OH)_6]_2 \cdot 24H_2O\}(SO_4)_3 \cdot [(CO_3)_2]$), which has a homologous structure to ettringite can form if Si replaces Al in the column structure and CO_3 replaces water molecules. EDAX point analyses revealed that highly variable numbers of silicon atoms replace Al in the mineral structures of Iowa highway concrete. Day (1992) concluded that thaumasite forms a solid solution series with ettringite, a conclusion supported by our analyses.

The CMA-treated blocks exhibited cracks and crumbling edges. Dark brown rims in the paste surrounded the coarse aggregate in both W/D and F/T experiments. Magnesium acetate and calcium acetate solutions did not have these deleterious effects.

Reaction rims formed at interface between reactive dolomite aggregate and cement paste in CMA-treated concrete were almost identical to those found in $MgCl_2$ -treated concrete where interstitial brucite was formed. Distinctive reaction rims also occurred in reactive dolomite aggregate margins (Plate V-A). The concentration of Mg in the light-colored outer dolomite rim (Zone Ce) increased due to experimentally-induced brucite growth like that observed in the light-colored dolomite rims of $MgCl_2$ -treated concrete (Fig. 36; cf. Fig. 22). Light-colored paste rims, Zone De, were considerably broadened by CMA treatment.

Both durable and nondurable concrete showed severe paste deterioration regardless of wet/dry or freeze/thaw conditions. The main cause of cement paste deterioration by CMA solution appears to be due to the formation of brucite and non-cementitious MSH. Brucite readily formed in air voids and at paste-fine aggregate interfaces (Plate V-B Figs. 37, 38). The CSH phase in the cement paste was converted to MSH by contact with the CMA solution (Figs. 37, 38, 39). Abundant shrinkage cracks developed in MSH. Calcium ions displaced by the MSH-forming reaction formed thin layers of calcite in open spaces such as air voids, or in boundary areas between the aggregate and cement paste, where brucite also precipitated (Figs. 37, 38).

Another aggressive feature of CMA treatment was debonding of fine aggregate. As shown in Plate VI-A and Figure 39, CMA solution penetrates the cement paste; especially through the weak boundaries between the fine aggregate quartz and the cement

paste where it reacts with the CHS phase of cement paste interface and forms a thin layer of non-cementitious MHS. The formation of a MHS layer results in debonding of fine aggregate from the paste, and causes the release of fine aggregate particles. Secondary brucite was then precipitated in the large voids created by loss of fine aggregate. As result of this process, a series of newly-formed minerals are frequently observed in those open spaces. A typical sequence from the outer margins of open spaces inward is magnesium silicate hydrate - silica gel - calcite - brucite - calcite (Figs. 37, 38, 39). Silica gel was only rarely observed in the sequence, possibly because it was removed in sample preparation.

CMA solutions also moved along micro-cracks inside fine aggregate quartz grains (Plate VI-A), and in rare instances, silica gel formed at the margins of those solution paths (Fig. 39). Coarse dolomite aggregate is generally not subject to debonding. The CSH in the paste reaction rim (Zone De) does not appear to change to MSH (Fig. 36), possibly because calcite had precipitated there during pre-treatment dedolomitization. Calcite mineralization lowered the permeability of the paste reaction rim and impeded solution penetration.

Several processes are involved in paste deterioration by CMA: (1) shrinkage cracking of cement paste by MSH formation, (2) debonding of fine aggregate from the cement paste by non-cementitious MSH at the paste - aggregate interfaces, (3) clogging of voids by newly-formed minerals such as brucite, calcite, and magnesium silicate hydrate, and (4) dissolution of cracked quartz grains.

As in the MgCl_2 -treated concrete, significant amounts of new brucite formed in air entrainment voids where only ettringite was previously seen, and the ettringite in the voids was dissolved (Figs. 40, 41).

To determine the roles that the cations Mg^{2+} and Ca^{2+} have in deterioration of concrete by CMA solutions, we conducted additional experiments with magnesium acetate and calcium acetate. Concrete with non-reactive Sundheim quarry dolomite aggregate was used in order to eliminate aggregate-related parameters.

Effects of Magnesium Acetate Solutions

Brucite, with thin calcite layers, formed in the air entrainment voids in the durable concrete under both wet/dry and freeze/thaw condition (Fig. 42, 43). Non-cementitious MSH formed in the cement paste as a replacement of the CSH phase. The paste deterioration by Mg-acetate solution was very similar to that occurring with CMA in which the formation of MSH and brucite at the interface between fine aggregate and paste cause debonding of the two components. The magnesium acetate-treated blocks were also brown in color, had large cracks, and crumbling edges and corners. Fine aggregate grains stood in relief above the decomposed cement on sample surfaces as a result of cement loss.

Effects of Calcium Acetate Solutions

Concrete sample blocks treated with calcium acetate did not darken and turn brown. Their corners showed mild crumbling, and there was an occasional crack. The paste rims around coarse aggregate particles appeared darker in color than before

treatment. No new minerals formed in the air entrainment voids, and the fine aggregates were present in their pre-treatment condition. No significant change was observed in the cement paste, except that calcium increased in the paste adjacent to coarse dolomite aggregate from freeze/thaw experiments (Fig. 44). Calcium increase was probably due to calcite precipitation. Ca-acetate produced much less paste deterioration than CMA and Mg-acetate.

PART III

SUMMARY AND RECOMMENDATIONS

SUMMARY OF PART I. EXPANSIVE MINERAL

FEATURES OF IOWA CONCRETES

Eleven samples taken from Iowa concrete highways were studied, and results are summarized in Tables V-A and V-B. Concrete containing aggregate from Crawford-Lee, Nelson, Paralta, and Smith quarries were characterized by reactive coarse aggregate that underwent dedolomitization producing relatively large quantities of secondary ettringite, brucite and MSH, and calcite mineralization, in addition to abundant cracks. The service lives of these concretes are generally less than 15 years, and there is good correlation between service record and secondary mineralization. In contrast, concretes containing coarse aggregate from the Sundheim quarry have non-reactive coarse aggregate, small quantities of secondary mineralization, and little cracking or other signs of deterioration. Concrete with coarse aggregate from Dotzler and Portland West are intermediate in characteristics. Highway I 35 with non-reactive Portland West aggregate contains reactive pyrite that forms large quantities of ettringite and some cracking. IA 9 with Dotzler quarry aggregate exhibits reactive aggregate, abundant brucite and ettringite, and cracking. Both these highways were constructed about 25 years ago, and both are showing signs of deterioration. The following secondary minerals were identified in the concretes studied:

1. Calcite was the most abundant secondary mineral in cements of poorly performing concretes. It occurred chiefly in the light-colored cement paste regions surrounding reactive dolomite coarse aggregate. Much of the calcite was formed as a result of dedolomitization of reactive dolomite coarse aggregate which releases magnesium and carbonate ions. The carbonate reacts with portlandite, $\text{Ca}(\text{OH})_2$, of the paste to form calcite. Additional calcite was formed by reaction of atmospheric CO_2 with portlandite.

We found no evidence that secondary calcite was expansionary. Cracks were not more abundant in highly calcified paste regions of Zone D, compared to non-calcified paste. Calcification may be beneficial in that it could reduce rates of migration of detrimental solutions from reactive coarse aggregate into the cement paste.

2. Delayed, or secondary, ettringite was next in volume abundance, with most occurring in poorly-performing concretes. It completely filled smaller air-entrainment voids and partially filled larger voids. Some ettringite was present as microscopic crystals in the cement paste. It also filled narrow cracks along margins of fine aggregate particles aiding in their debonding. Ettringite is often concentrated near reactive carbonate coarse aggregate containing oxidized pyrite, suggesting that pyrite supplied the sulfur necessary for ettringite formation. Another source of sulfur for ettringite may have been introduced by applications of sulfate-bearing rock salt deicer.

Void-fill ettringite formed by direct precipitation from solution. Microscopic ettringite deposits in the paste most likely were formed by replacement of calcium aluminate. Expansion cracks radiating from ettringite-filled air-entrainment voids are common, and may have been produced by crystal growth pressures generated by the

ettringite, by swelling associated with water adsorption by ettringite, and/or by reduction of freeze resistance because of clogging of air-entrainment voids by the ettringite.

3. Brucite is common but less abundant than secondary calcite or ettringite. Small quantities are widely disseminated in the cement paste of poorly-performing concretes. Most brucite is microscopic in size although a few crystal masses are larger. It is also associated with Mg-rich pore solutions that replace CSH with non-cementitious MSH. We believe that most of the brucite in cement paste was formed by crystal surface mediated (topochemical) reactions between magnesium pore solutions and portlandite $\text{Ca}(\text{OH})_2$. Microscopic crystals in the outer rim zones of reactive dolomite aggregate were produced by direct precipitation from pore solutions.

No expansion cracks are spatially associated with brucite deposits, but this is not conclusive evidence against brucite-induced expansion. Brucite is widely disseminated, so that expansion at innumerable micro-locations will cause general concrete expansion which would be relieved by cracking at weaker locations in the concretes.

4. As a broad generalization, we conclude from our research that reactive dolomite aggregate, especially that containing pyrite, is highly deleterious to concrete durability. Dedolomitization of reactive aggregate leads to a variety of problems including formation of secondary minerals such as calcite and brucite, and possible formation of magnesium silicate hydrate as a result of Mg release to pore solutions. Coarse and fine aggregate with pyrite inclusions are harmful because pyrite oxidation produces sulfate which reacts with C_3A to produce ettringite. The most easily oxidized pyrite masses are those exposed to oxidizing solutions by being located adjacent to

abundant micropores and intercrystalline channels that most commonly occur in reactive types of coarse aggregate.

SUMMARY OF PART II. EXPERIMENTAL DETERIORATION OF IOWA HIGHWAY CONCRETES

In the experiments, concrete samples were exposed to freeze/thaw and wet/dry cycling in solutions containing different chloride and acetate salts. These salts are currently used as deicers or have been proposed as alternatives to those currently used. Sodium sulfate was also tested to characterize decomposition caused by sulfate groundwaters. We observed that:

1. **Acetates.** Calcium magnesium acetate solutions were the most damaging of all solutions tested. Wet/dry and freeze/thaw cycling in CMA produced widespread and severe damage with cracking from replacement of calcium silicate hydrate with non-cementitious magnesium silicate hydrate. Brucite formation was extremely copious, and it was disseminated throughout the cement paste and in voids. It also occurred at the paste-fine aggregate interface where it furthered debonding of fine aggregate. Magnesium acetate produced similar but slightly less damage, and calcium acetate solutions produced much less alteration. CMA appeared to dissolve the cement paste and to alter quartz fine aggregate but it is still not clear why CMA is more deleterious than magnesium chloride or magnesium acetate.

2. **Sulfates.** Sodium sulfate solutions were next to CMA and Mg-acetate in aggressiveness. Both wet/dry and freeze/thaw cycling in these solutions produced severe expansion cracking, with wet/dry conditions being worse. Sulfate solutions applied to

Sundheim concrete that previously did not contain ettringite produced abundant ettringite disseminated throughout the paste and in voids, and cracking resulted. Our suggested mechanism of deterioration by ettringite expansion is clearly evidenced by these experiments.

3. **Chlorides.** Magnesium chloride produced significant concrete crumbling because of widespread replacement of CSH by non-cementitious MSH. Our research results show that calcium chloride deicing salts caused characteristic deterioration in concretes with reactive dolomite aggregates by enhancing dedolomitization reactions that release magnesium to form destructive brucite and MSH. Sodium chloride solutions did not cause significant change in reaction rims. All the chloride containing solutions cause the formation of chloroaluminate. Its morphology and occurrence in air-entrainment voids suggest that the chloroaluminate formed in concrete treated with chloride solutions is tri-chloroaluminate resulting from the transformation of pre-existing ettringite.

4. **Magnesium.** In our experiments, the magnesium component of deicer salts proved to be the most deleterious. Magnesium promoted replacement of CSH by non-cementitious MSH with resultant paste shrinkage and cracking. The growth of abundant, potentially-expansive brucite especially in the paste-fine aggregate interface furthered debonding of the fine aggregate.

5. White chert in fine aggregate that was unreactive in concrete became a highly expansive silica hydrate when exposed to the road deicers NaCl, CaCl₂, and MgCl₂.

RECOMMENDATIONS

Based on our research, several recommendations can be made.

1. **Dolomite coarse aggregate should be carefully evaluated for reactivity to cement**

paste, especially for its potential for dedolomitization. Our observations of poorly performing Iowa highway concrete document strong evidence that dedolomitization of reactive dolomite coarse aggregate contributes to brucite formation, which is closely associated with concrete cracking and premature deterioration.

Our experiments with magnesium chlorides and acetates document that magnesium from any source will cause deterioration of the strength-producing aluminosilicate structure of concrete paste, so that we are convinced that similar effects will occur with magnesium derived from dedolomitization.

Coarse aggregate reactivity can be rapidly evaluated by standard petrographic microscope study, supplemented with minor SEM and EDAX observation. Iowa dolomite rocks that are most susceptible to dedolomitization are those composed of fine-grained, poorly crystallized, dolomite crystals with abundant pore space between loosely intergrown crystals. This type of material can be easily detected with standard petrographic microscope observation.

2. **Reactive dolomite aggregate could be used in combination with non-reactive**

aggregate. Our experimental work shows secondary mineral formation and concrete destruction to be proportional to the quantity of reactive aggregate.

Diluting the amount of magnesium-producing coarse aggregate should lessen its

destructiveness. Consequently, poorly-performing reactive dolomite aggregate from local quarries might be used if blended with high-performance limestone or dolomite rock.

3. **The pyrite content of coarse aggregate should be minimized, particularly if the aggregate rock is poorly crystallized and contains abundant pore spaces and channel ways where oxidizing solutions can make contact with the sulfide inclusions.** Easily-oxidized pyrite adjacent to rock pores and channels provides sulfur that is necessary for delayed ettringite formation. Fine aggregate should also be monitored for pyrite, and for silicates that become highly expansive in deicer solutions.
4. **Sulfur contamination from rock salt deicers should be minimized.** Rock salt is the least deleterious road deicer and should produce the least amount of damage over long term use, but sulfur, an essential substance for ettringite formation, may be added to concrete as a result of applying sulfate-contaminated rock salt. We conclude that low-Mg rock salt should be required for highway use wherever economically feasible.
5. **Close attention should be given to concrete which has been subjected to deicers containing magnesium and calcium.** Magnesium deicer salts such as CMA, Mg-acetate, and Mg-chloride, proved highly deleterious to concrete in experimental systems. It is difficult to discount the potential damage that these salts may have on concrete when used over long terms as deicers. If deicers containing magnesium are used, concrete cores should be obtained ever few years

and comparative petrographic analyses of the material should be performed in order to determine if harmful changes are occurring.

ACKNOWLEDGMENTS

This project was funded primarily by the Iowa Department of Transportation, Project No. HR-384. This support is gratefully acknowledged. We particularly want to thank Messers. Vernon Marks, Jim Myers, and Wendell Dubberke as well as Dr. Ken Bergenson for their advice, suggestions, and support of this project. Without their help the project would not have been possible. We thank Drs. Jerry Amenson and Scott Schlorholtz, of the ISU Materials Research Laboratory, for their assistance with SEM analyses. Appreciation is also extended to Mr. Scott Thieben for assistance with x-ray diffraction analyses and for reading a preliminary draft of this report.

REFERENCES

- AL-AMOUDI, O. S. B.; ABDULJAUWAD S. N.; RASHEEDUZZARFAR; AND MASLEHUDDIN, M., 1992, Effect of chloride and sulfate contamination in soils on corrosion of steel and concrete: *Transportation Research Record*. No. 1345, pp. 67-73.
- BERNTSSON L. AND CHANDRA, S., 1982, Damage of concrete sleepers by calcium chloride: *Cement & Concrete Research*, Vol. 12, No. 1, pp. 87-92.
- BISQUE, R. E. AND LEMISH, J. L., 1958, Chemical characteristics of some carbonate aggregate as related to durability of concrete: *Highway Research Board Bulletin*, Vol. 196, pp. 29-45.
- BONEN, D., 1992, Composition and appearance of magnesium silicate hydrate and its relation to deterioration of cement-based materials: *Journal of the American Ceramic Society*, Vol. 75, No. 10, pp.2904-2906.
- BONEN, D. AND COHEN, M. D., 1992, Magnesium sulfate attack on Portland cement paste: I. Microstructural analysis: *Cement and Concrete Research*, Vol. 22, pp.169-180.
- BONEN, D. AND COHEN, M. D., 1992, Magnesium sulfate attack on Portland cement paste: I. Microstructural analysis: *Cement and Concrete Research*, Vol. 22, pp. 169-180.
- BONEN, D. AND SARKAR, S. L, 1994, Environmental attack on concrete, in *Proceedings of the 16th International Conference on Cement Microscopy*, Eds. GOUDA, G. R.; NISPEROS, A.; AND BAYLES J., International Cement Microscopy Association, Texas, pp.11-23.

- BRITISH CEMENT ASSOCIATION, 1992, The diagnosis of alkali-silica reaction (Report of a working party): *British Cement Association*, Publication 45:042, 44 p.
- CASANOVA, L. A. AND AGUADO, A., 1996, Aggregate expansivity due to sulfide oxidation. I. Reaction system and rate model: *Cement and Concrete Research*, Vol. 26, No. 7, pp. 993-998.
- CHATTERJI, S., 1976, Discussion of scanning electron micrographic studies of ettringite formation by P. K. Metha: *Cement and Concrete Research*, Vol. 6, No. 5, pp. 711-712.
- CHATTERJI, S., 1978, Mechanism of the CaCl_2 attack on Portland cement concrete: *Cement and Concrete Research*, Vol. 8, No. 40, pp. 461-468.
- CHATTERJI, S. AND JEFFERY, J. W., 1963, A new hypothesis of sulphate expansion: *Magazine of Concrete Research*, Vol. 15, pp. 83-86.
- CHINCHON, J. S.; AYORA, C.; AGUADO, A.; AND GUIRADO, H., 1995, Influence of weathering of iron sulfides contained in aggregates on concrete durability: *Concrete Cement and Research*, Vol. 25, No. 6, pp. 1264-72.
- COHEN M. D., 1983a, Modeling of expansive cement: *Cement and Concrete Research*, Vol. 13, No. 4, pp. 519-528.
- COHEN M. D., 1983b, Theories of expansion in sulfoaluminate-type expansive cements: schools of thought: *Cement and Concrete Research*, Vol. 13, pp. 809-818.

- COHEN, M. D.; CAMPBELL, E.; AND FOWLE, W., 1985, Kinetics and morphology of ettringite formation, in *Proceedings of the 7th International Conference on Cement Microscopy*, Ft. Worth, Texas, pp. 360-381.
- CODY, R. D.; SPRY, P. G.; CODY, A. M.; AND GAN, G., 1994, *The role of magnesium in concrete deterioration*: Iowa Department of Transport, Final Report HR-355, 171p.
- CODY, R. D.; CODY, A. M.; SPRY, P. G.; AND GAN G., 1996, Experimental deterioration of highway concrete by chloride deicing salts: *Environmental and Engineering Geoscience*, Vol. 2, No. 4, pp. 575-588.
- DIAMOND, S., 1996, Delayed ettringite formation - processes and problems: *Cement & Concrete Composites*, Vol. 18, No. 3, pp. 205-215.
- DAY, R. L., 1992, The effect of secondary ettringite formation on durability of concrete: A literature analysis: *PCA Research and Development Bulletin* RD108T, pp.1-115.
- DENG M. AND TANG M. SH., 1993, Mechanism of dedolomitization and expansion of dolomitic rocks: *Cement and Concrete Research*, Vol. 23, No. 6, pp. 1397-1408.
- DENG M.; HAN, S. F.; LU, Y. N.; LAN, X. H.; HU, Y. L.; AND TANG, M. SH. 1993, Deterioration of concrete structures due to alkali - dolomite reaction in China: *Cement and Concrete Research*, Vol. 23, pp. 1040-1046.
- DENG, M.; WANG, Q.; MU, X. F.; AND TANG, M. SH., 1994, The chemical reaction in dolomite - KOH solution systems autoclaved at high temperatures: *Advances in Cement Research*, Vol. 6, No. 22, pp. 61-65.

- DENG, M. AND TANG, M., 1994, Formation and expansion of ettringite crystals: *Cement and Concrete Research*, Vol. 24, No. 6, p.119-126.
- DIAB, Y. AND PRIN, D., 1992, Alkali-aggregate reaction structural effects: A finite element model, in *Proceedings of the 9th International Conference on Alkali-Aggregate Reaction In Concrete*, London, Vol.1, pp. 261-268.
- DIAMOND, S., 1996, Delayed ettringite formation - processes and problems: *Cement and Concrete Composites*, Vol. 18, No. 3, pp. 205-215.
- DURAND, B.; ROUX, R.; HOUDE, J.; AND BLANCHETTE, A., 1992, Free expansions and stresses in concrete released to alkali-aggregate reaction, *Proceedings of the 9th International Conference on Alkali-Aggregate Reaction In Concrete*, London, Vol.1, pp. 298-310.
- FTIKOS CH. AND PARISSAKIS, G., 1985, The combined action of Mg^{2+} and Cl^- ions in cement paste. *Cement and Concrete Research*, Vol. 15, No. 4, pp. 593-599.
- FU, Y.; XIE, P.; GU, P.; AND BEAUDOIN, J. J., 1995, Preferred nucleation of secondary ettringite in pre-existing cracks of steam-cured cement paste: *Journal of Materials Science Letters*, Vol. 12, pp. 1864-1865.
- FU, Y. AND BEAUDOIN, J. J., 1995, A through-solution mechanism for delayed ettringite formation in pre-existing cracks in Portland cement mortar: *Journal of Materials Science Letters*, Vol. 14, pp. 217-219.
- FU, Y. AND BEAUDOIN, J. J., 1996, Mechanisms of delayed ettringite formation in Portland cement system: *ACI Material Journal*, July-August, pp. 327-333.

- GAN, G.; SPRY, P. G., CODY, R. D.; AND CODY A. M., 1996, Rim formation on Iowa highway concrete dolomite aggregate: the effects of dedolomitization reactions: *Environmental and Engineering Geoscience*, Vol. 2, No. 1, pp. 59-72.
- GILLOTT, J. E., 1964, Mechanism and kinetic of expansion in alkali - carbonate rock reaction: *Canadian Journal of Earth Science*, Vol. 1, pp. 121-145.
- GILLOTT, J. E., 1975, Alkali - aggregate reactions in concrete: *Engineering Geology*, Vol. 9, No. 4, pp. 303-326.
- GILLOTT, J. E. AND SWENSON, E. G., 1969, Mechanism of the alkali - carbonate rock reaction: *Quarterly Journal of Engineering Geology*, Vol. 2, No. 1, pp.7-23.
- GLASSER, F. P.; DAMIDOT, D.; AND ATKINS, M., 1995, Phase development in cement in relation to the secondary ettringite problem: *Advances in Cement Research*, Vol. 7, No. 26, pp. 57-68.
- GRATTAN-BELLOW, P. E., 1992, Microcrystalline quartz, undulatory extinction and the alkali-silica reaction, in *Proceedings of the 9th International Conference on Alkali-Aggregate Reaction In Concrete*, London, Vol.1, pp. 383-394.
- HADLEY, D. W., 1961, Alkali reactivity of carbonate rocks-expansion and dedolomitization. *Highway Research Board*, Vol. 40, pp. 463-474.
- HADLEY, D. W., 1964a, Alkali reactive carbonate rocks in Indiana: A pilot regional investigation: *Highway Research Record*, Vol. 45, pp. 196-221.
- HADLEY, D. W., 1964b, Alkali reactivity of dolomitic carbonate rocks: *Highway Research Record*, Vol. 45, pp. 1-19.

- HANSEN, W. C., 1976, A discussion of the paper "Scanning electron micrographic studies of ettringite formation" by P. K. Metha: *Cement and Concrete Research*, Vol. 6, No. 4, 595-596 p.
- HEFFMANN, D. W., 1984, Changes in structures and chemistry of cement mortars stressed by a sodium chloride solutions: *Cement and Concrete Research*, Vo. 14, pp. 49-56.
- HELLER L. AND BEN-YAIR, M., 1966, Effect of chloride solutions on Portland cement: *Journal of Applied Chemistry*, Vol. 16, pp. 223-226.
- KELHAM, S., 1996, The effect of cement composition and fineness on expansion associated with delayed ettringite formation: *Cement & Concrete Composites*, Vol. 18, No. 3, pp. 171-186.
- KOSMATKA, S. H. AND PANARESE, W. C., 1988, *Design and Control of Concrete Mixtures*: Portland Cement Association, Skokie, Illinois, 13 ed., pp 205.
- KURDOWSKI, W.; TRYBALSKA, B.; AND DUSZAK, S., 1994, SEM studies of corrosion of cement paste in chloride solution, in *Proceedings of the 16th International Conference on Cement Microscopy*, Eds. GOUDA, G. R.; NISPEROS, A.; AND BAYLES J., International Cement Microscopy Association, Texas, pp.80-89.
- LEMISH J. L. AND MOORE, W. J., 1964, Carbonate aggregate reactions: Recent studies and an approach to the problem: *Highway Research Record*, p.57-71.
- LEMISH J.; RUSH, F. E.; AND HILTROP, C. L., 1958, Relationship of physical properties of some Iowa carbonate aggregate to durability of concrete: *Highway Research Board Bulletin*, Vol. 196, pp. 1-16.

- LOCHER, F. W., 1969, Influence of chloride and hydrocarbonate on the sulphate attack, in *Proceedings of the 9th International Symposium on the Chemistry of Cement*, Tokyo, Part III, Vol. 3, pp. 328-335.
- MATHER, BRYANT, 1984, A discussion of the paper "Theories of expansion in sulfoaluminate-type expansive cements: Schools of thought, " by M. D. Cohen: *Cement and Concrete Research*, Vol. 14, No. 4, pp. 603-609.
- MATHER, KATHARINE; BUCK, ALAN D.; AND LUKE, WILBUR I., 1964, Alkali-silica and alkali-carbonate reactivity of some aggregates from South Dakota, Kansas, and Missouri, Highway Research Board Record, Vol. 45, pp.72-109.
- METHA, P. K., 1969, Morphology of calcium sulphoaluminate hydrate: *Journal of the American Ceramic Society*, Vol. 52, No. 9, pp. 521-522
- METHA, P. K., 1973, Mechanism of expansion associate with ettringite formation: *Cement and Concrete Research*, Vol. 3, No. 1, pp.1-6.
- METHA, P. K., 1976a, Scanning electron micrographic studies of ettringite formation: *Cement and Concrete Research*, Vol. 6, No. 2, pp.169-182.
- METHA, P. K., 1976b, Reply to discussion by S. Chatterji of "Scanning electron micrographic studies of ettringite formation": *Cement and Concrete Research*, Vol. 6, No. 5, pp. 713-714.
- METHA, P. K., 1976c, Reply to discussion by W. C. Hansen of "Scanning electron micrographic studies of ettringite formation": *Cement and Concrete Research*, Vol. 6, No. 4, pp. 597-598.

- METHA, P. K., 1983, Mechanism of sulfate attack on Portland cement concrete - another look: *Cement and Concrete Research*, Vol. 13, No. 3, pp. 401-406.
- METHA, P. K. AND HU, F., 1978, Further evidence for expansion of ettringite by water adsorption: *Journal of the American Ceramic Society*, Vol. 61, No. 3, pp. 179-181.
- METHA, P. K. AND WANG, S., 1982, Expansion of ettringite by water adsorption: *Cement and Concrete Research*, Vol. 12, No. 1, pp. 121-122.
- MILANESI C. A. AND BATIC, O. R., 1994, Alkali reactivity of dolomitic rocks from Argentina: *Cement and Concrete Research*, Vol. 24, No. 6, pp. 1073-1084.
- MONTEIRO, P. J. M., 1985, Ettringite formation on the aggregate-cement paste interface: *Cement and Concrete Research*, Vol. 15, No. 2, pp. 378-380.
- MU, X., 1996, *Studies on alkali-carbonate reaction*: Ph.D dissertation, Nanjing University of Chemical Technology, 124 p.
- NEVILLE, A. M., 1969, Behavior of concrete in saturated and weak solutions of magnesium sulphate or calcium chloride: *Journal of Materials*, Vol. 4, No. 4, pp.781-816.
- NICHOLSON, R. V.; GILLHAM, R. W.; AND REARDON, E. J., 1988, Pyrite oxidation in carbonate-buffered solution: 1. Experimental kinetics: *Geochimica et Cosmochimica Acta*, Vol. 52, pp.1077-1085.
- OBERHOLSTER, R. E.; TOIT, P. DU.; AND PRETORIUS, J. L., 1984, Deterioration of concrete containing a carbonaceous sulphide-bearing aggregate, in, *Proceedings of the 6th International Conference on Cement Microscopy*, Bayles, K., ed., Albuquerque, New Mexico, pp. 360-373.

- OBERSTE-PADTBURG, R., 1985, Degradation of cements by magnesium brine: A microscopic study, in *Proceedings of the 7th International Conference on Cement Microscopy*, Ft. Worth, Texas. pp.24-36.
- OGAWA, K. AND ROY, D. M., 1981, C_4A_3S hydration ettringite formation and its expansion mechanism: I. Expansion; ettringite stability: *Cement and Concrete Research*, Vol. 11, pp. 741-750.
- OGAWA, K. AND ROY, D. M., 1982a, C_4A_3S hydration ettringite formation and its expansion mechanism: II. Microstructural observation of expansion: *Cement and Concrete Research*, Vol. 12, No. 1, pp. 101-109.
- OGAWA, K. AND ROY, D. M., 1982b, C_4A_3S hydration ettringite formation and its expansion mechanism: III. Effect of CaO, NaOH and NaCl; conclusions: *Cement and Concrete Research*, Vol. 12, pp. 247-256.
- OLDER, L. AND YAN, P., 1994, Investigation on ettringite: *Advances in Cement Research*, Vol. 4, No. 24, pp. 165-171.
- PETTIFER, K. AND NIXON, P. J., 1980, Alkali-metal sulphate - a factor common to both alkali aggregate reaction and sulphate attack on concrete: *Cement and Concrete Research*, Vol. 10, No. 2, pp. 173-181.
- PIASTA, W. G. AND HEBDA, L., 1991, Sulphate expansion and permeability of concrete with limestone aggregate: *Magazine of Concrete Research*, Vol. 43, No. 155, pp. 81-85.

- PING, X, AND BEAUDOIN, J. J., 1992, Mechanism of sulphate expansion: I. Thermodynamic principle of crystallization pressure: *Cement and Concrete Research*, Vol. 22, No. 4, pp. 631-640.
- PITT, J. M.; SCHLUTER, M. C.; LEE D.Y.; AND DUBBERKE, W., 1987, Sulfate Impurities from deicing salt and durability of portland cement mortar: *Transportation Research Record*, Vol. 1110, pp.16-23.
- POOLE, A. B., 1981, Alkali - carbonate reactions in concrete, in *Proceedings 5th International Conference on the Concrete Alkali-Aggregate Reaction*, Pretoria, South Africa, pp.327-334.
- RAMACHANDRAN, V. S.; PHILL, M. SC. D.; AND CERAM, F. I. 1976, *Calcium Chloride in Concrete*: Applied Science Publishers Ltd, 207 p.
- ROGERS, C. A., 1993, Alkali-aggregate reactivity in Canada: *Cement & Concrete Composites*, Vol. 15, pp. 13-19.
- SALOMON, M.; GAUDE, J.; AND HASNI, L., 1992, Diagnosis of concrete structures affected by alkali aggregate reaction, in *Proceedings of the 9th International Conference on Alkali-Aggregate Reaction in Concrete*, London, Vol. 2, pp. 902-915.
- SCRIVENER, K. L. AND TAYLOR, H. F. W., 1993, Delayed ettringite formation: a microstructural and microanalytical study: *Advances in Cement Research*, Vol. 5, No. 20, pp. 139-146.

- SCHLORHOLTZ, S. AND AMENSON, J., 1995, Evaluation of microcracking and chemical deterioration in concrete pavements: Iowa Department of Transportation, Project HR-358, 205 p.
- SHAYAN, A. AND QUICK, G. W., 1992, Relative importance of deleterious reactions in concrete: formation of AAR products and secondary ettringite: *Advances in Cement Research*, Vol. 4, No. 16, pp. 149-157.
- SHAYAN, A. AND IVANUSEC, I., 1996, An experimental clarification of the association of delayed ettringite formation with alkali-aggregate reaction: *Cement & Concrete Composites*, Vol. 18, No. 3, pp. 161-170
- SMITH, A. S.; DUNHAM A. C.; AND WEST, G., 1992, Undulatory extinction of quartz in British hard rocks: *Proceedings of the 9th International Conference on Concrete Alkali-Aggregate Reaction*, London, Vol.2, pp. 1001-1006.
- SWENSON E. G. AND GILLOTT, J. E. 1960, Characteristics of Kingstone carbonate rock reaction: *Highway Research Board Bulletin*, Vol. 275, pp.18-31.
- SWENSON E. G. AND GILLOTT, J. E. 1964, Alkali - carbonate rock reaction: *Highway Research Record*, Vol. 45, pp. 21-45.
- SWENSON E. G. AND GILLOTT, J. E. 1967, Alkali reactivity of dolomitic limestone aggregate. *Magazine of Concrete Research.*, Vol. 19, No. 59, pp. 95-104.
- TANG, M.; LIU, ZH.; AND HAN, S. F., 1986, Mechanism of alkali - carbonate reaction, *Proceedings 7th International Conference on Concrete Alkali-Aggregate Reaction*,

- Ottawa, Canada, GRATTAN-BELLEW, P. E., ed., New Jersey, Noyes Publications, pp. 275-279.
- TANG M.; LU, Y. N.; AND HAN, S. F., 1989, Kinetics of alkali - carbonate reaction, *Proceedings 8th International Conference on Concrete Alkali-Aggregate Reaction*, eds. OKADA, K.; NISHIBAYASHI S.; AND KAWAMURA, M., New York, Elsevier Applied Science, pp. 147-152.
- TANG M.; LIU, ZH.; LU, Y. N.; AND HAN, S. F., 1991, Alkali - carbonate reaction and pH value: *Il Cemento*, Vol. 88, No. 3, pp. 141-150.
- TANG, M., 1992, Classification of alkali-aggregate reaction, in *Proceedings of the 9th International Conference on Concrete Alkali-Aggregate Reaction*, London, Vol. 2, pp. 648-653.
- TANG, M.; DENG, M.; LAN, X. H.; AND HAN S. F., 1994, Studies on alkali - carbonate reaction: *ACI Materials Journal*, Vol. 91, No. 1, pp. 26-29.
- TAYLOR, H. F. W., 1990, *Cement Chemistry*: London, Academic Press Ltd. 475 p.
- TUMIDAJSKI, P. J. AND CHAN, G. W., 1996, Durability of high performance concrete in magnesium brine: *Cement and Concrete Research*, Vol. 26, No. 4, pp. 557-565.
- WEST, G., 1996, *Alkali-Aggregate Reaction in Concrete Roads and Bridges*: London, Thomas Telford Ltd. Chapter, 161p.
- WOLTER, S., 1996, *Ettringite. Cancer of Concrete*: New York, Burgess Publishing Co., 172 p.

WORTHINGTON, J. C.; BONNER, D. G.; AND NOWELL, D. V., 1988, Influence of
cement chemistry on chloride attack of concrete: *Materials Science and Technology*,
Vol. 4, pp. 305-313.

Appendix I

PLATES AND FIGURES

Expansive Mineral Growth in

Iowa Highway Concrete Samples

PLATE I

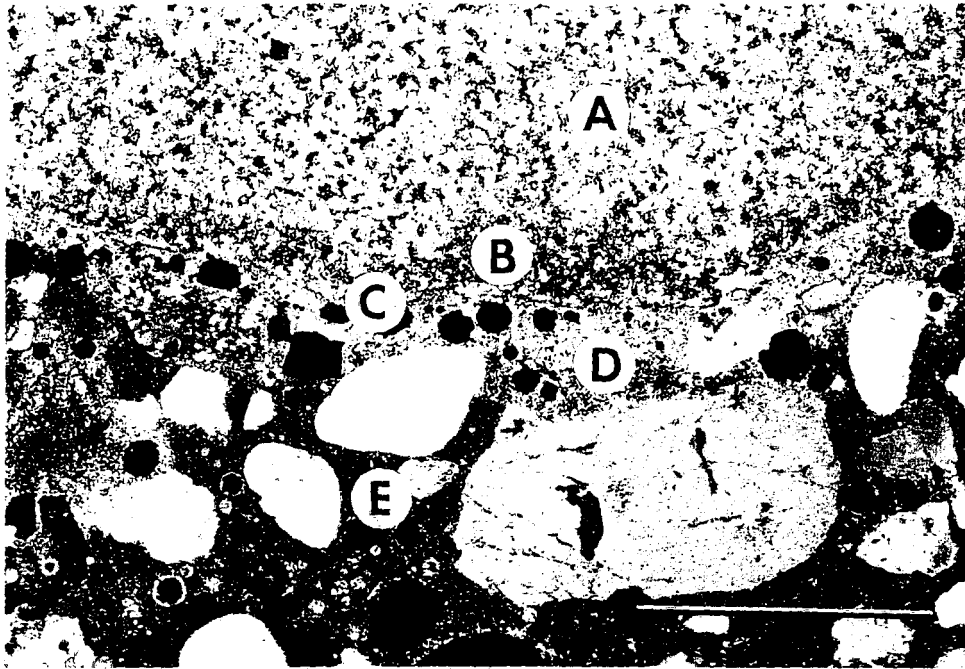
A. Light micrograph showing typical characteristics of reactive dolomite aggregate

(Crawford-Lee quarry; US 30). It consists of fine-grained, poorly-crystallized dolomite crystals with abundant void spaces. Dedolomitization reaction rims, which show the best developed zone patterns, occur at aggregate-cement paste interfaces. (Zone A = interior of dolomite particle; B = dark-colored inner dolomite rim area; C = light-colored exterior or outer dolomite rim area; D = light-colored cement paste region; E = normal cement paste). In the photo, Zones D and E are easily distinguishable. The rounded particles are quartz fine aggregate. Transmitted light with crossed-polarizers x 40. Scale bar = 1 mm.

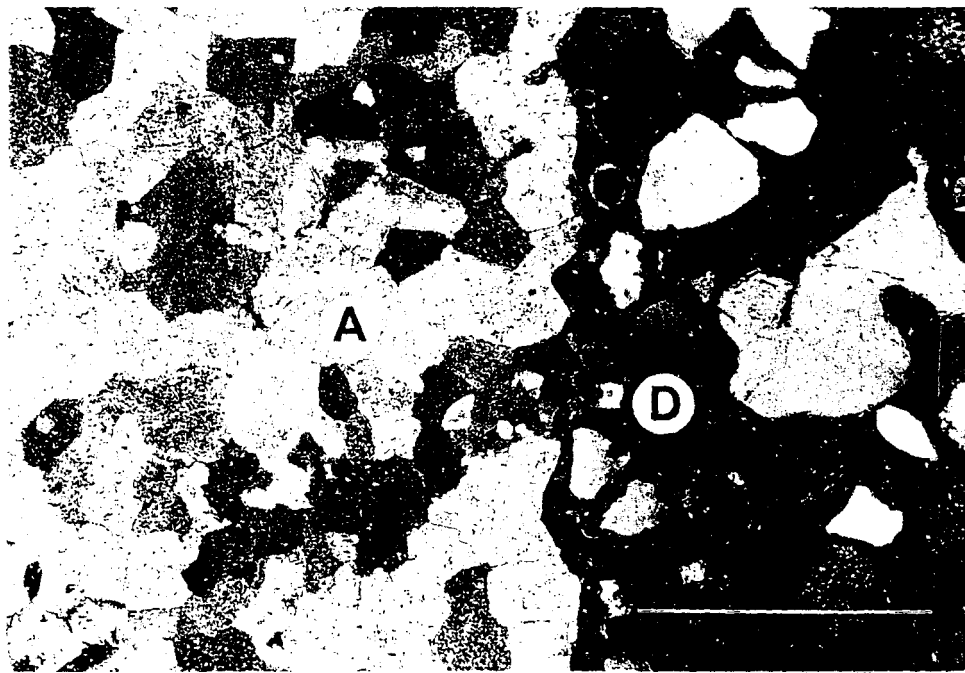
B. Light micrograph showing typical characteristics of non-reactive dolomite

aggregate (Sundheim quarry; US 20). It consists of coarse-grained, well-crystallized dolomite crystals that are tightly intergrown with little void space between crystals. No reaction rims are formed at the interface. Transmitted light with crossed-polarizers, x 40. Scale bar = 1 mm.

PLATE I.



A



B

Plate II.

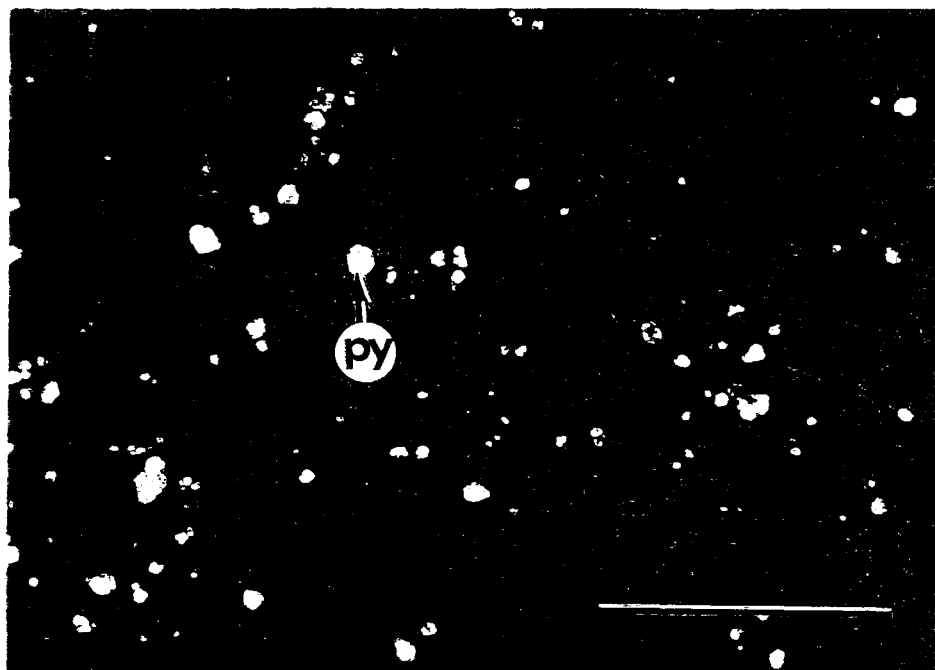
A. Light micrograph of unoxidized pyrite inclusions in dolomite aggregate. Small

pyrite masses (py) enclosed within large, well-crystallized dolomite crystals are not oxidized because the pyrite has little chance to be exposed to oxidizing solutions. Reflected light, x200. Scale bar = 200 μm .

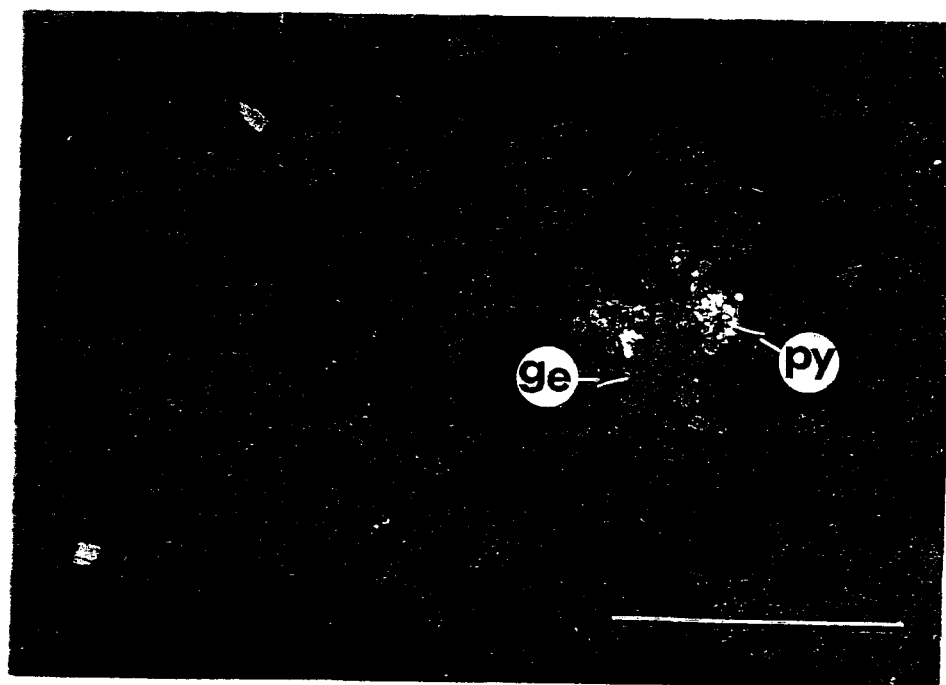
B. Light micrograph of oxidized pyrite inclusions in dolomite aggregate. Pyrite

masses (py) located in open spaces such as interstitial pores or intercrystalline boundaries are typically well-oxidized to goethite (ge) because the pyrite was exposed to oxidizing solutions. Reflected light, x200. Scale bar = 200 μm .

PLATE II.



A



B

Plate III.

A. Light micrograph showing a typical occurrence of fine aggregate in Iowa

highway concrete. Rounded to subrounded quartz grains (q) are the major constituent of fine aggregate. They generally appear to be unaltered by exposure to cement paste environments. Some are composed of strained quartz (qu) with undulatory extinction. Transmitted light with crossed-polarizers, x40. Scale bar = 1mm.

B. Light micrograph showing microcracks in quartz fine aggregate, US 20 highway.

The microcracks may be caused by expansion resulting from alkali-silica reaction, but there is little evidence of a significant amount of silica gel adjacent to the grains or in the microcracks. Transmitted light with crossed-polarizers, x40. Scale bar = 1 mm.

PLATE III.



A



B

Fig. 1. SEM micrograph and EDAX maps of Crawford Lee quarry concretes from

US 30. Reactive dolomite coarse aggregate is shown on the left side of the SEM micrograph. It consists of poorly-crystallized, very small, dolomite crystals with abundant voids between the crystals. Reaction rims are observable in the dolomite aggregate and cement paste; interface type sequence is A+B+C+D+E, with Zone A lying outside the micrograph view. The rim zones are indicated on the photograph by the appropriate capital letter, for example Zone A is shown by the letter 'A'. Both void-fill and void-rim ettringite crystals are present in air-entrainment voids in the cement paste. There is more abundant ettringite in the paste outside the light-colored paste rim (Zone D) compared to the amount in the rim (D). EDAX area maps show that brucite is widely disseminated throughout the cement paste.

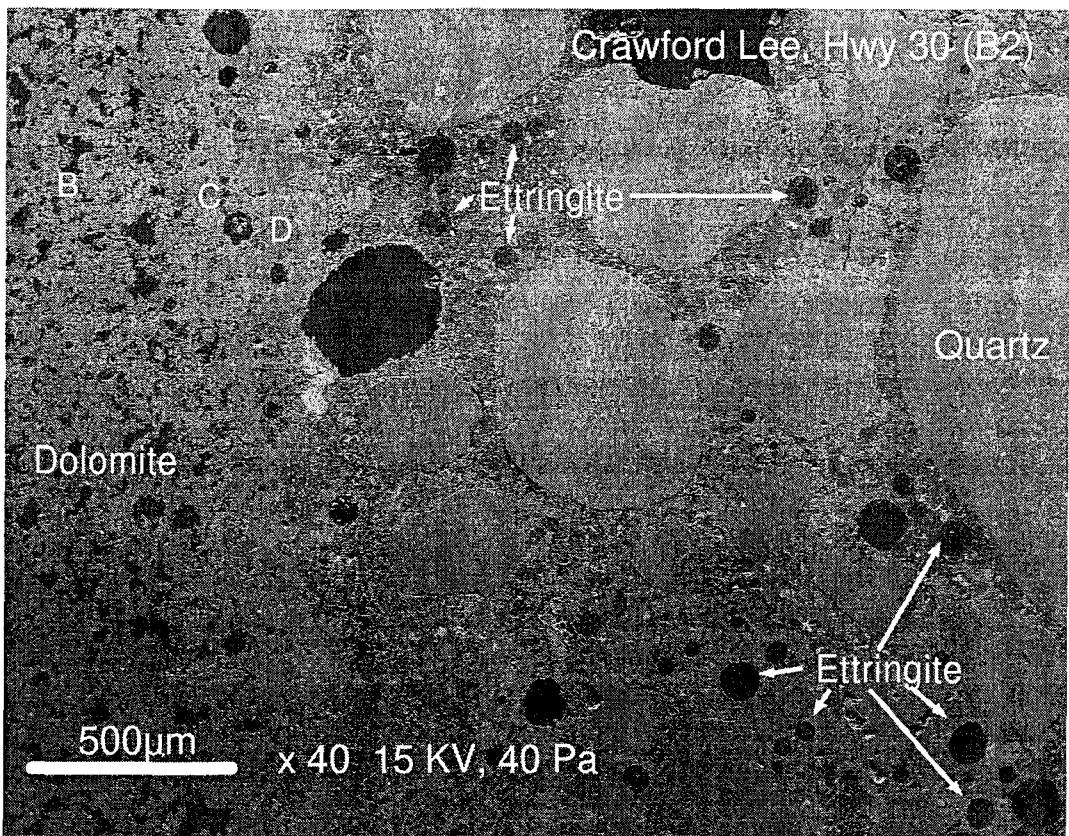


Fig. 1

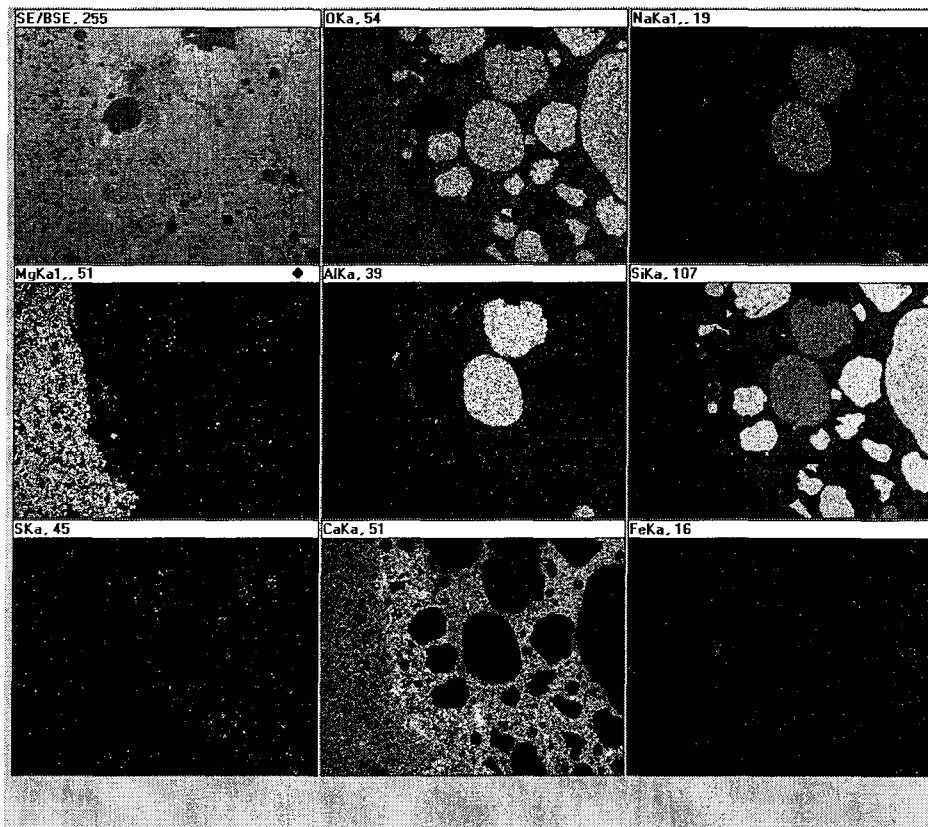


Fig. 2. SEM micrograph and EDAX area maps of Nelson quarry concretes from US

63. The SEM view shows the interface area between dolomite aggregate and cement paste. The reactive dolomite aggregate particles consist of poorly-crystallized, fine-grained, dolomite crystals with abundant voids. Well-developed reaction rims are clearly seen in the dolomite aggregate and cement paste; interface sequence is A+B+C+D+E, with Zone A lying outside of the micrograph. Note that no ettringite forms in air-voids in the light colored cement paste Zone E. Cracks are often spatially associated with ettringite void-fillings. Note also the calcium-rich cement paste region, Zone D, immediately outside the aggregate particle (evident in the Ca-map).

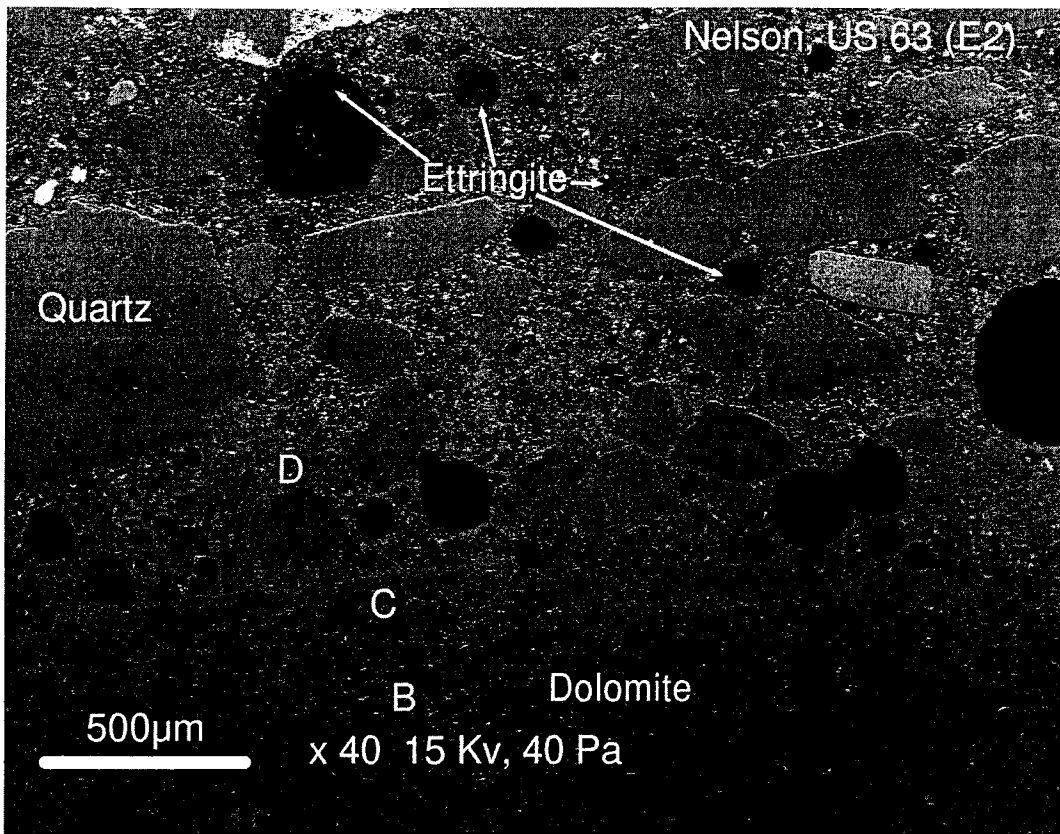


Fig. 2

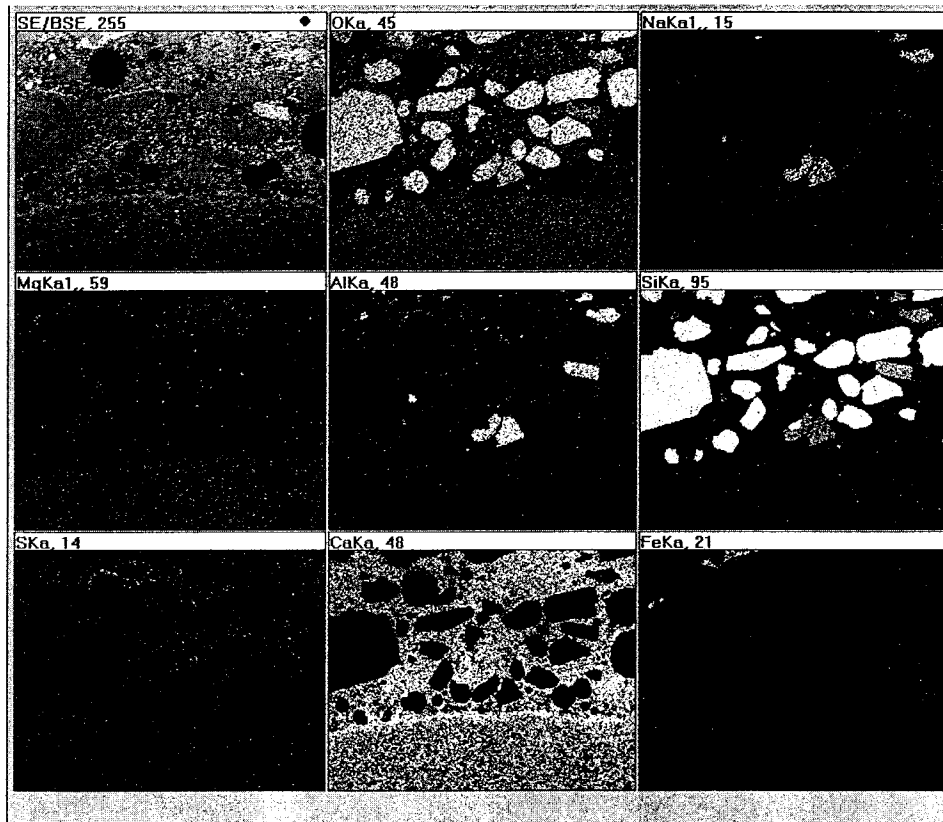


Fig. 3. SEM micrograph and EDAX area maps of Paralta quarry concrete from IA

13. Reactive coarse aggregate is composed of very small, poorly-crystallized dolomite. Well-developed reaction rims clearly seen in the aggregate and paste exhibit the sequence A+B+C+D+E. Ettringite is visible in air-entrainment voids in cement paste Zone E. The EDAX element maps show that abundant brucite crystals are disseminated throughout the paste. More abundant and larger-sized brucite crystals are present in the cement paste Zone E.

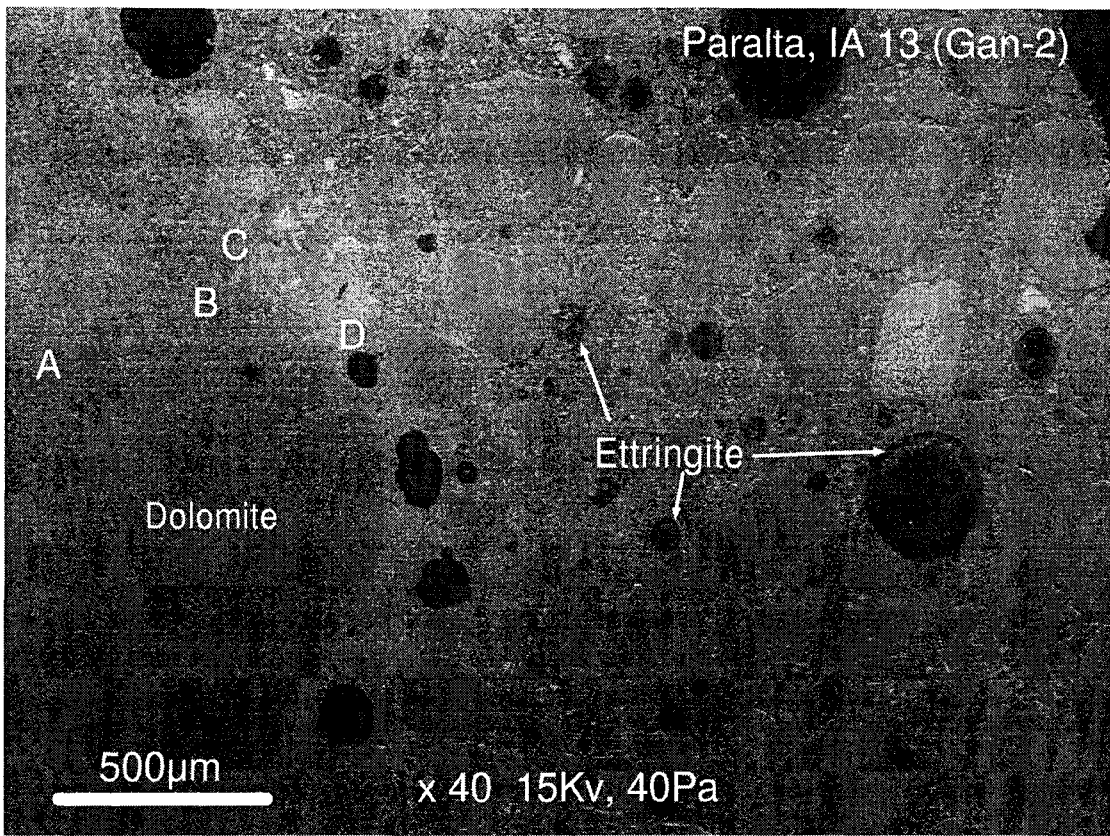


Fig. 3

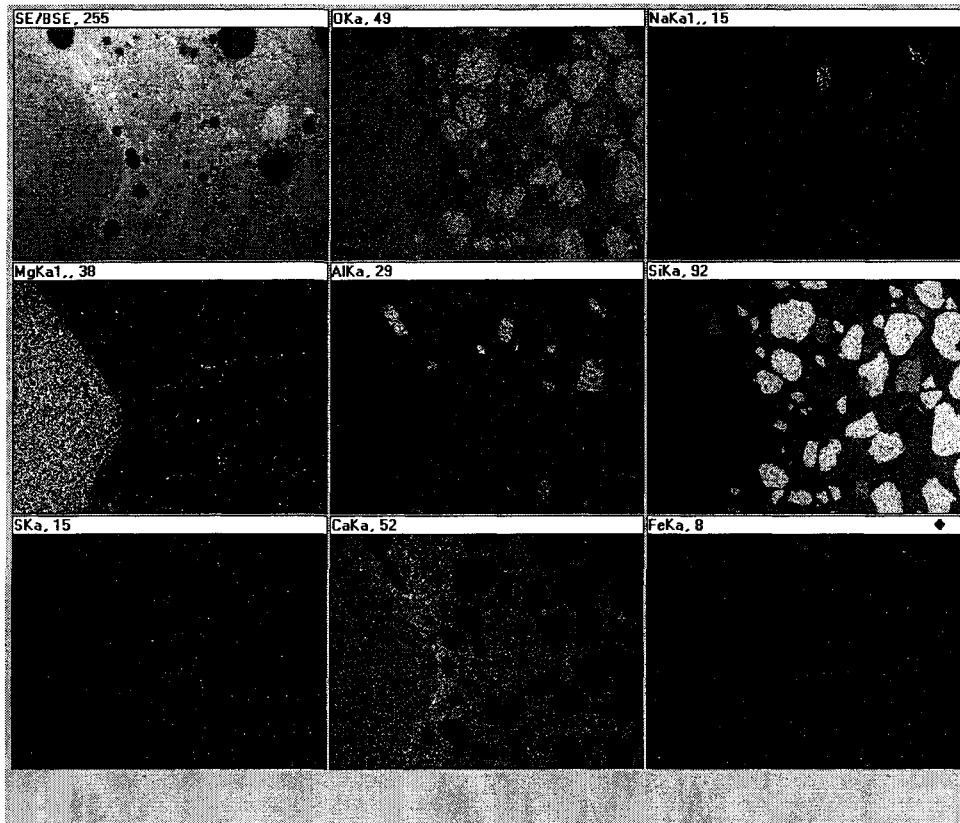


Fig. 4. SEM micrograph and EDAX maps of Crawford Lee quarry concretes from IA 21. The SEM micrograph shows the dolomite aggregate-cement paste interface in highway concrete taken from IA 21, back-scattered electron image. Abundant voids are evident in the dolomite aggregate, and the interface sequence is (A or B)+C+D+E. Both void-fill and void rim ettringite occur in small air-entrainment voids in the cement paste. The corresponding EDAX maps show that brucite occurs throughout the cement paste. Ettringite is more abundant outside the light-colored paste rim (Zone D) than it is in this zone.

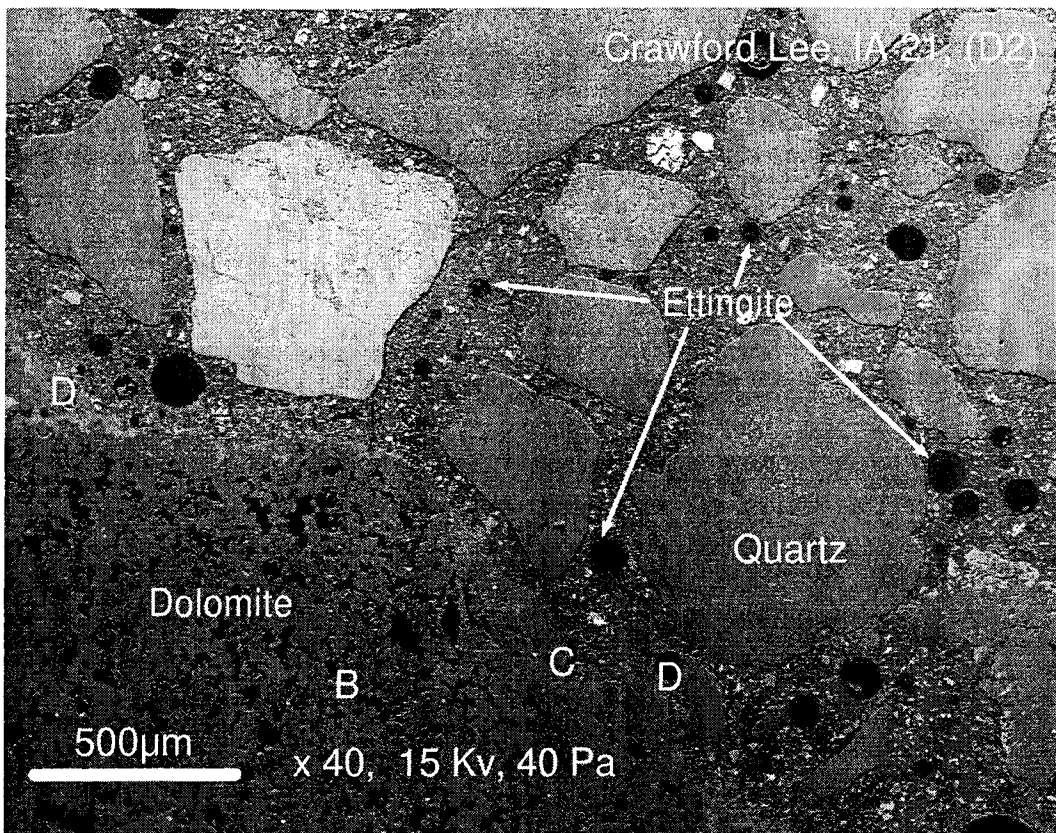


Fig. 4

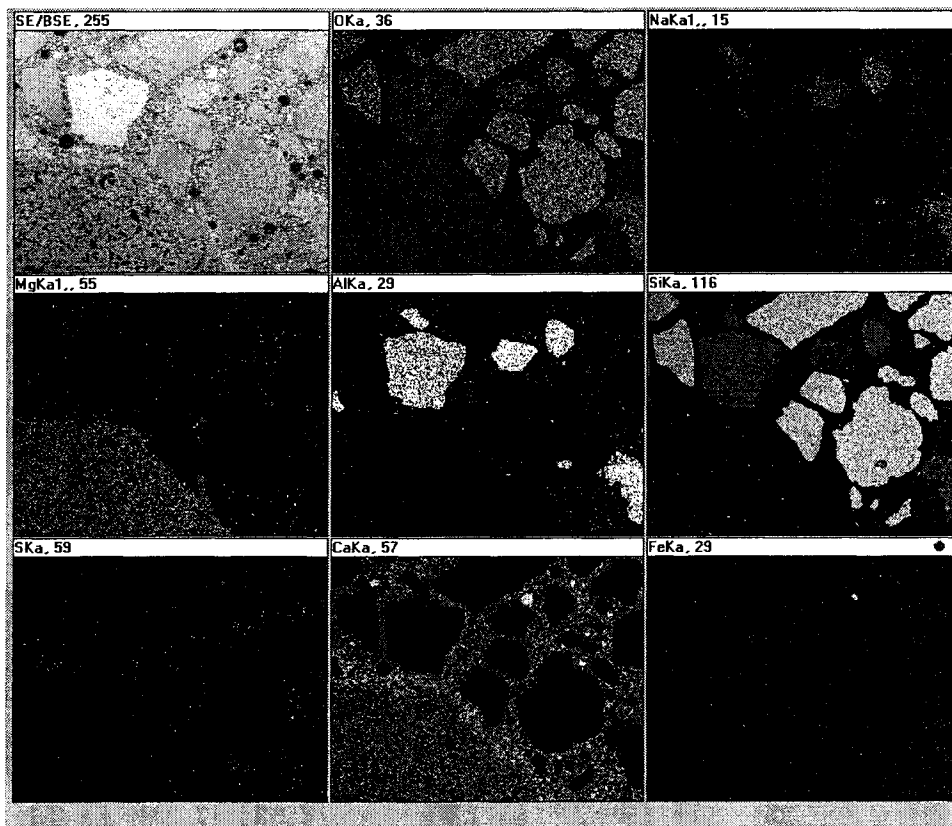


Fig. 5. SEM micrograph and EDAX area maps of Dotzler quarry concrete from IA 9. The dolomite aggregate-cement paste interface area is shown in the back-scattered electron image and in corresponding EDAX area maps. The two reactive coarse aggregate particles consist of very fine-grained and poorly-crystallized dolomite. Reaction rims observable in the dolomite aggregate and paste show the sequence A+B+C+D+E and A+B+D+E, with Zone A lying outside of the micrograph. Both types of ettringite are present in air-entrainment voids in the paste Zone E. The Mg and O EDAX element maps show that abundant brucite crystals are disseminated throughout the paste.

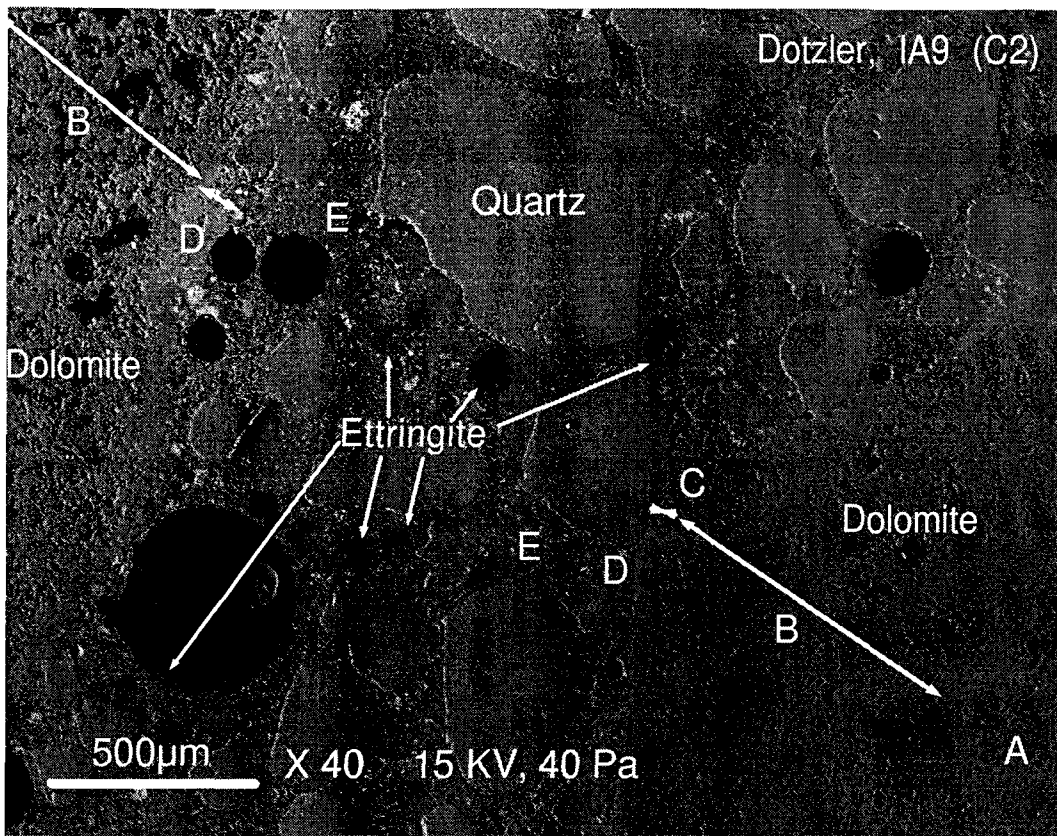


Fig. 5

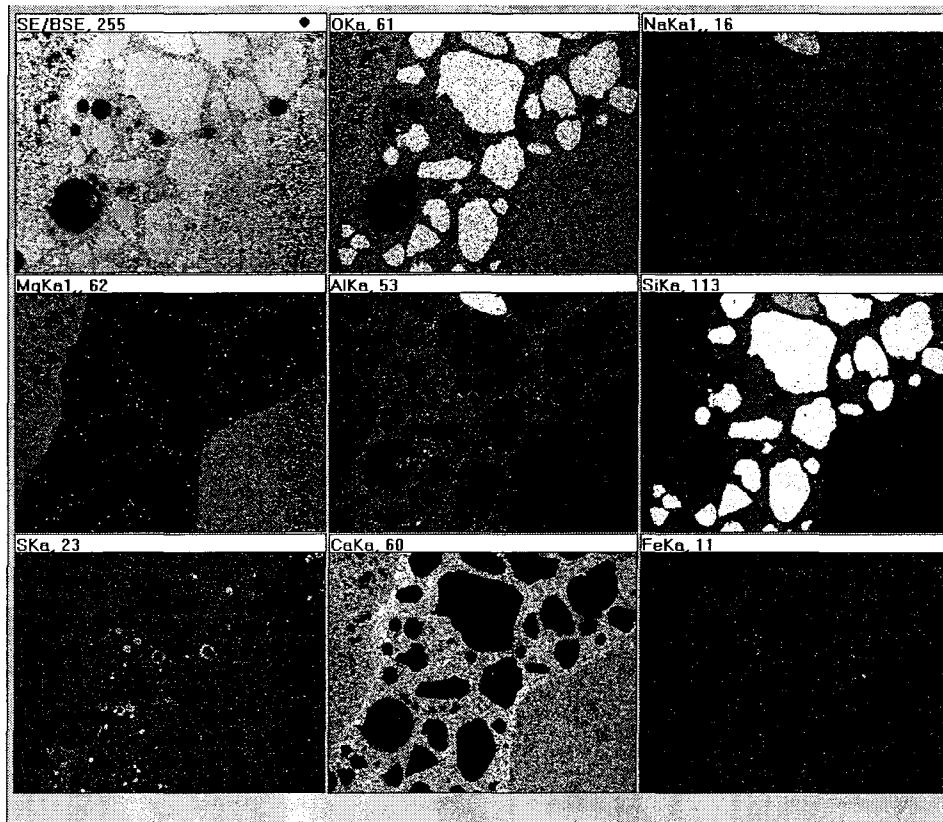


Fig. 6. SEM micrograph and EDAX area maps of Sundheim quarry concrete from US 20. Non-reactive coarse aggregate is composed of coarse-grained, well-crystallized dolomite. No significant reaction rims are observable in the A+(D)+E sequence. Limited amounts of ettringite form in the very small air-entrainment voids in the cement paste. EDAX element maps show that a little brucite is present in the cement.

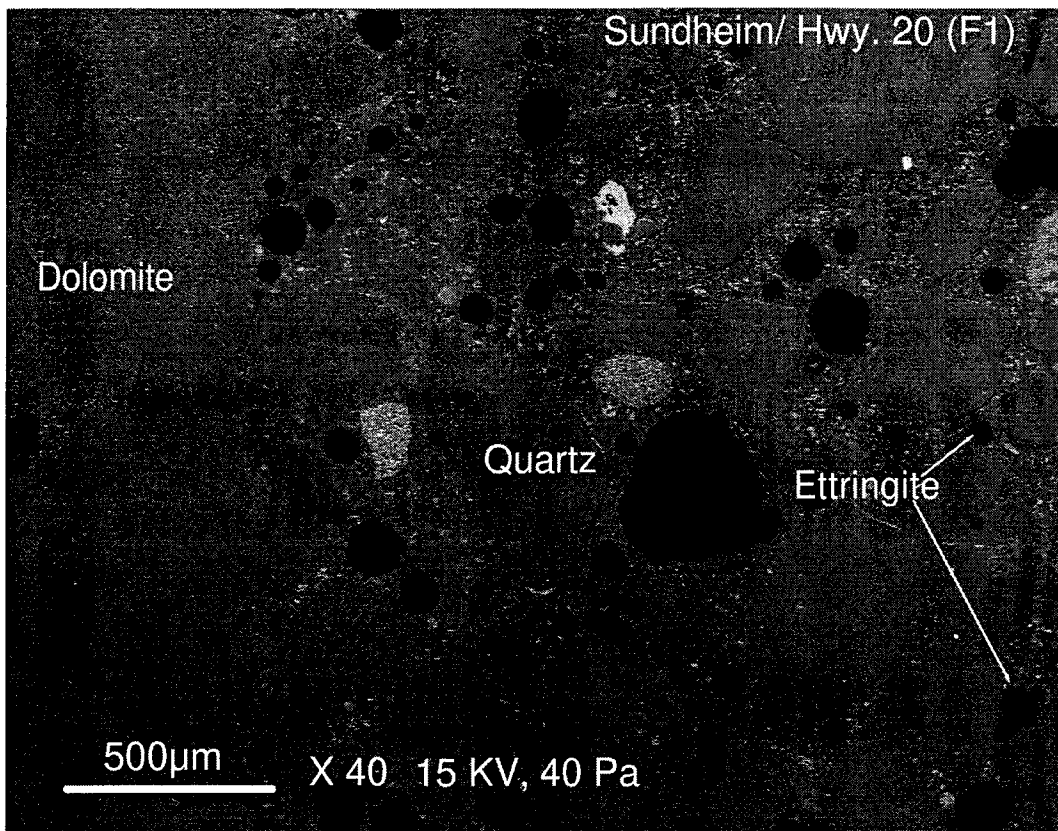


Fig. 6

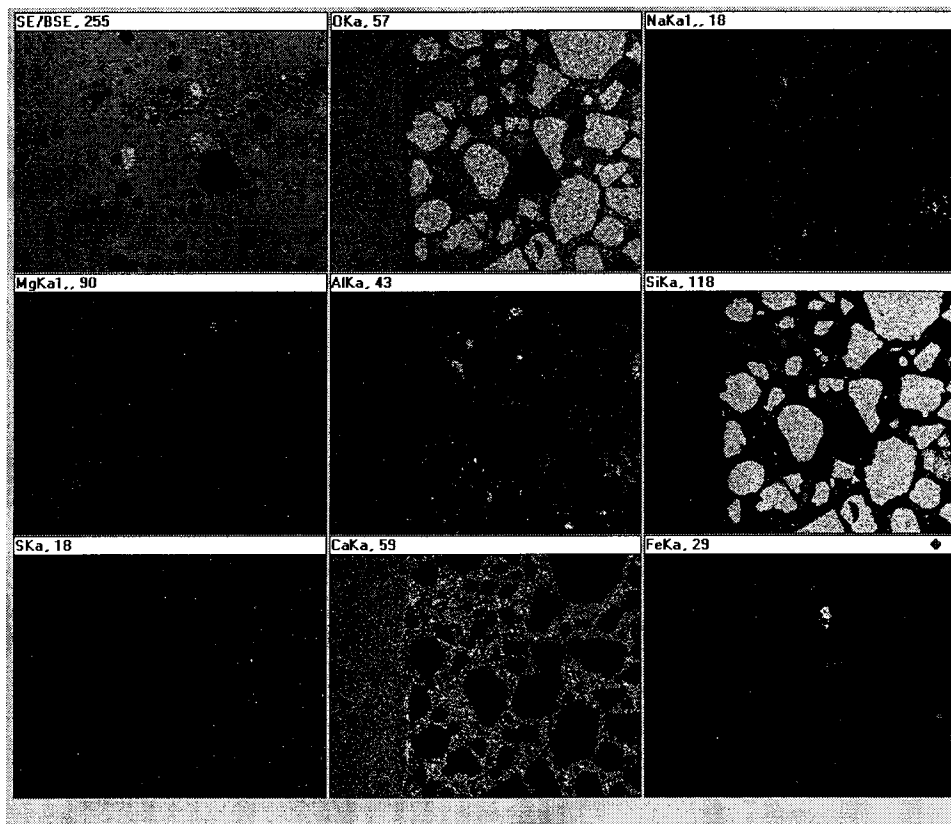


Fig. 7. SEM micrograph and EDAX element maps showing the oxidation of large pyrite inclusions in dolomite aggregate from Portland West quarry, I 35.

Note the large pyrite mass on right side of photograph. Oxidation occurs on its outer surface and along fractures. The pyrite mass shown on the left side of photograph has been almost entirely replaced by goethite.

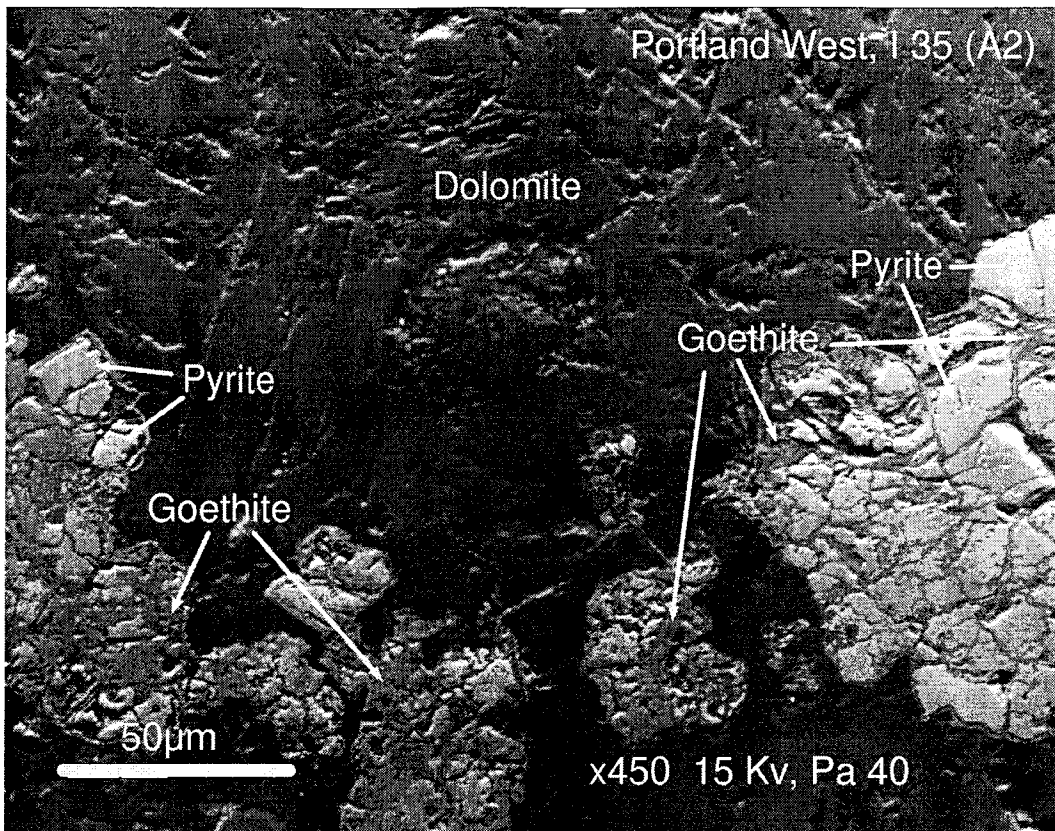


Fig. 7

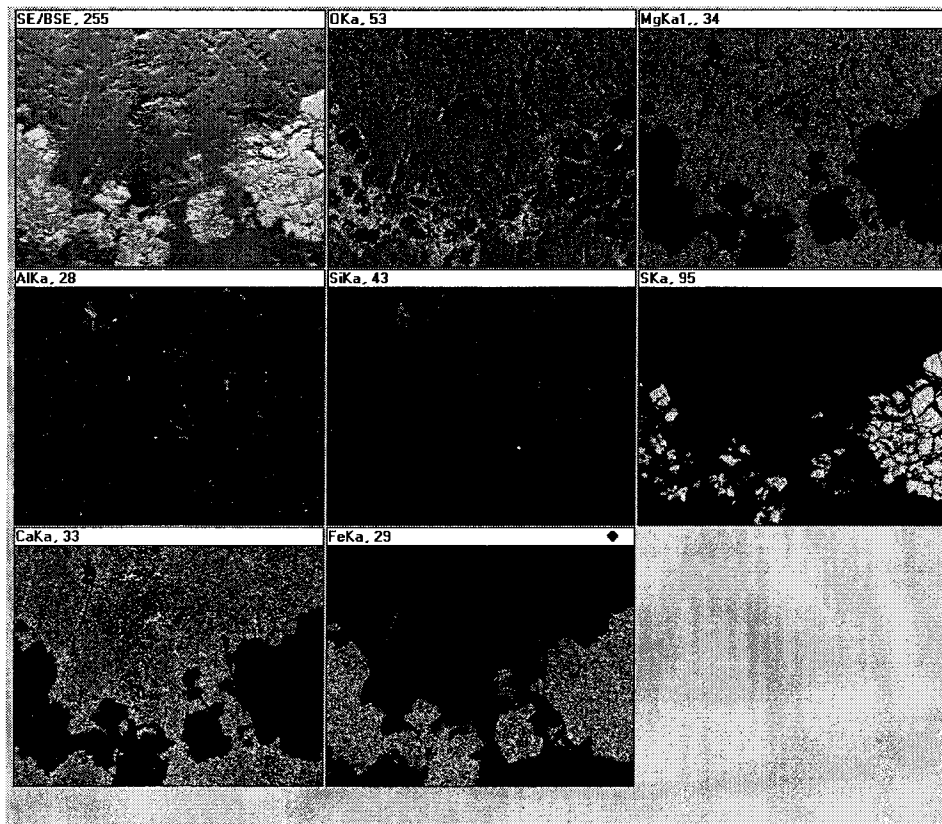


Fig. 8. SEM micrograph and EDAX area maps of Crawford Lee quarry concrete from IA 100. The coarse aggregate is mostly limestone. No reaction rims are observable at the interface and this fact indicates that the aggregate is essentially non-reactive. Ettringite occurs in the extremely small air-entrainment voids and is evenly distributed in the paste. A very small amount of brucite is identified with the EDAX element maps.

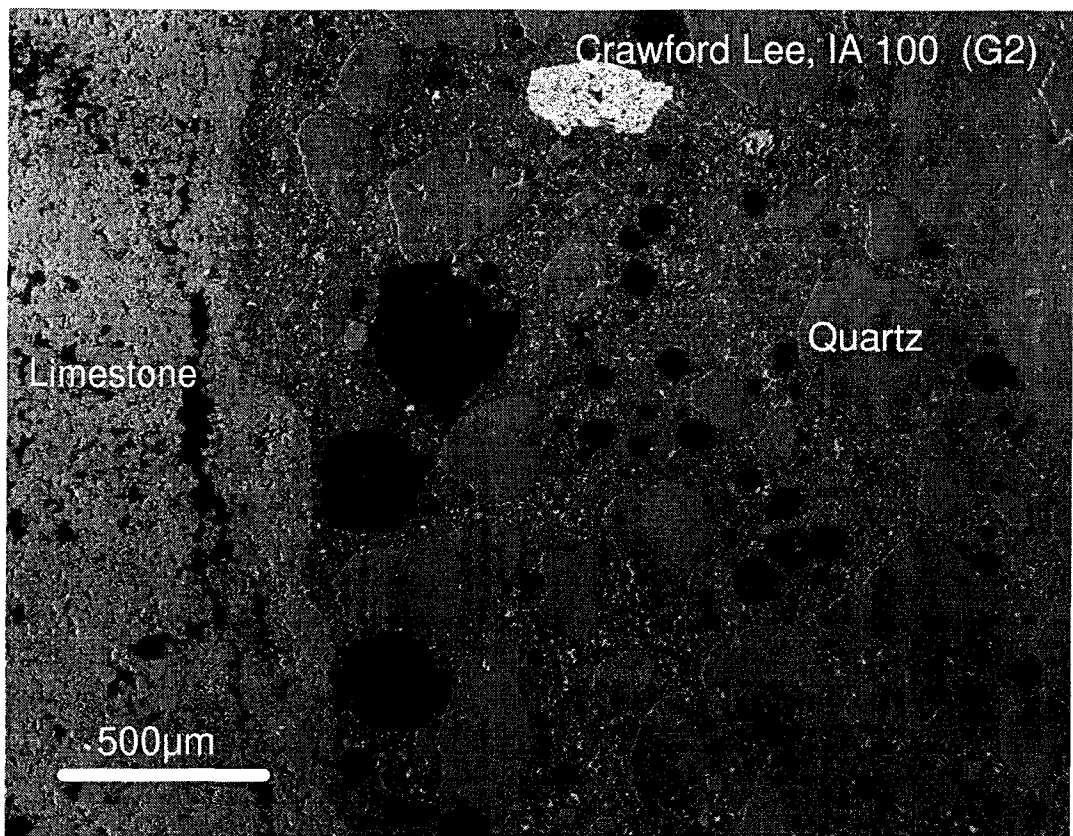


Fig. 8

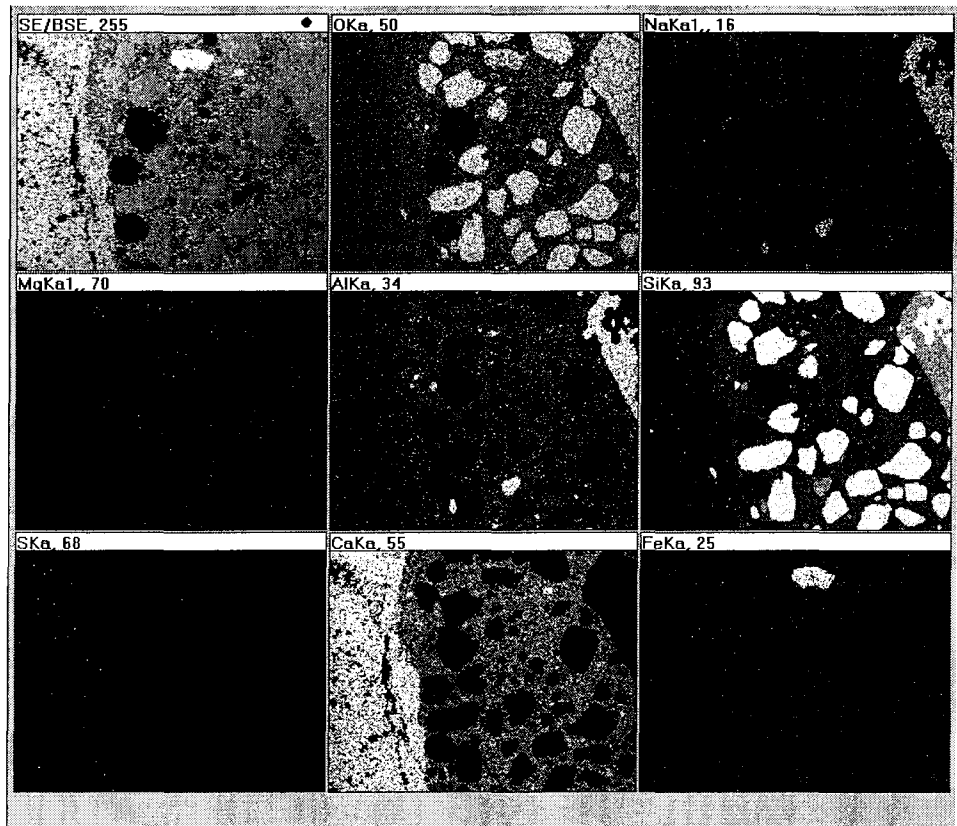


Fig. 9. SEM micrograph and EDAX area maps showing brucite occurrence in the dolomite aggregate and cement paste. Relatively larger, euhedral to subhedral, brucite is present in the calcite-rich matrix of the light-colored cement paste rim (Zone D). The EDAX area maps show that magnesium concentrations correspond to the oxygen concentrations, and verify brucite locations. Larger brucite crystals form in the paste compared to those in the dolomite aggregate interior where only extremely-small white spots are visible in corresponding Mg-O element maps. The extremely small grain size and dissemination along interstitial spaces in dolomite aggregate indicate that most of the brucite in dolomite aggregate interiors may exist as microcrystalline coatings on the surface of dolomite crystals. It can be clearly seen that much calcite accumulated in interstitial voids in the dolomite aggregate and in the reaction rim (zone D) of the cement paste.

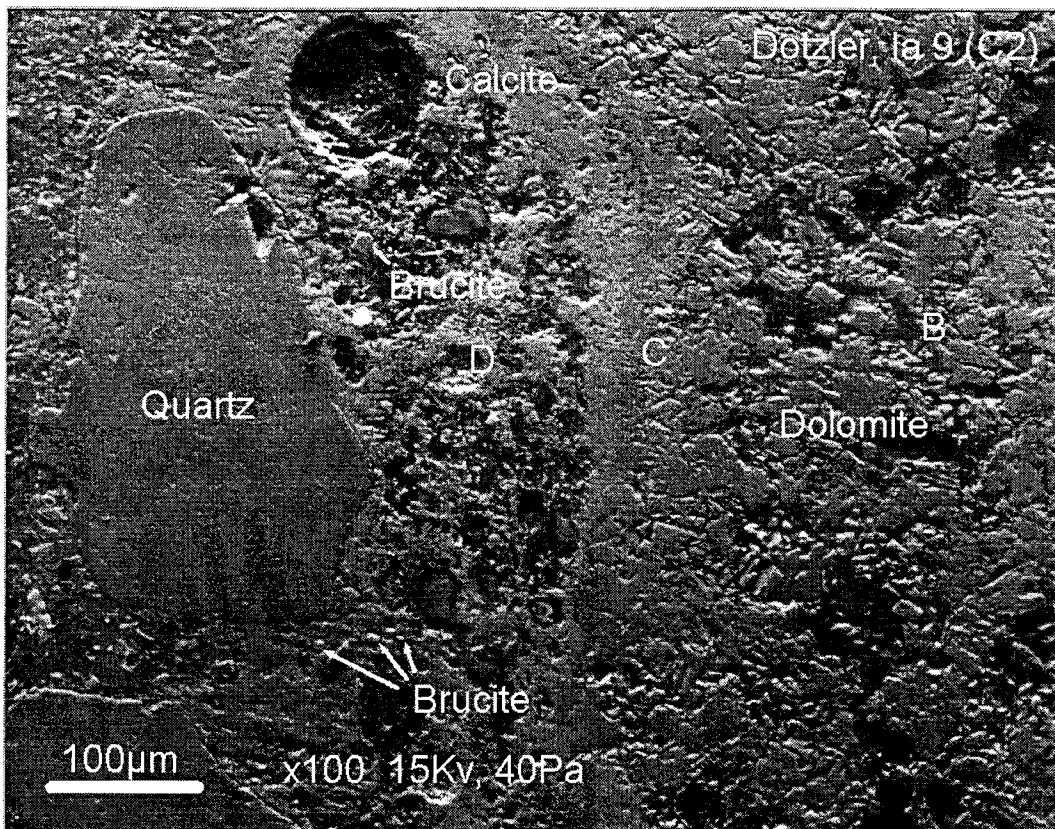


Fig. 9

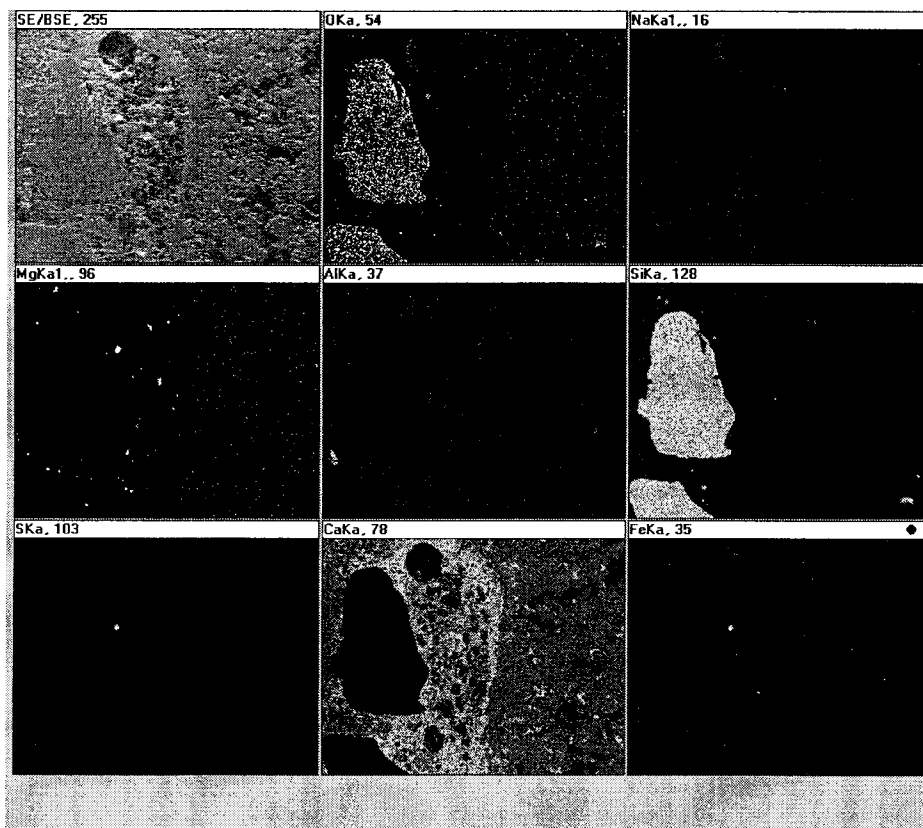


Fig. 10. SEM micrograph and EDAX area maps showing the brucite and ettringite formation in the unaltered cement paste. Small brucite crystals, < 20 μm size, occur in irregular-shaped nodules in the cement matrix. Note that open spaces are developed in the vicinity of brucite. Ettringite completely fills the large air-entrainment voids and interstitial pores in the cement paste. Cracks developed in ettringite and extend into the paste, and probably were caused by ettringite expansion or ice expansion in ettringite-clogged voids. Very small ettringite deposits also occur in the cement matrix.

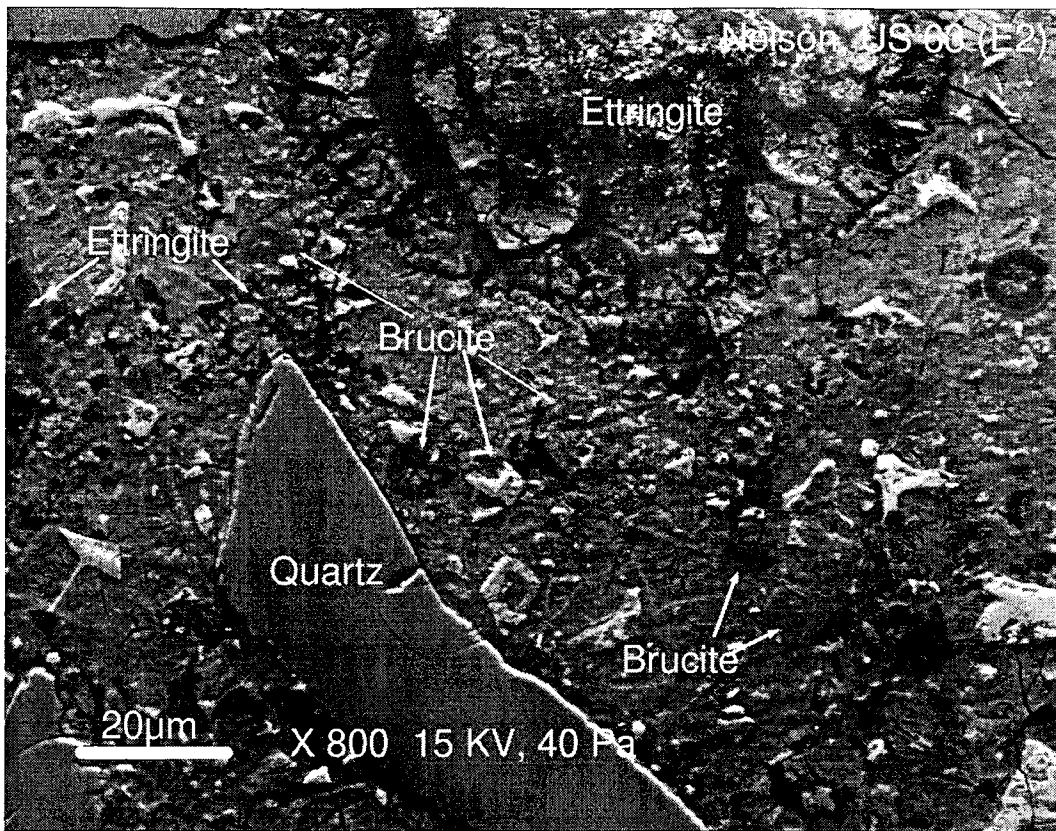


Fig. 10

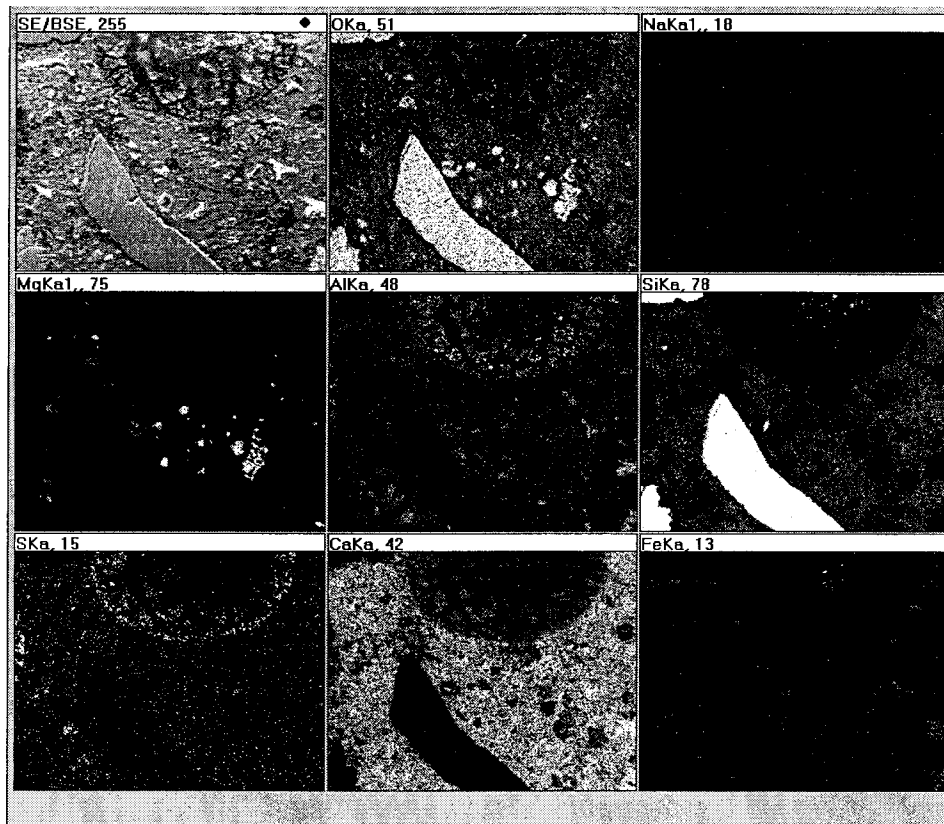


Fig. 11. SEM micrograph and EDAX element maps of ettringite in paste from US

63. An SEM view of acicular ettringite crystals on the wall of an air entertainment void in Iowa highway concrete. Energy-dispersive X-ray analysis of the crystals reveals strong Ca, Al, S peaks which confirm that these crystals are ettringite. The occurrence of a weak Si peak indicates that Si partially substitutes for Al in the ettringite structure.

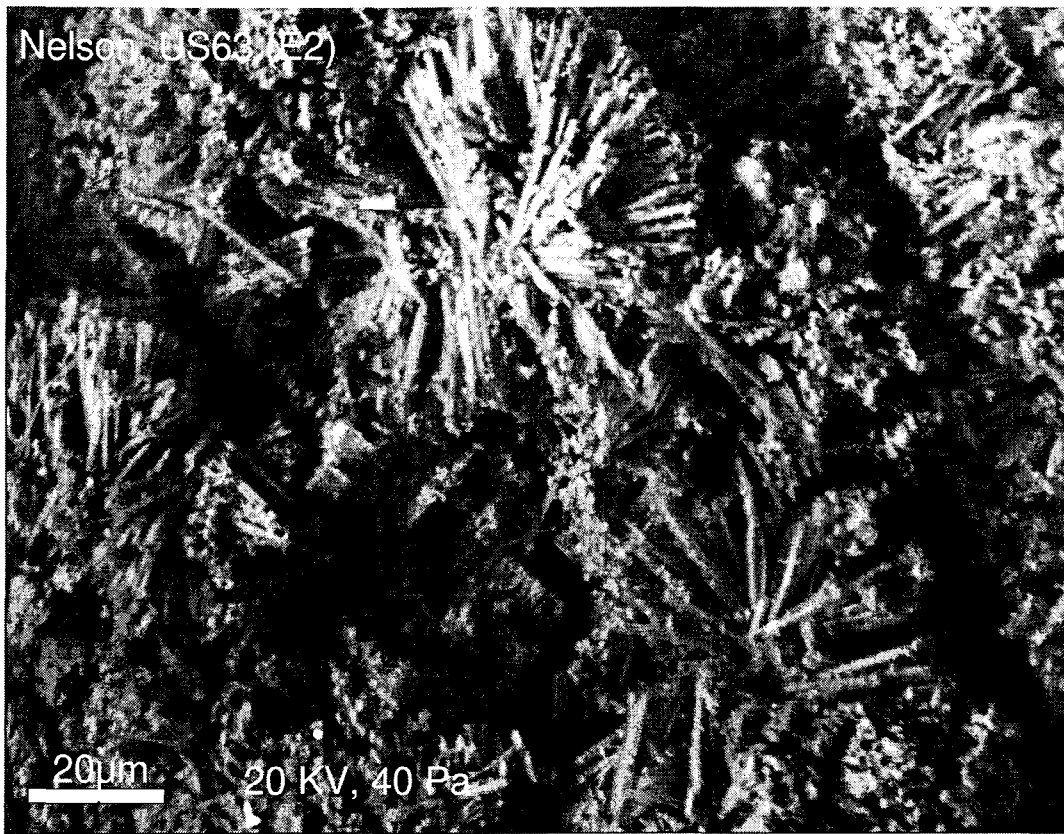


Fig. 11

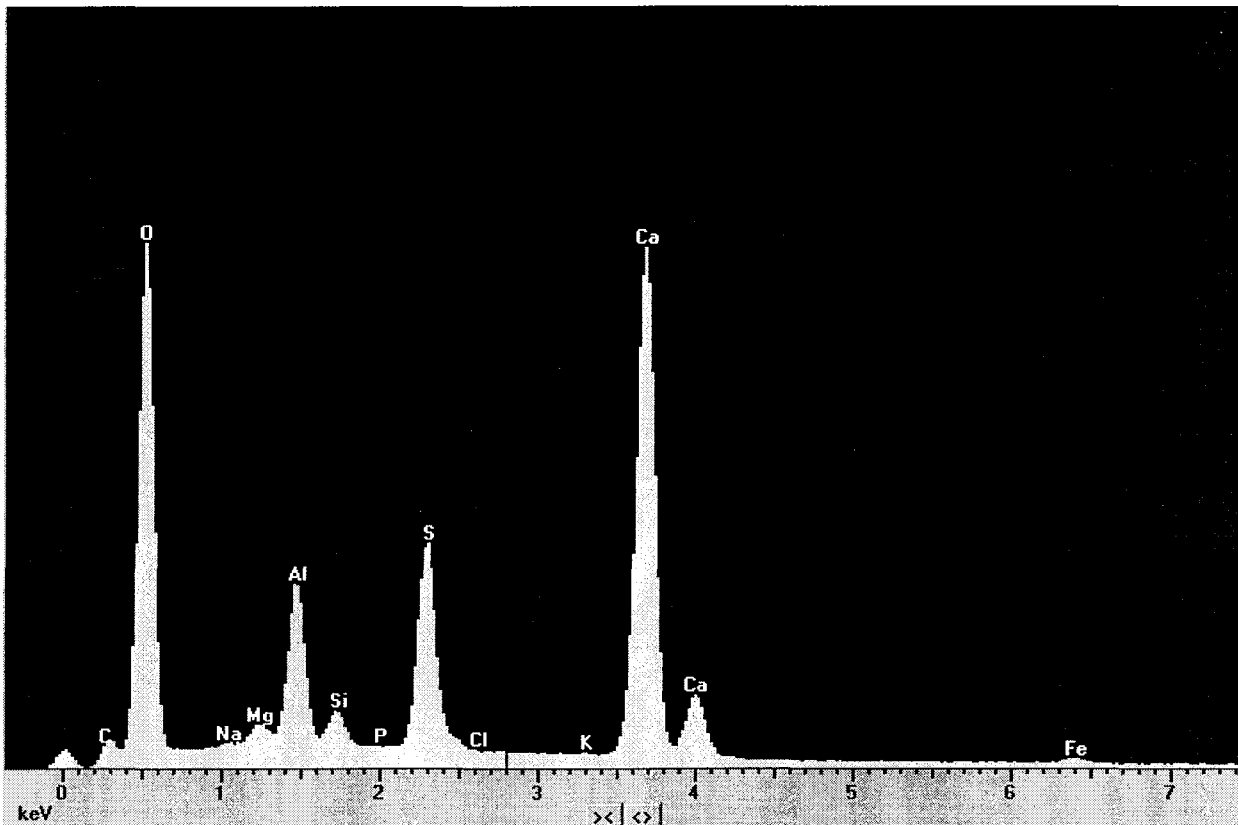


Fig. 12. SEM micrograph and EDAX area maps showing void-fill ettringite in

cement paste. Ettringite completely fills air-entrainment voids ($< 100 \mu\text{m}$) in the cement paste. Irregular disruptive cracks are associated with this type of ettringite. Microcracks propagate outward into the cement paste from the ettringite. Also observable are very small areas of ettringite that formed around residual aluminate particles in the cement matrix.

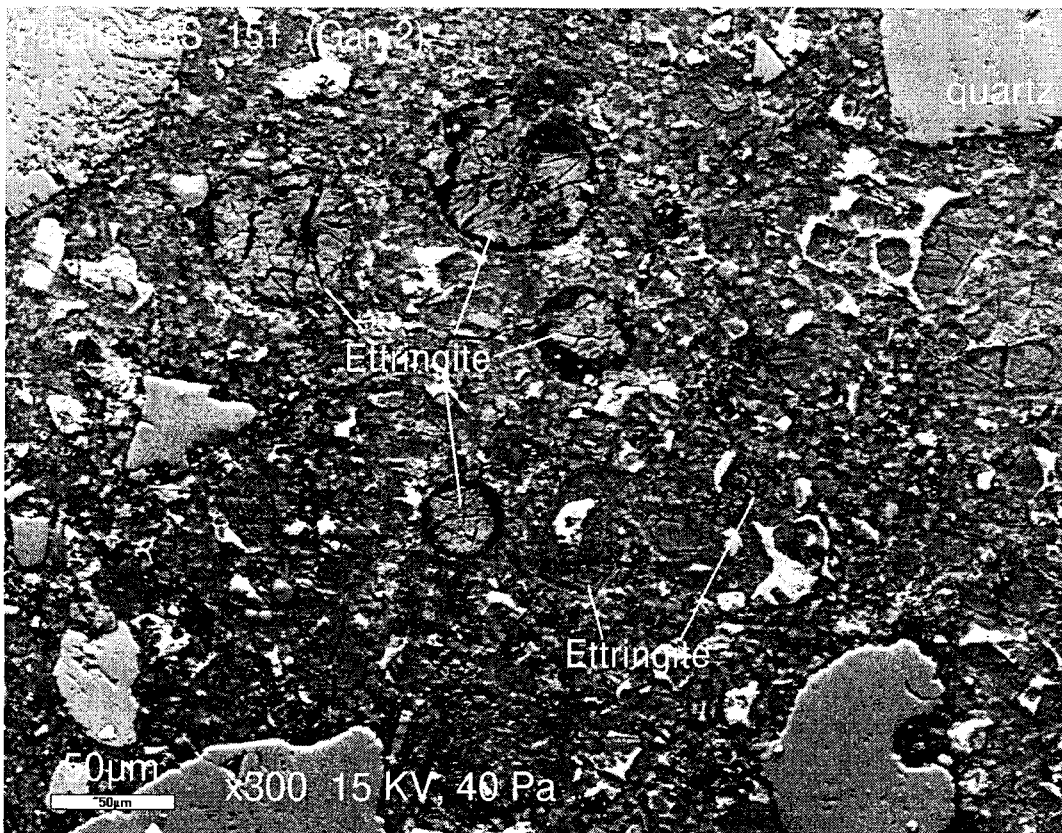


Fig. 12

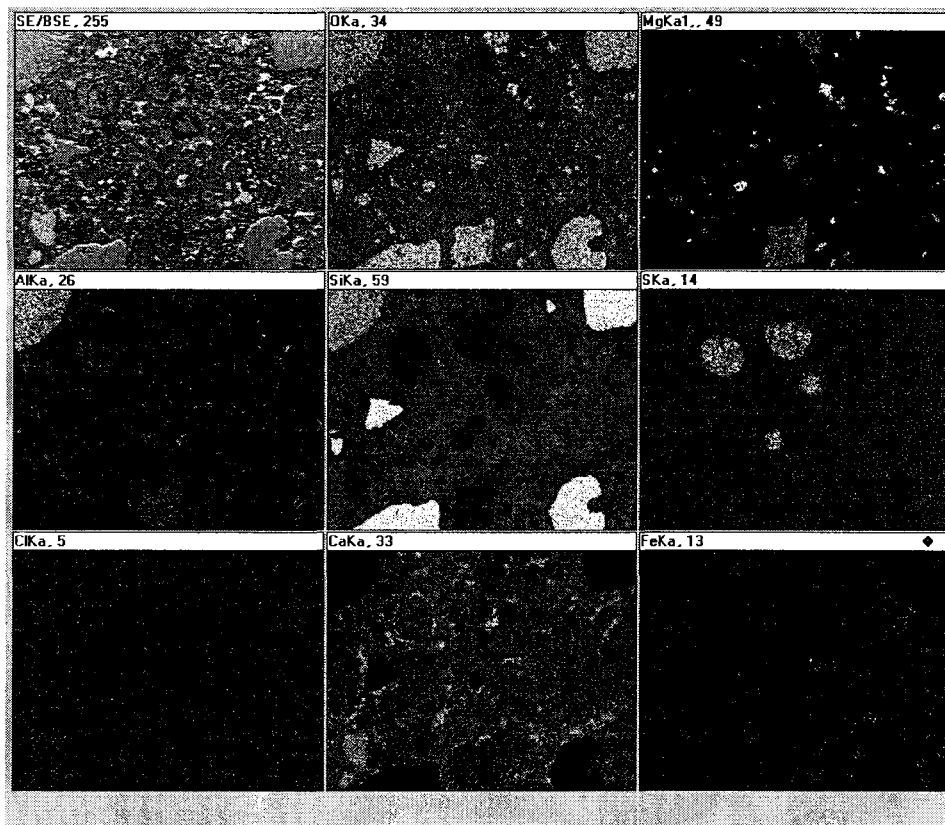


Fig. 13. SEM micrographs showing both void-rim and void-fill types of ettringite in cement paste. Void-rim ettringite occurs as a rim that lines the margin of air-entrainment voids ($>100\ \mu\text{m}$) in the cement paste. Radial cracks are well-developed in this type of ettringite. Void-fill ettringite occurs in small air-entrainment voids ($<100\ \mu\text{m}$), and microcracks propagate out into cement from them.

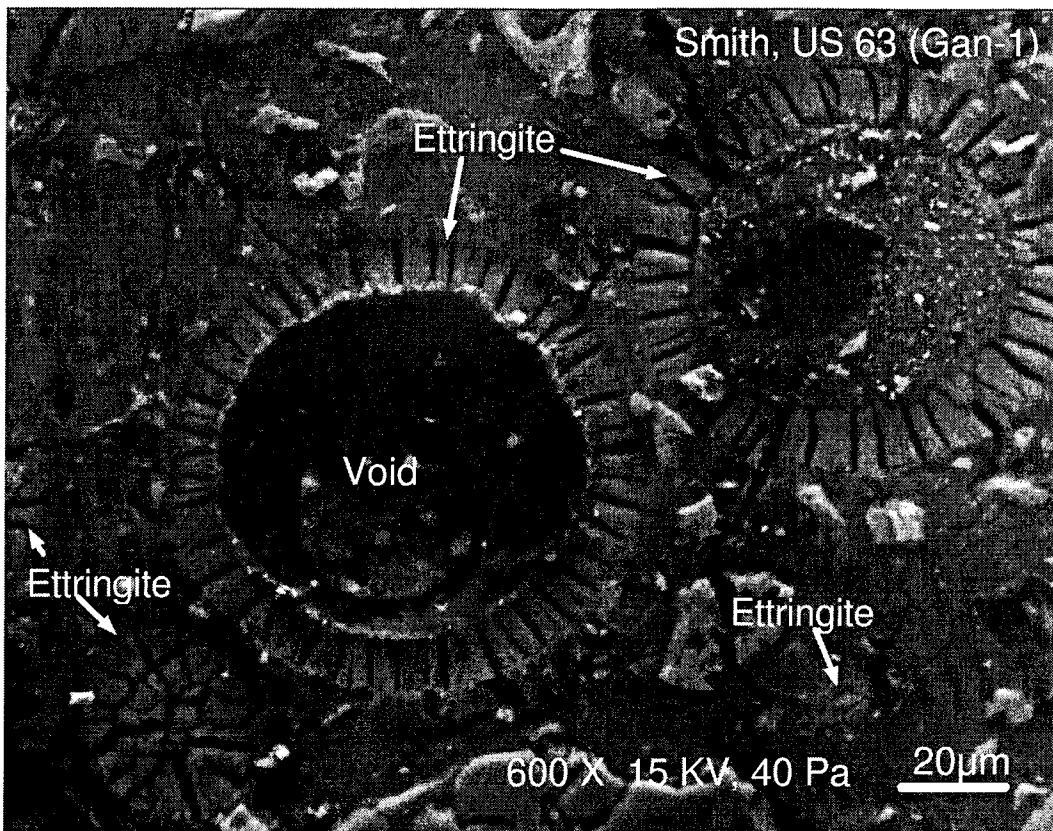


Fig. 13

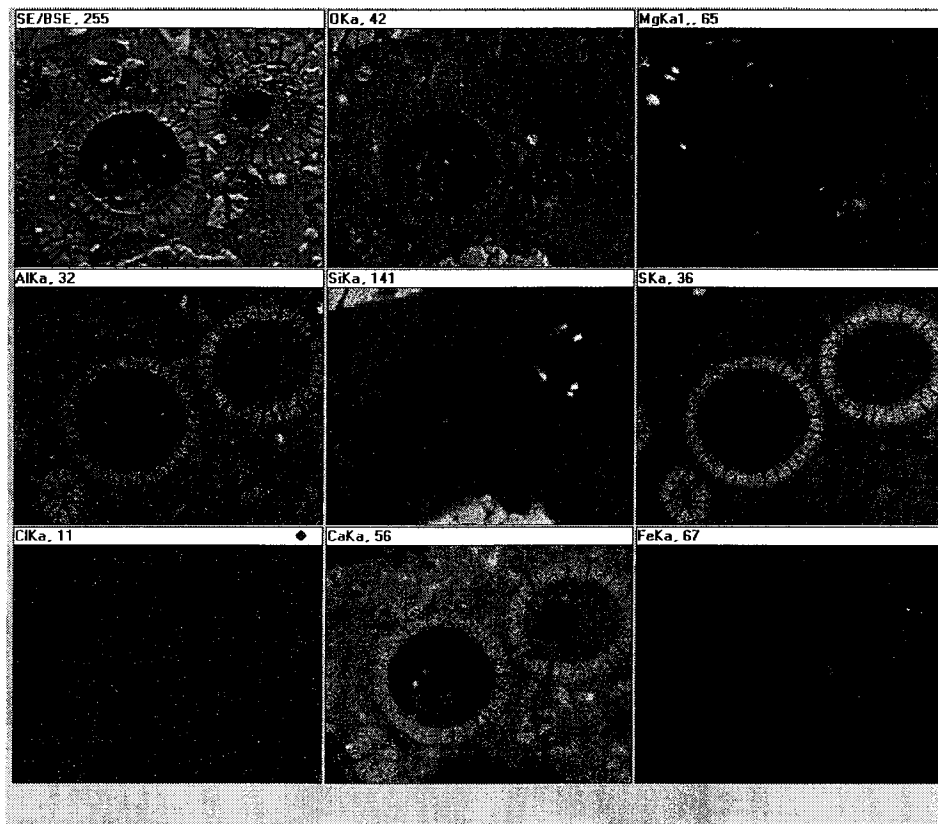


Fig. 14. SEM micrograph and EDAX area maps showing ettringite in pre-existing cracks. Ettringite forms along the pre-existing cracks between quartz aggregate and cement paste. The cracks appear to be formed by expansive alkali-aggregate reaction. Microcracks extend from ettringite into the cement paste.

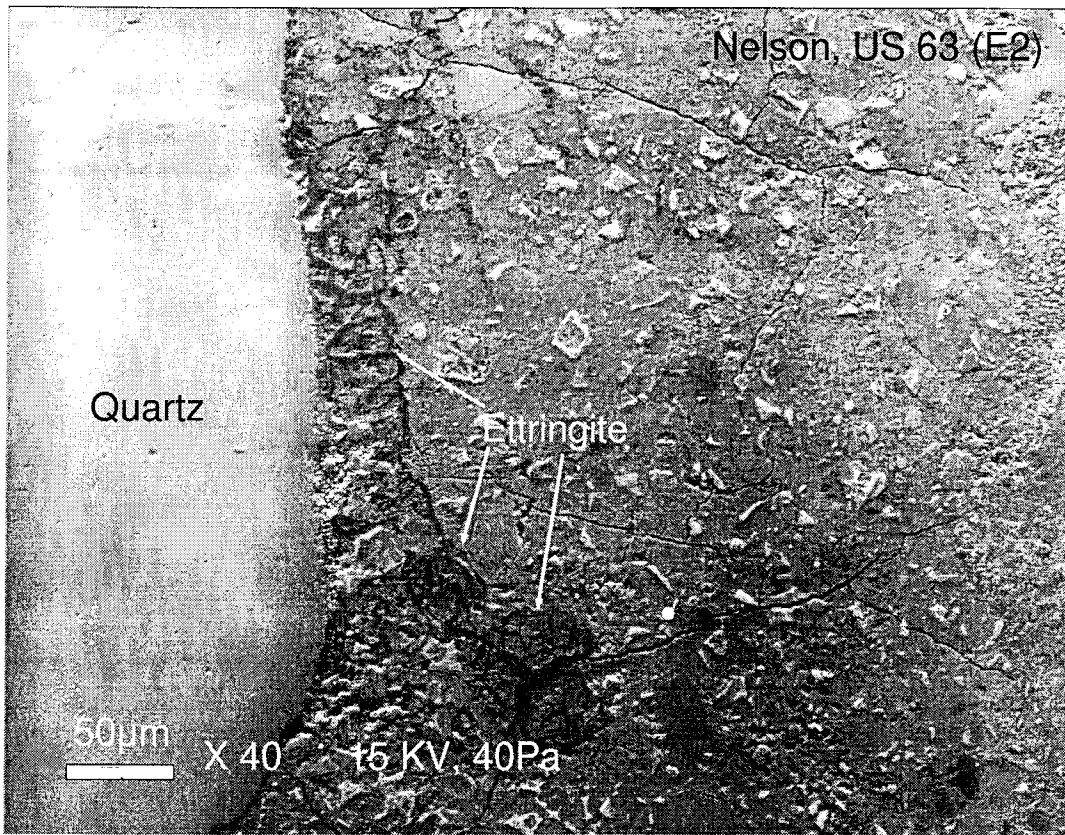


Fig. 14

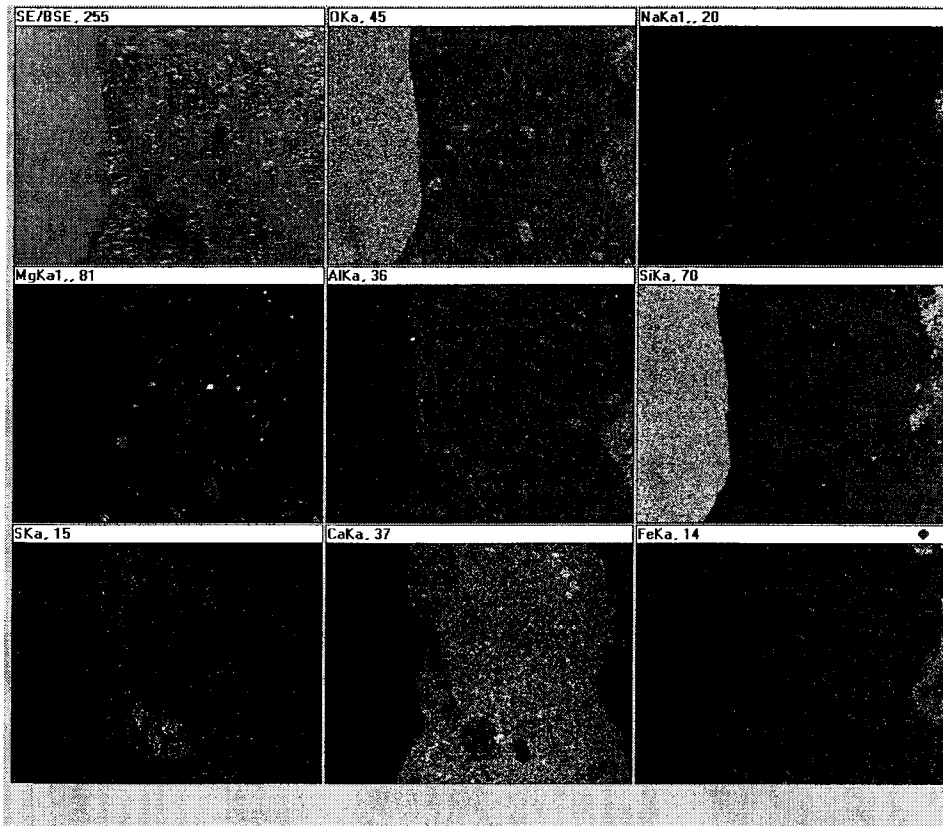


Fig. 15. High magnification SEM micrograph and EDAX area maps showing lack of ettringite in microcracks. The cracks originate at ettringite void fills and rims, and the lack of ettringite accumulation in them indicates that the cracks developed after ettringite formation.

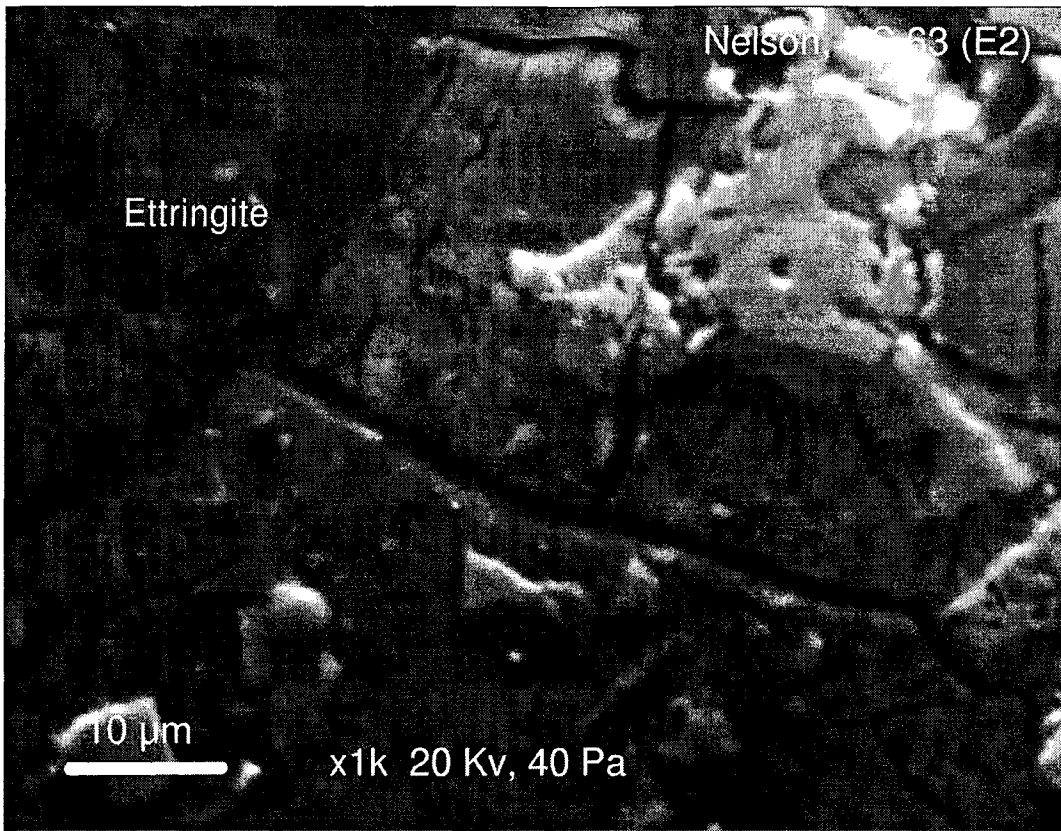


Fig. 15

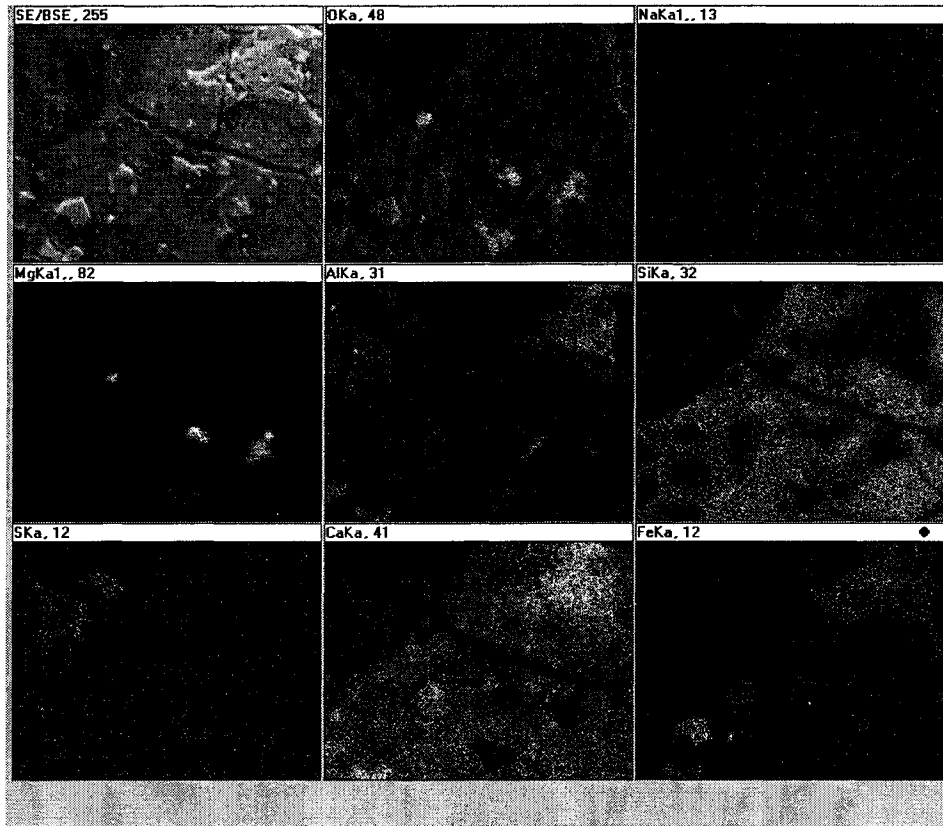


Fig. 16. SEM micrograph and EDAX area maps showing abundant ettringite close to coarse aggregate containing oxidized pyrite inclusions.

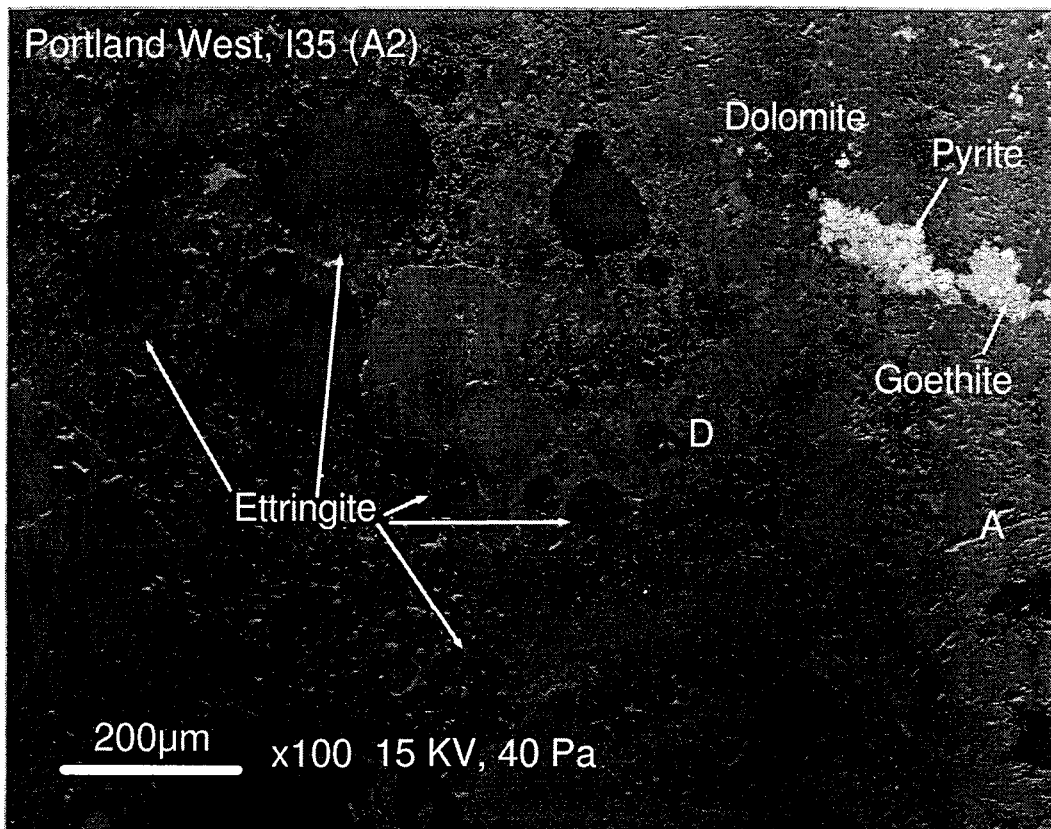


Fig. 16

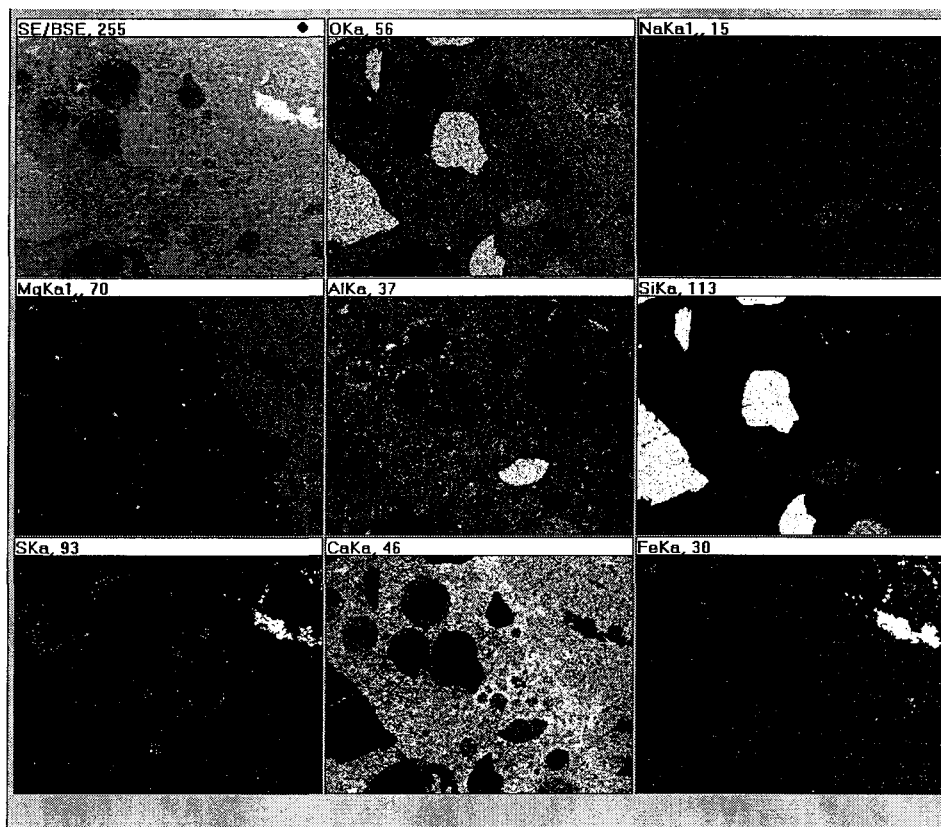


Fig. 17. High magnification SEM micrograph and EDAX area maps showing small ettringite deposits around aluminate particles in cement matrix. This type of ettringite appears to form as a result of a topochemical reaction mechanism between calcium aluminate, CA, and SO_4 pore solutions. No significant microcracks are developed around this type of ettringite.

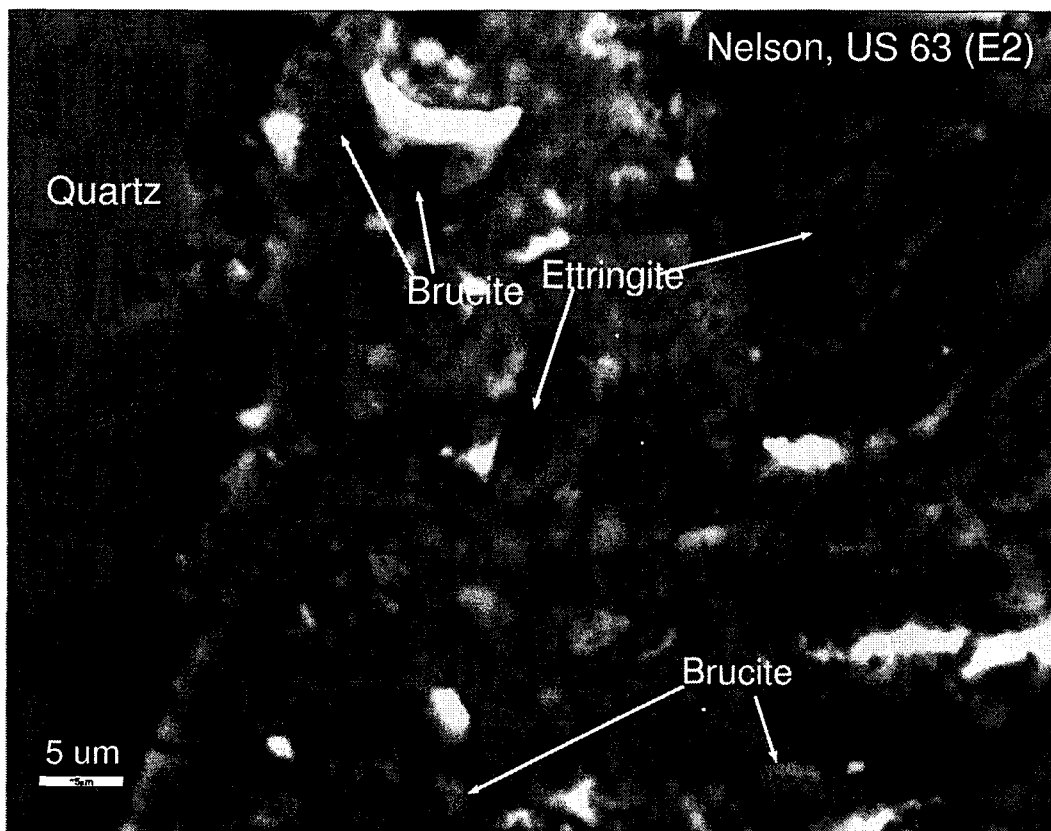
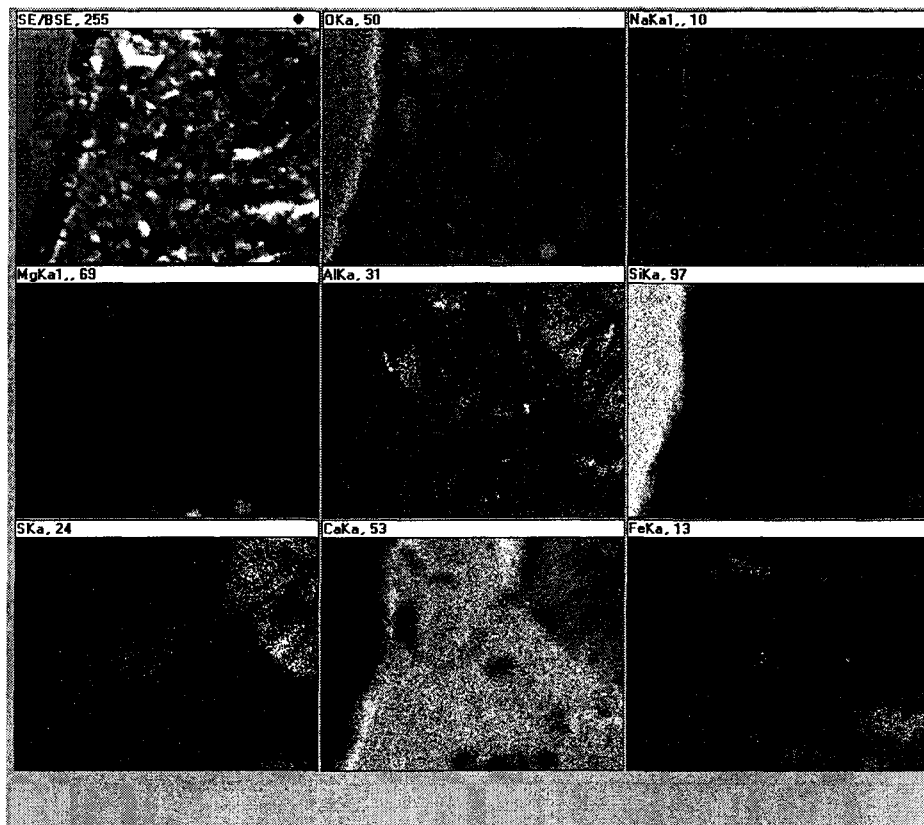


Fig. 17



Appendix II

PLATES AND FIGURES

Experimentally Altered

Iowa Highway Concrete Samples

Plate IV.

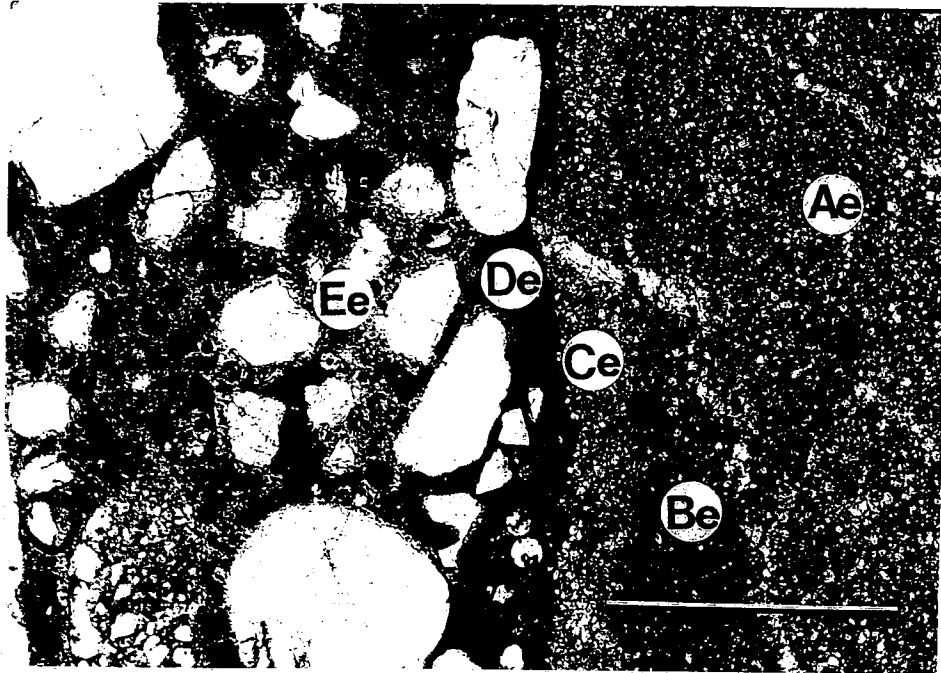
A. Light micrograph showing experimentally-induced deterioration after wet/dry

cycling in CaCl₂, Nelson quarry concrete from US 63. On the right side of the photograph is a reactive dolomite coarse aggregate particle. The dolomite aggregate-paste interface exhibits well-developed dark and light-colored dolomite rims, Zones Be and Ce. The two rims appear similar to, but are much wider than corresponding rims in untreated concrete (See Plate I-A), and have significant differences as shown in Fig. 19 which presents an SEM view and EDAX element maps of corresponding areas. Cement paste Zone, Ee, is strongly discolored. Plane-polarized light, x40. Scale bar = 1 mm.

B. Light micrograph showing experimentally-induced deterioration after

freeze/thaw cycling in MgCl₂, Nelson quarry concrete from US 63. The dolomite aggregate-paste interface exhibits dark and light-colored dolomite rims, Zones Be and Ce. These two rims appear similar to those of untreated concrete (See Plate I-A), but there is a significant difference in characteristics in the light-colored dolomite rims (Zone Be) as shown in Fig. 22 which presents an SEM view and EDAX element maps of the corresponding area. Brucite crystals (br) grow as a thin-lining in the large void space. Plane-polarized light, x40. Scale bar = 1 mm.

PLATE IV.



A



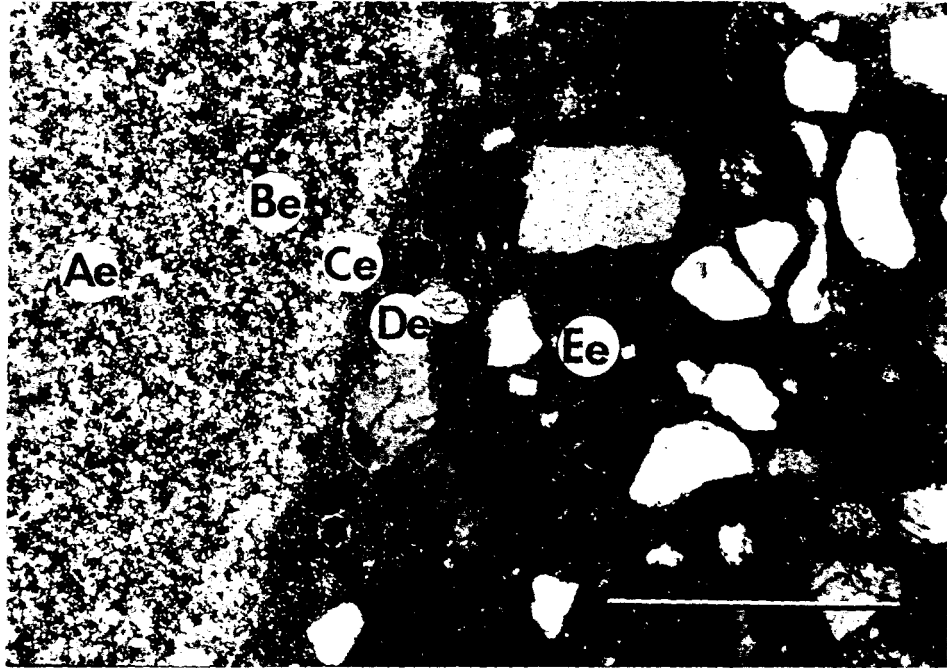
B

Plate V.

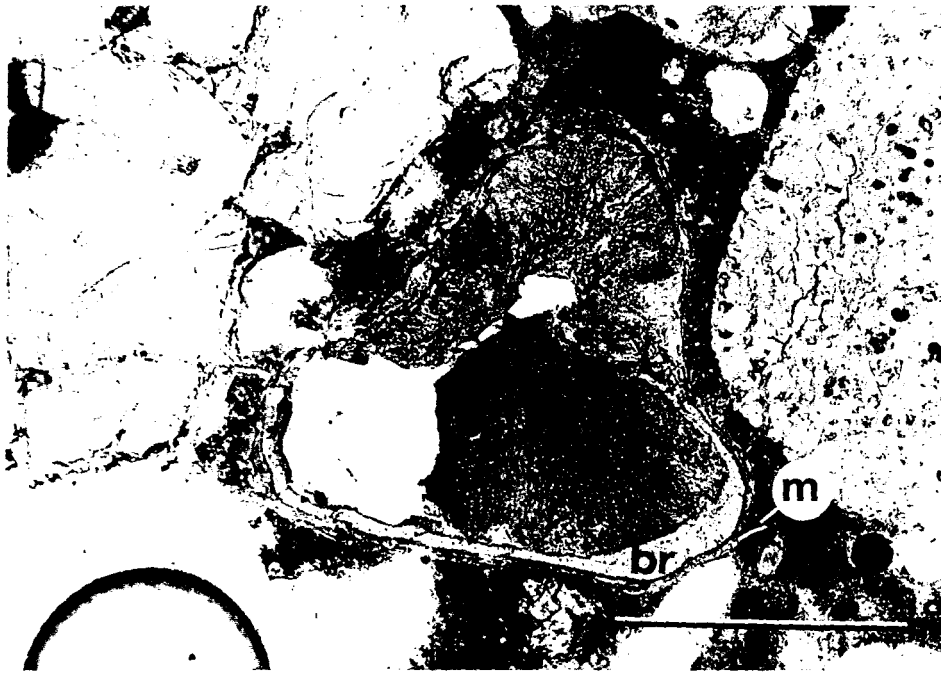
A. Light micrograph showing experimentally-induced deterioration after wet/dry cycling in CMA, Nelson quarry concrete from US 63. The dolomite aggregate-paste interface reaction rims look almost identical to those in MgCl_2 treated concrete (See Plate III-A.), as shown in Fig. 36 of an SEM view and EDAX element maps of the corresponding area. Transmitted light with cross-polarizers, x40. Scale bar = 1 mm.

B. Light micrograph showing secondary mineral growth after freeze/thaw cycling in CMA of Sundheim quarry concrete from US 20. Brucite crystals (br) grow as a thin lining in open spaces, and magnesium silicate hydrate (m) occurs as a thin layer between brucite crystals and the cement paste. Brownish matter, which is a Mg- and Ca- rich microcrystalline phase, fills open spaces (refer to Fig. 37 for an SEM view and EDAX element maps of the corresponding area). We concluded these open spaces occur as a result of debonding of fine aggregate due to formation of non-cementitious magnesium silicate hydrate and brucite at the fine aggregate-cement interface where solution can easily penetrate. Plane-polarized light, x100. Scale bar = 400 μm .

PLATE V.



A



B

Plate VI.

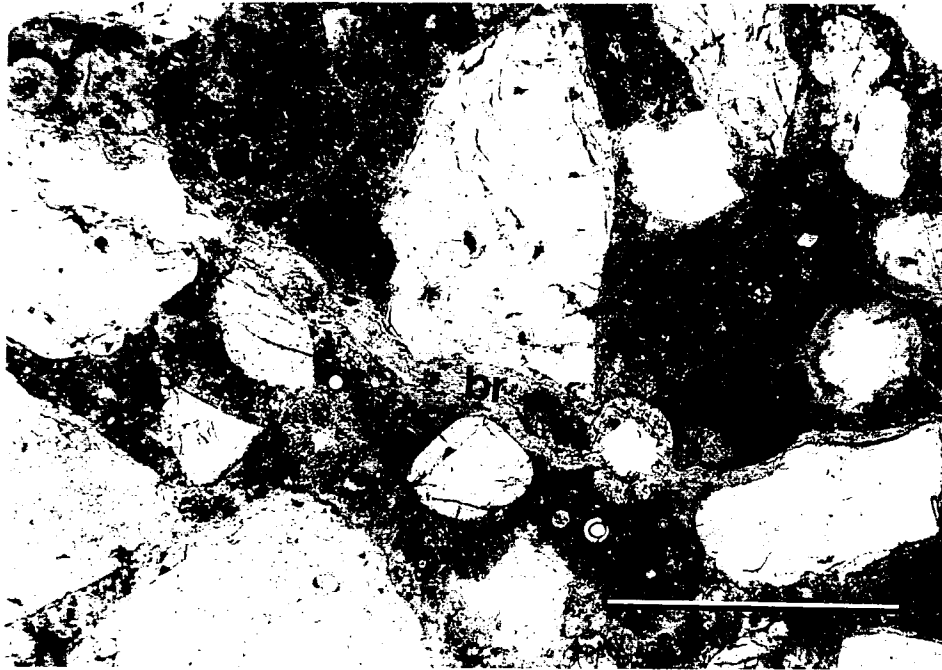
A. Light micrograph showing the crack-filling minerals after wet/dry cycling in

CMA of Sundheim quarry concrete from US 20. Cracks typically form at the boundaries between quartz particles and cement paste, but, in many case, they cut through the quartz. These cracks appears to be generated by dissolution of cement paste as CMA solution penetrates along the boundary spaces. Refer to Fig. 39 for EDAX element maps of the corresponding area, and for further discussion. Plane-polarized light, x100. Scale bar = 400 μm .

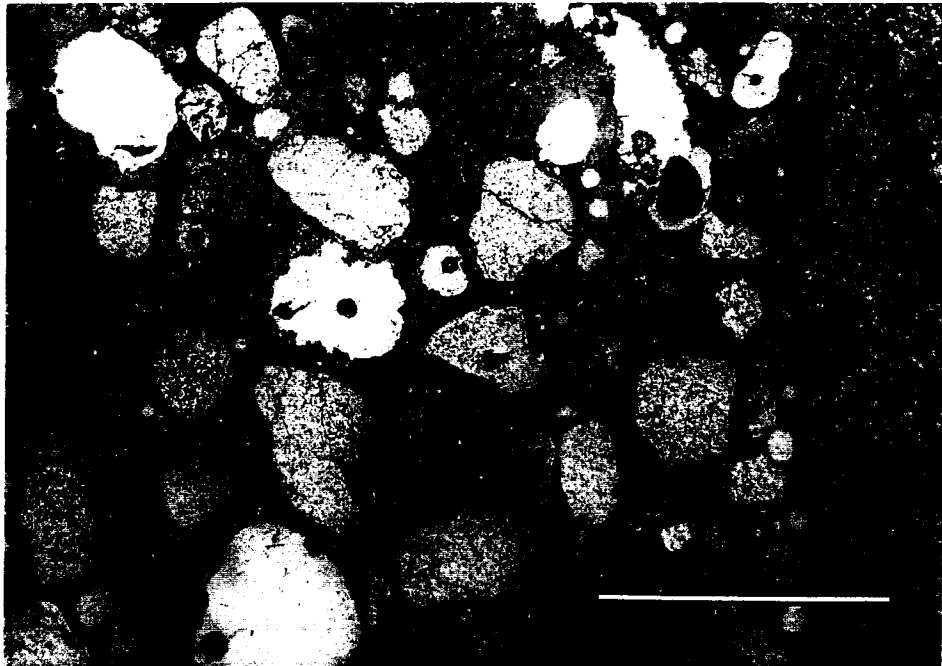
B. Light micrograph showing experimentally-induced deterioration after wet/dry

cycling in Na_2SO_4 of Sundheim quarry concrete from US 20. The cement paste is discolored. Refer to Fig. 32 for an SEM view and EDAX element maps of corresponding area and for further discussion. Reflected light, x40. Scale bar = 1 mm.

PLATE VI.



A



B

Fig. 18. SEM micrograph and EDAX area maps showing results of freeze/thaw cycling in H₂O of Nelson quarry concrete from US 63. Very few effects can be detected, but pre-treatment reaction rims appear to be slightly broadened in some samples. No new brucite was detected in the light-colored dolomite and light-colored paste rim Zones Ce and De.

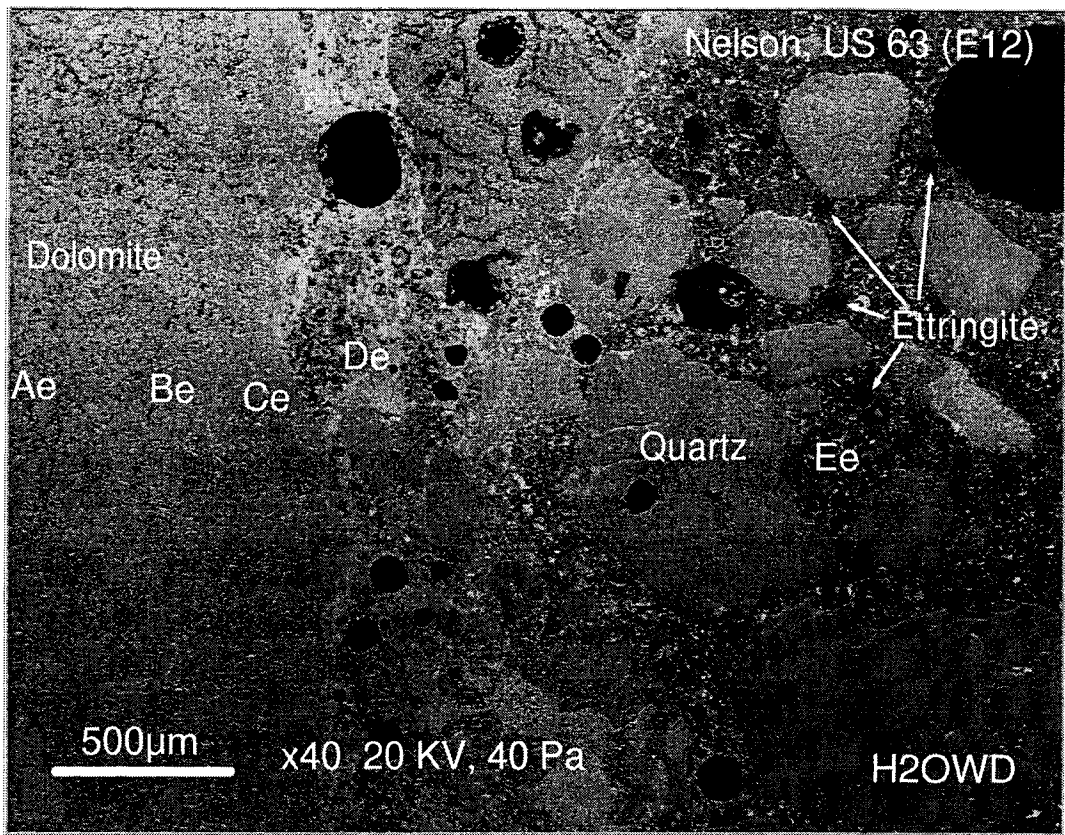


Fig. 18

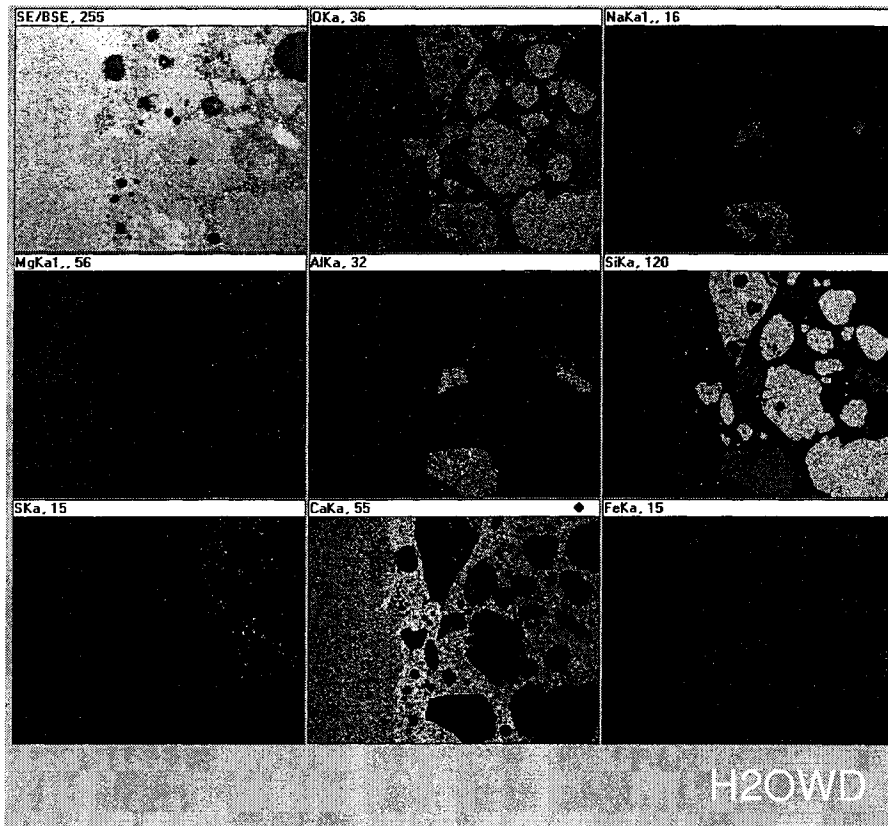


Fig. 19. SEM micrograph and EDAX area maps showing experimentally-induced deterioration after wet/dry cycling in CaCl_2 of Nelson quarry concrete, US 63.

These images include the corresponding area shown in Plate IV-A. The dark-colored Zone Be and light-colored dolomite rim Zone Ce, are apparent at the margins of coarse aggregate. EDAX element maps show a decrease in Ca and significant Mg concentration indicating brucite formation in the new light-colored dolomite rim (zone Ce). No significant brucite occurs in the old rim (zone C) in untreated concrete (See Fig. 2 for comparison). Significant Cl concentrations are present in the discolored cement paste (Zone Ee).

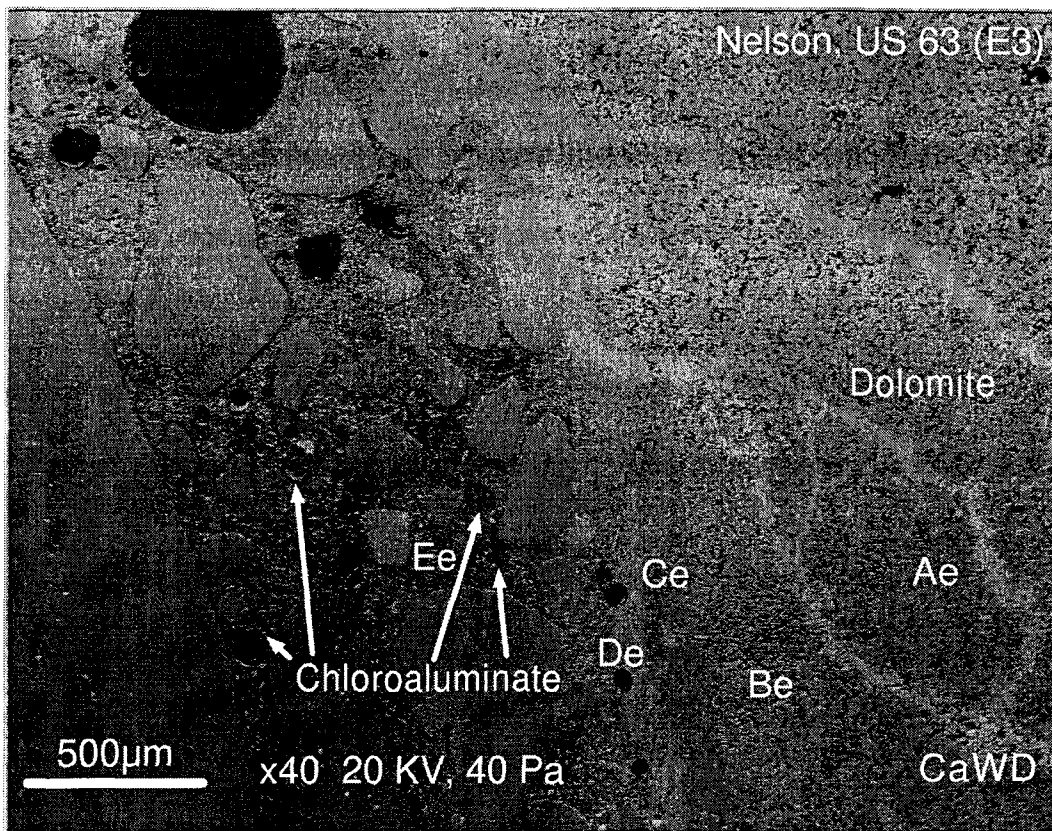


Fig. 19

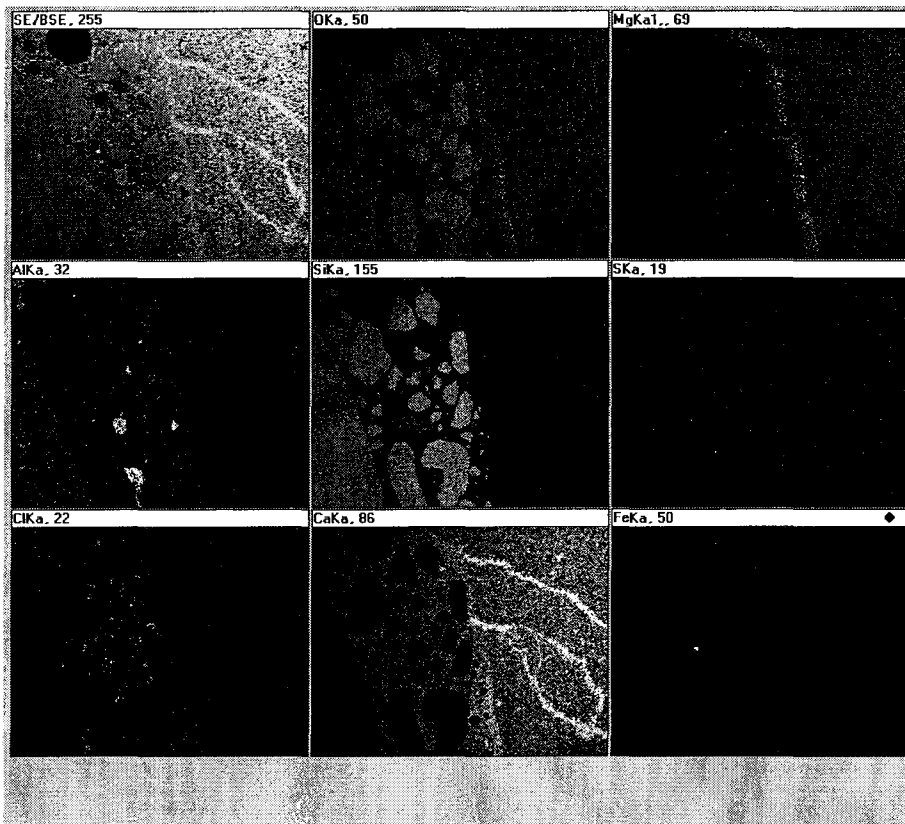


Fig. 20. SEM micrograph and EDAX element maps showing an enlarged area of Fig. 19.

Abundant brucite precipitated in the interstitial voids of the light-colored dolomite rim.

In air entrainment voids, areas rich in Ca, Al, and Cl probably are chloroaluminate. The

limited S concentrations at the margins of air-entrainment voids indicate that

chloroaluminates have replaced ettringite which occurs abundantly in untreated

concrete voids (See Fig. 2 for comparison).

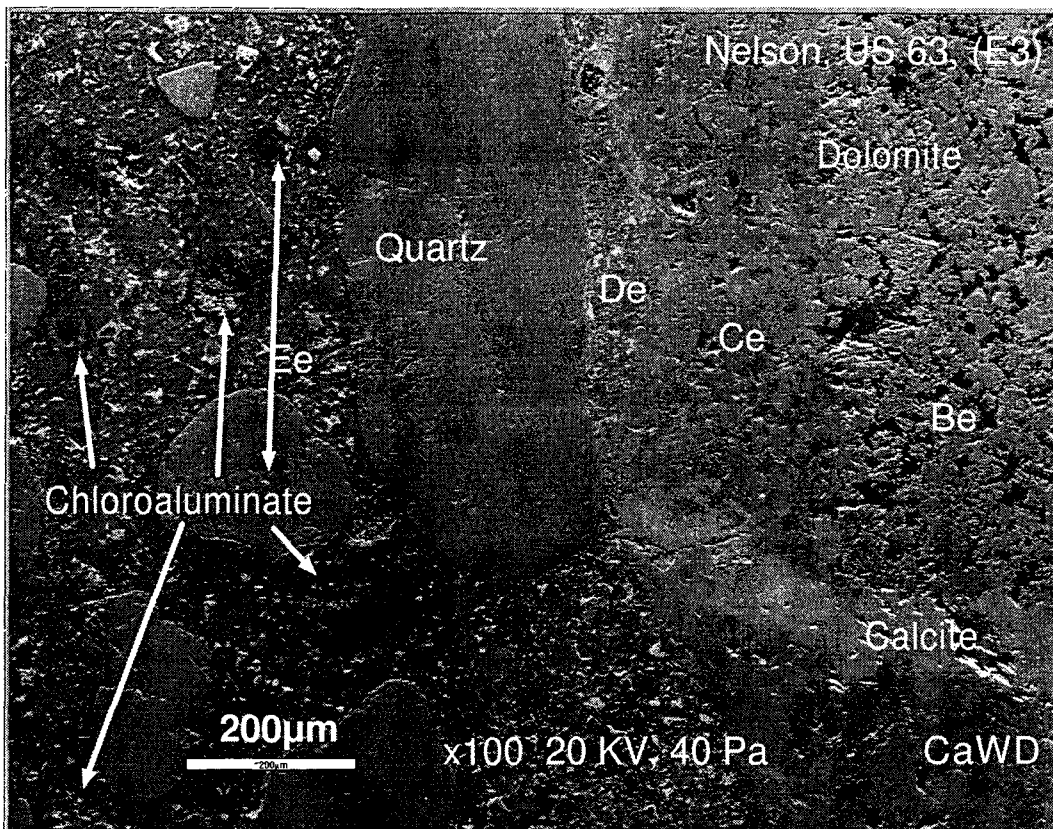


Fig. 20

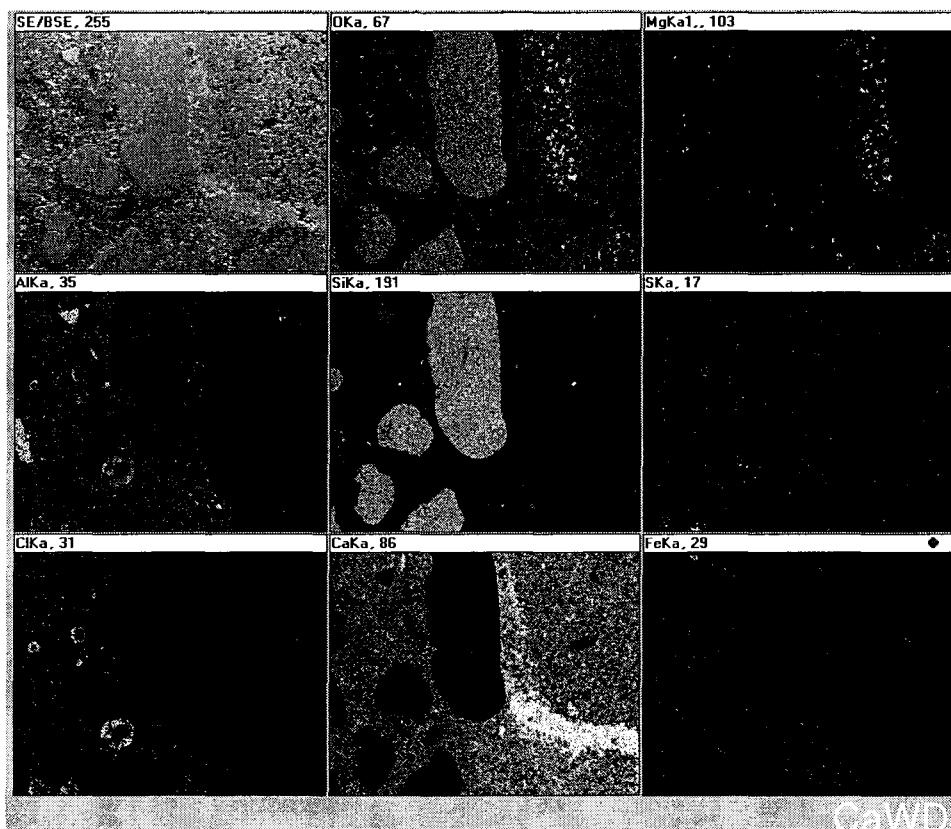


Fig. 21. SEM micrograph and EDAX area map showing experimentally-induced alteration of Sundheim quarry concrete from US 20 after wet/dry cycling in CaCl_2 . No reaction rims, either pre- or post-treatment are visible in the dolomite at the interface with the cement. Large concentrations of Cl and increased Ca are present in the cement paste (Zone Ee) as a result of soaking, but otherwise, the experiments failed to produce visible changes in this durable concrete.

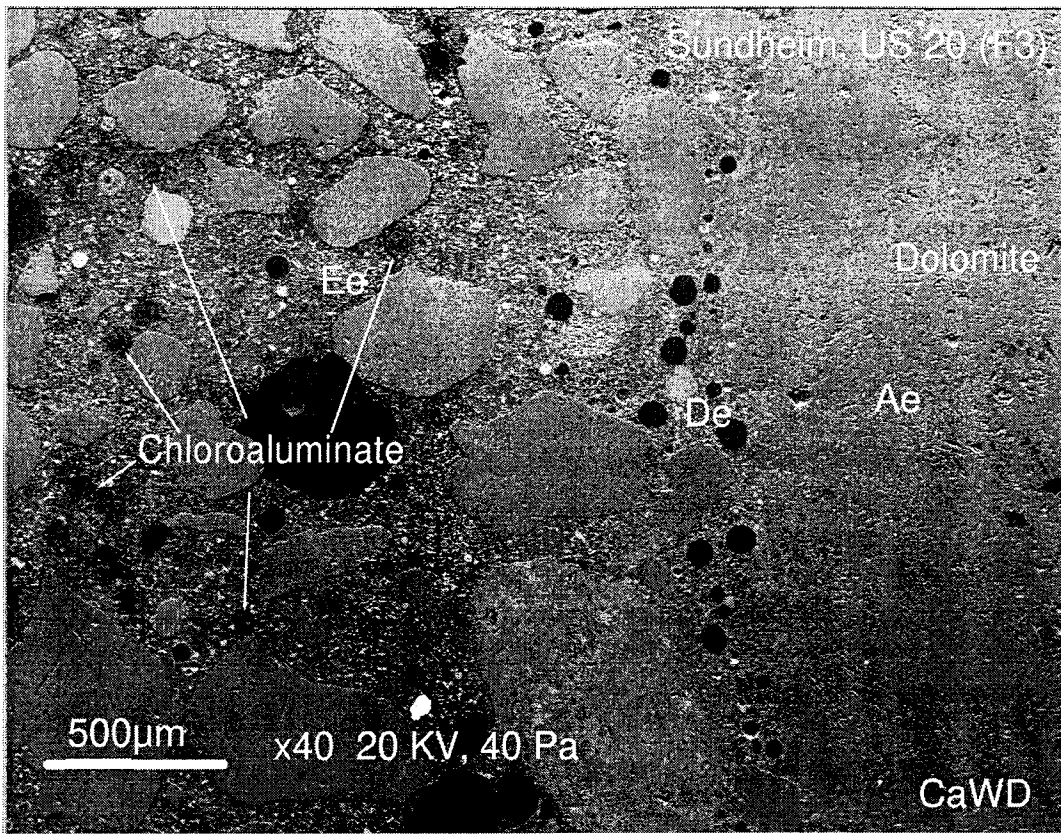


Fig. 21

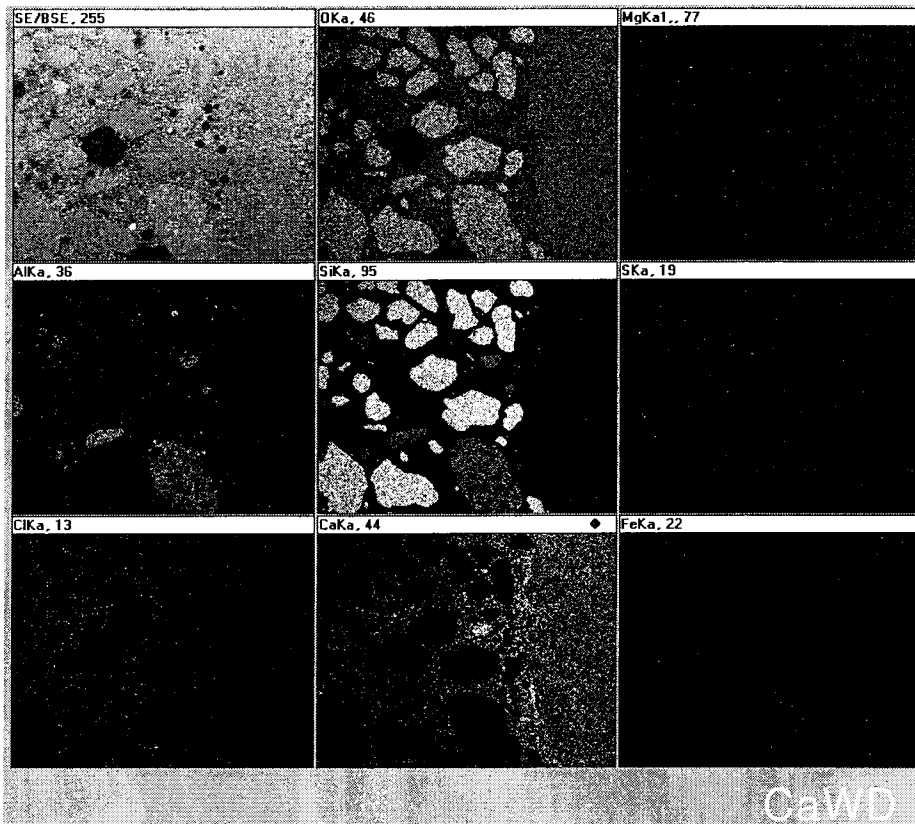


Fig. 22. SEM micrograph and EDAX area maps showing experimentally-induced deterioration of Nelson quarry concrete from US 63 after freeze/thaw cycling in $MgCl_2$. The images includes the corresponding area of Plate IV-B. Dark and light-colored dolomite rims Zones Be and Ce are well developed at the aggregate-paste interface. Significant Mg concentrations indicate that interstitial brucite precipitated in the light-colored dolomite rim Zone Ce as a result of the experimental treatment. No significant amounts of brucite occur in the untreated rim Zone C (See Fig. 2 for comparison). Brucite (Br) in the air void is shown as bright white spots in Mg and O maps. A thin layer of Ca-rich material indicates calcite (Cal) which precipitated at the outer and inner margins of the brucite rim which lines the air void. Increased Mg concentration in the cement paste is probably due to the formation of magnesium silicate hydrate (MSH) as well as brucite.

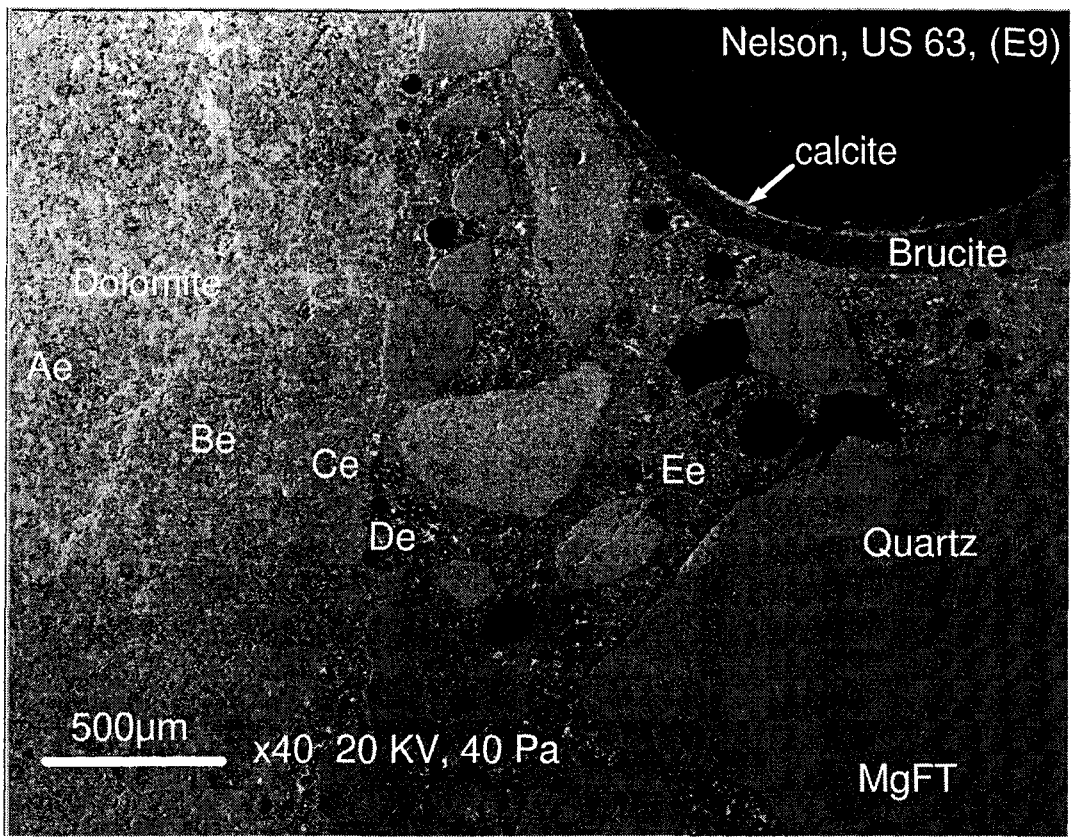


Fig. 22

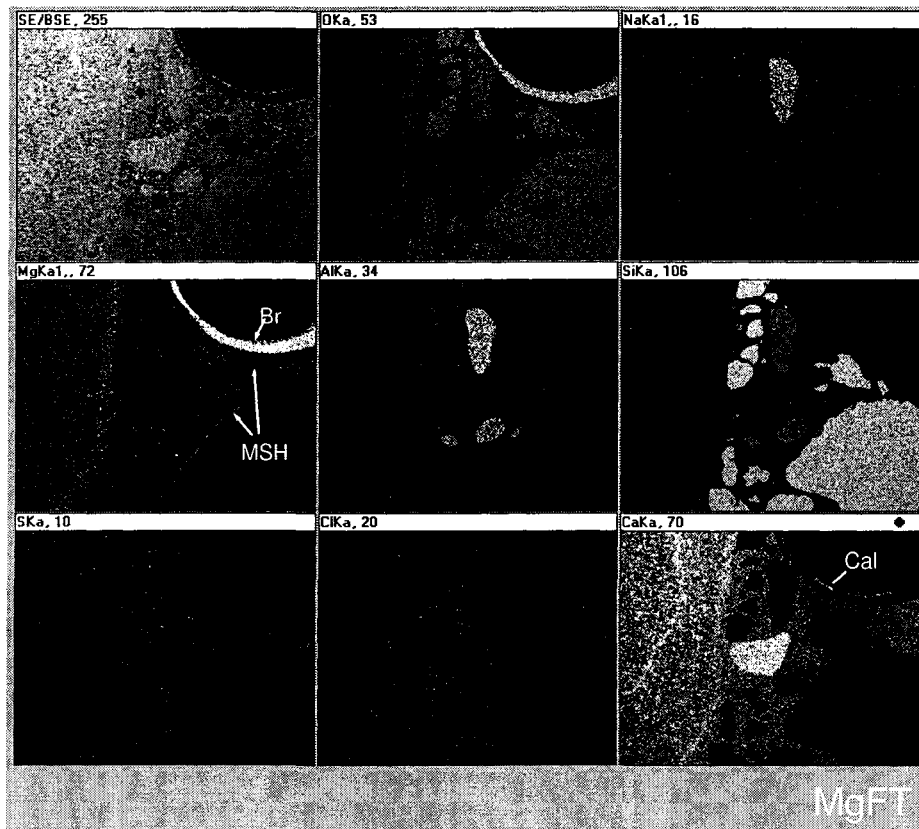


Fig. 23. SEM micrograph and EDAX element maps showing the aggregate-paste interface in Nelson quarry concrete from US 63 after wet/dry cycling in $MgCl_2$. The light-colored dolomite rim, Zone Ce, is absent. After treatment, the reaction rims are similar to rims of untreated concrete. A layer of brucite is seen in a void and calcite formed at the interface between brucite and the cement paste. EDAX element maps show that Mg concentration is elevated and Ca concentration is depleted in the cement paste. This indicates the alteration of calcium silicate hydrate, CSH, to magnesium silicate hydrate, MSH, in the cement. Note that the light-colored paste rim has not changed to MHS. Paste cracking and debonding of fine aggregate also occurred during wet/dry cycling.

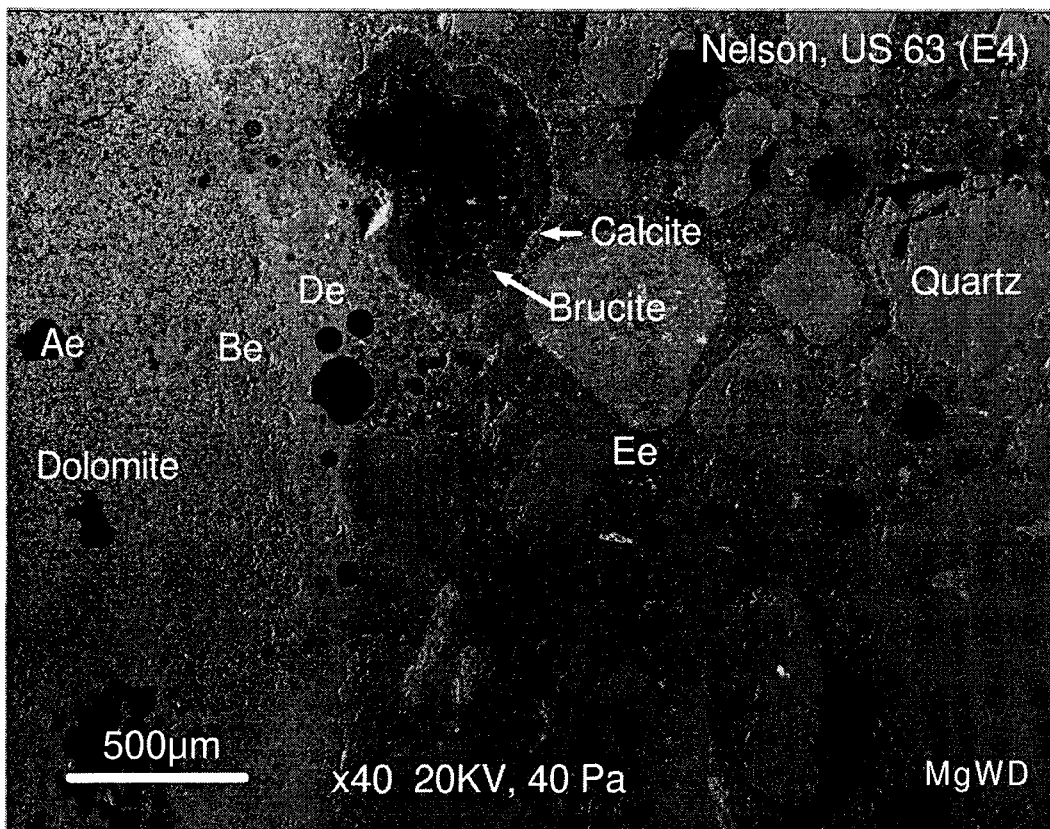


Fig. 23

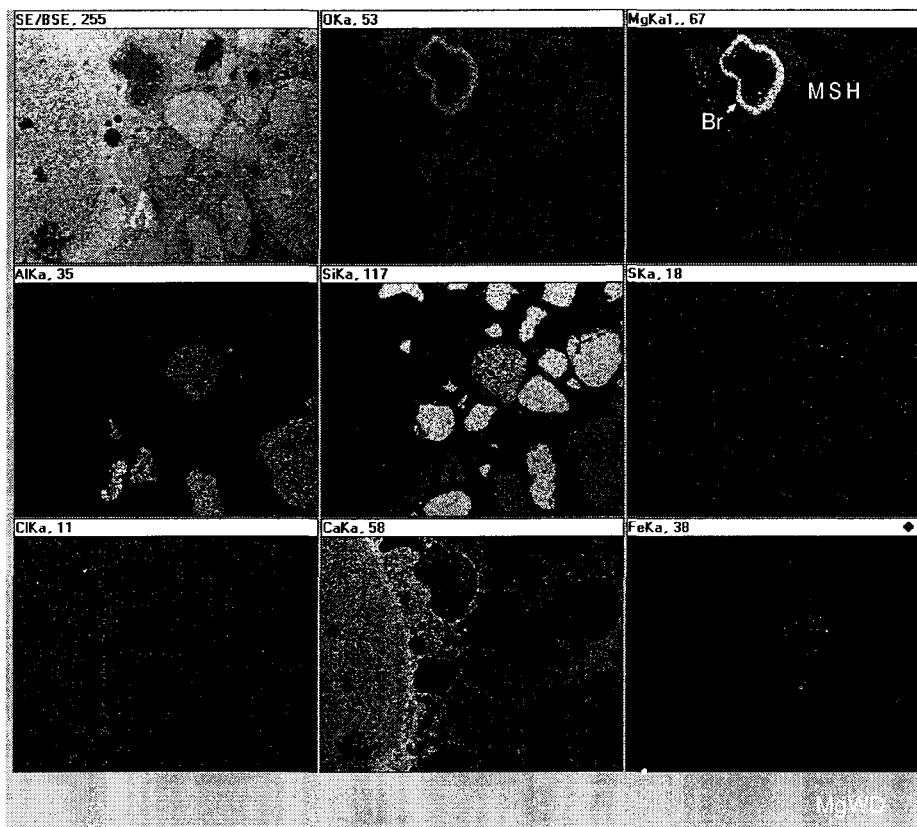


Fig. 24. SEM micrograph and EDAX area maps showing cement paste deterioration after wet/dry cycling in $MgCl_2$ of Nelson quarry concrete from US 63. In these images, several experimentally-induced features are evident. CSH in the cement paste was altered to MSH. Many shrinkage cracks developed in the MSH-enriched cement. Fine aggregate at the surface of the sample was debonded and separated from the cement paste because of the formation of non-cementitious MSH. Minerals of various compositions formed in many air entrainment voids. Voids in the less severely changed paste are filled with material rich in Ca, Mg, Al, and S, and with minor amounts of Si and Cl. This material is marked with 'B'. Voids in MSH are filled with material rich in Mg and O, and is marked with 'A'.

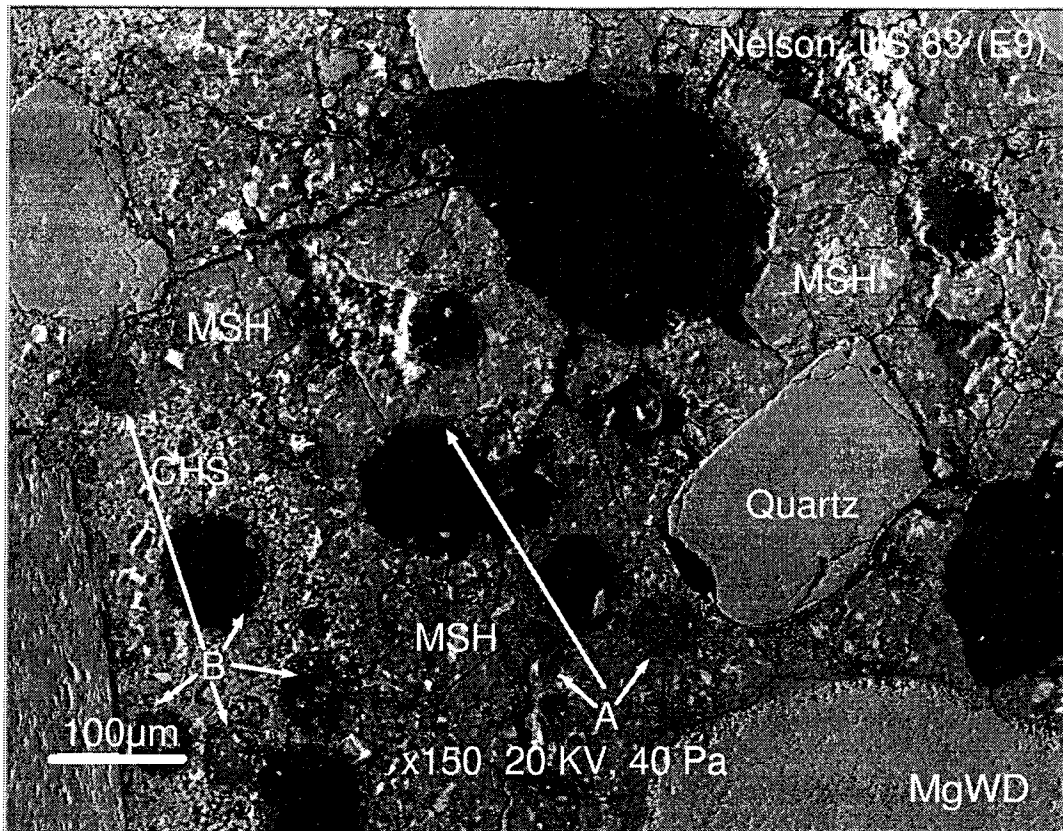


Fig. 24

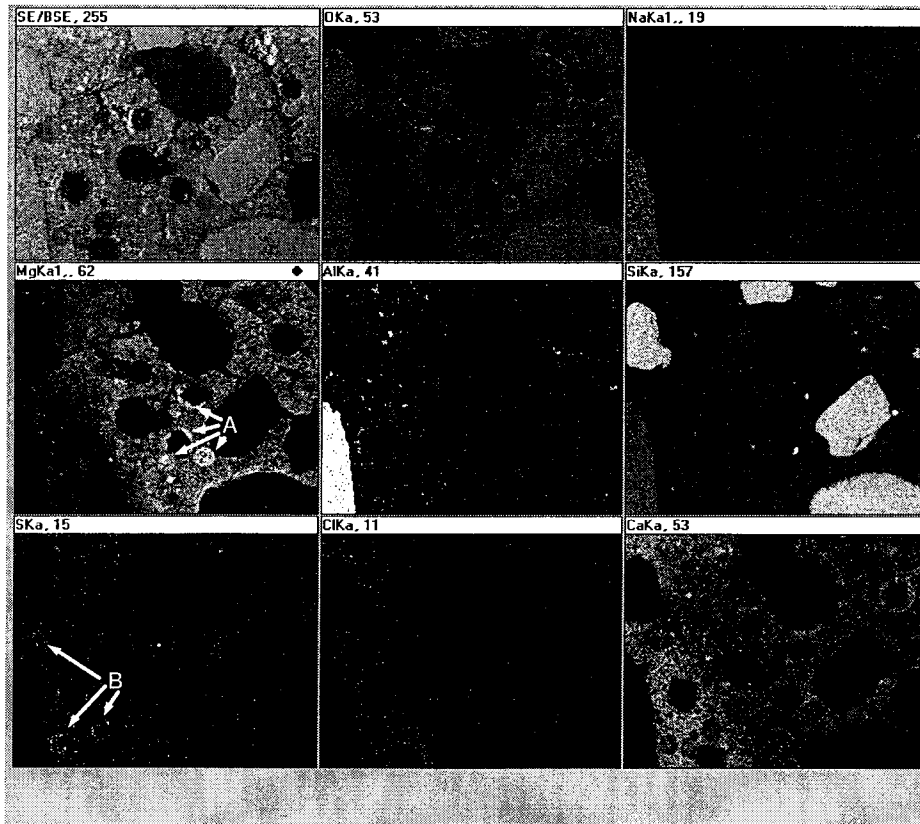


Fig. 25. High magnification SEM and EDAX maps showing MSH features in cement paste.

Abundant shrinkage cracks developed in the MSH as a result of experimental wet/dry cycling in MgCl_2 , and especially wide cracks formed at the boundary between quartz particles and cement paste. EDAX element maps and points analysis (Fig. 26) indicate that CSH in cement paste completely changed to MSH. Calcium released by MSH formation migrated into open spaces and precipitated as calcite. Mg-, Al-, and Cl-rich material with minor Si, marked as 'MACL' formed in air voids.

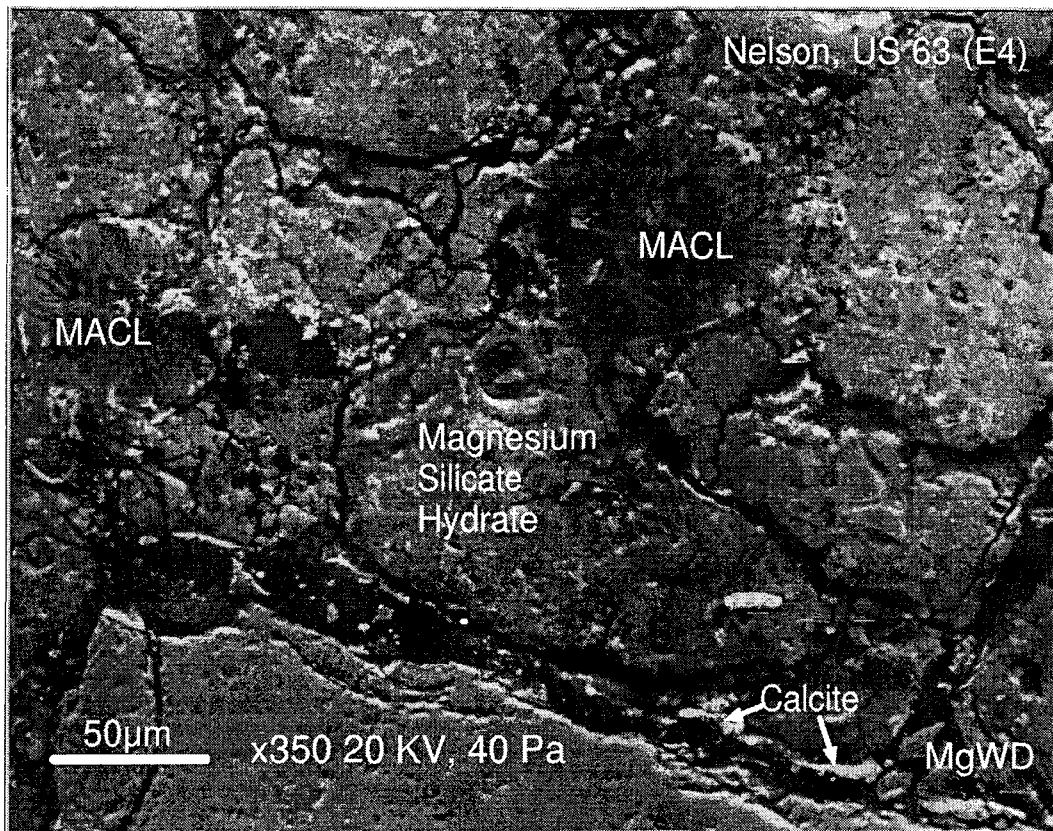


Fig. 25

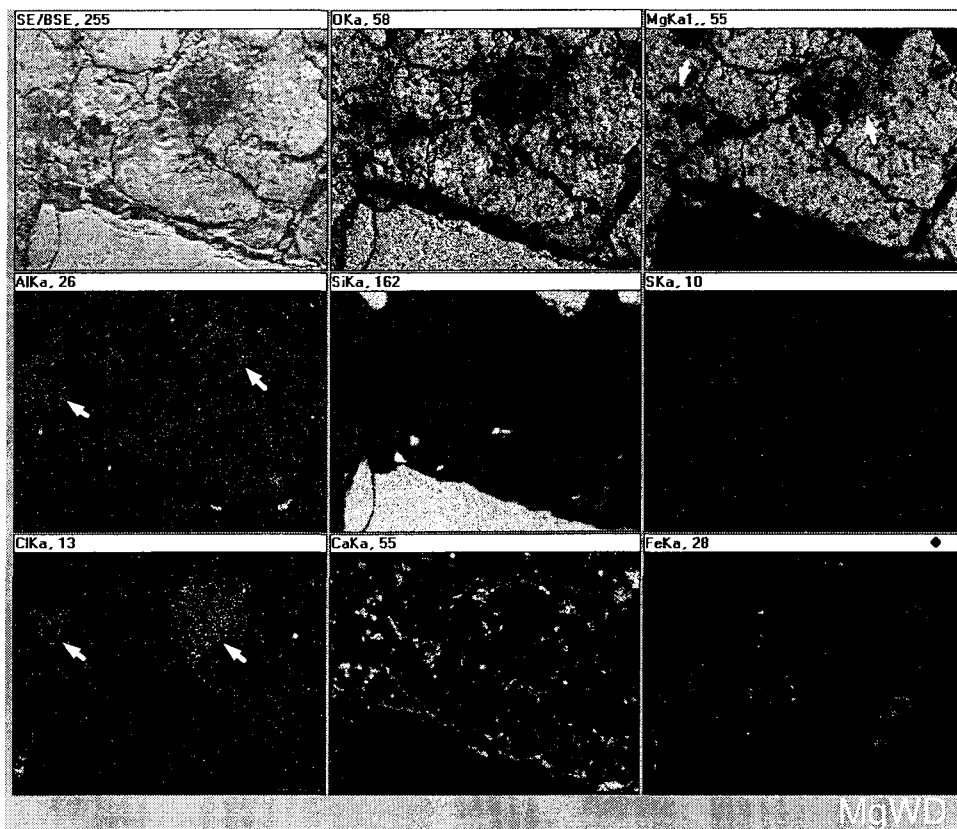


Fig. 26. EDAX point analysis of magnesium silicate hydrate (MSH) shown in Fig 25.

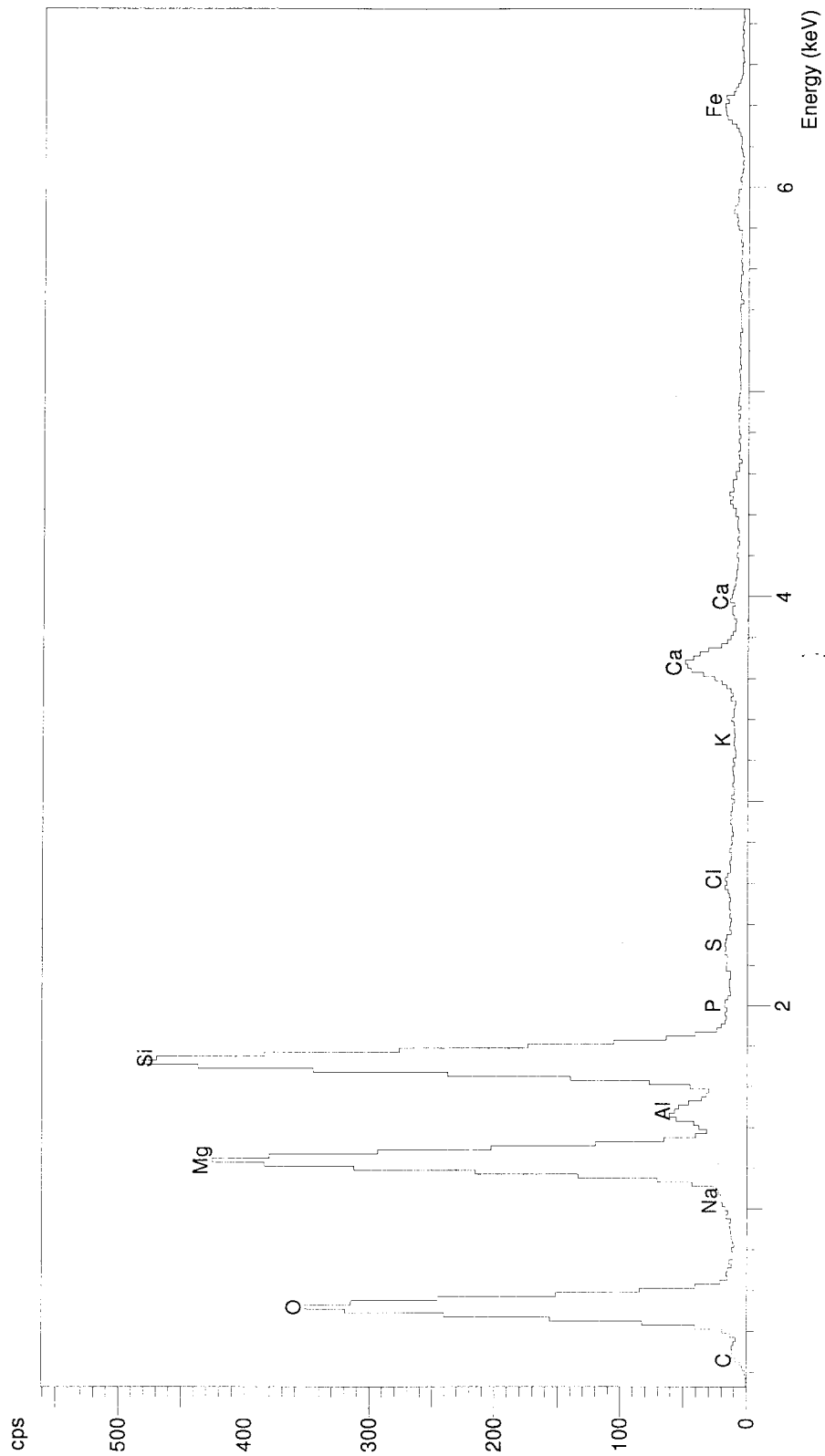


Fig. 26

Fig. 27. SEM micrograph and EDAX area maps showing the deposition of secondary minerals on the surface of concrete after wet/dry cycling in $MgCl_2$ of Portland West quarry concrete, I 35. Needles of calcite crystals and equant brucite crystals formed on the surface of both cement paste and dolomite coarse aggregate.

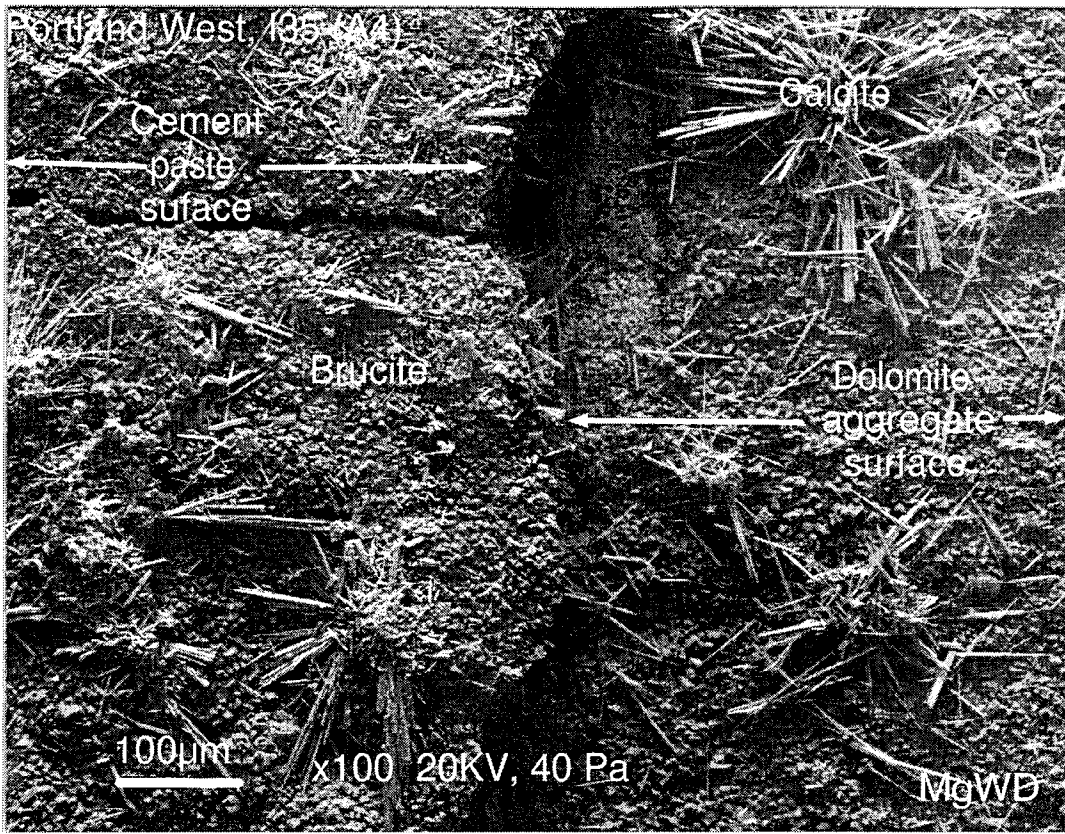


Fig. 27

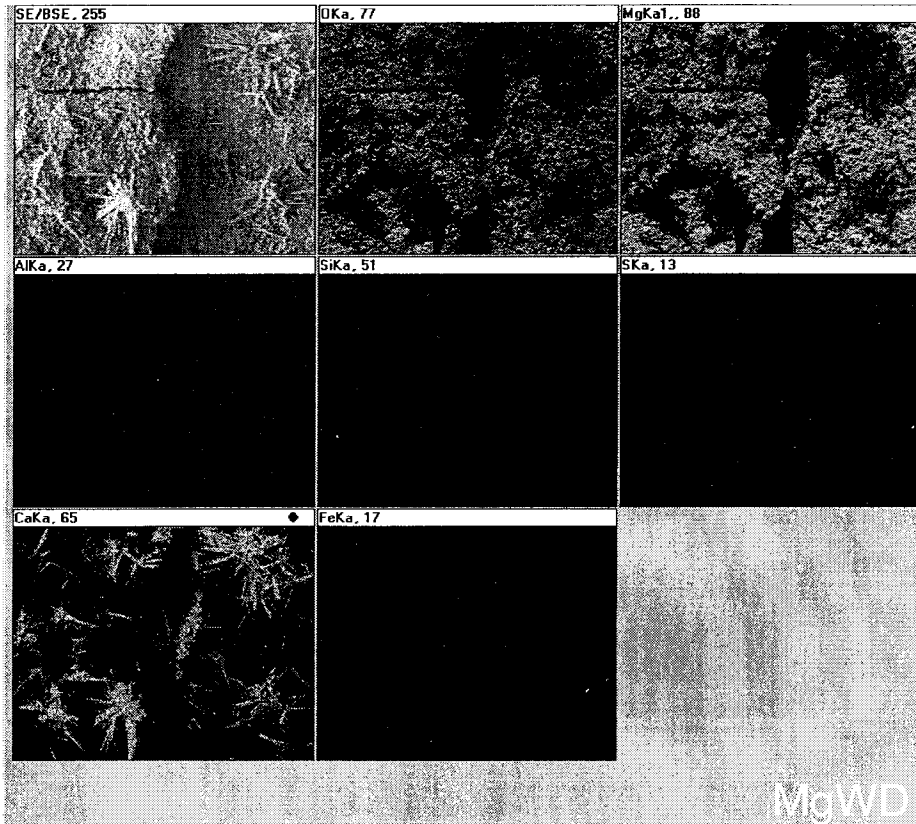


Fig 28. EDAX point analysis of void-filling matter shown in Fig. 24. The material marked 'B' in Fig. 24 has a complex composition of Mg, Ca, Al, Si, S, and minor Cl.

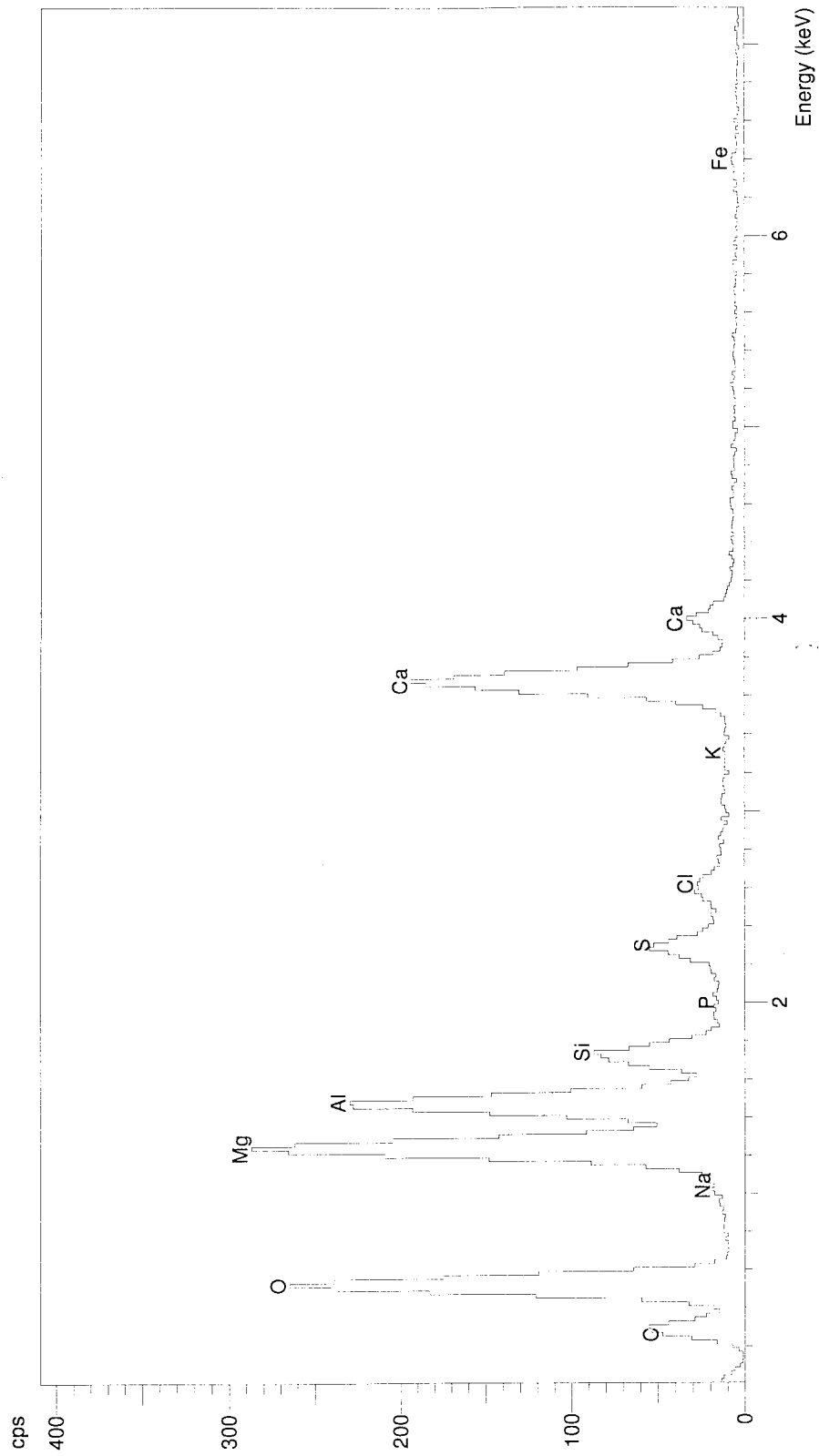


Fig. 28

Fig. 29. SEM micrograph and EDAX area maps showing Nelson quarry concrete from US 63 after wet/dry cycling in NaCl. Very little experimental alteration is visible, and the dolomite aggregate and cement paste reaction rims appear to be identical to those present in untreated concrete (see Fig 2 for composition). EDAX element maps show that no significant concentration of Mg occurs in the light-colored dolomite rim Zone Ce, and brucite only occurs in the cement paste Zones De and Ee, as in untreated concrete. Note that Cl is concentrated in air-entrainment voids where ettringite occurs. The small white-outlined rectangle shows the magnified area shown in the next figure (Fig. 30).

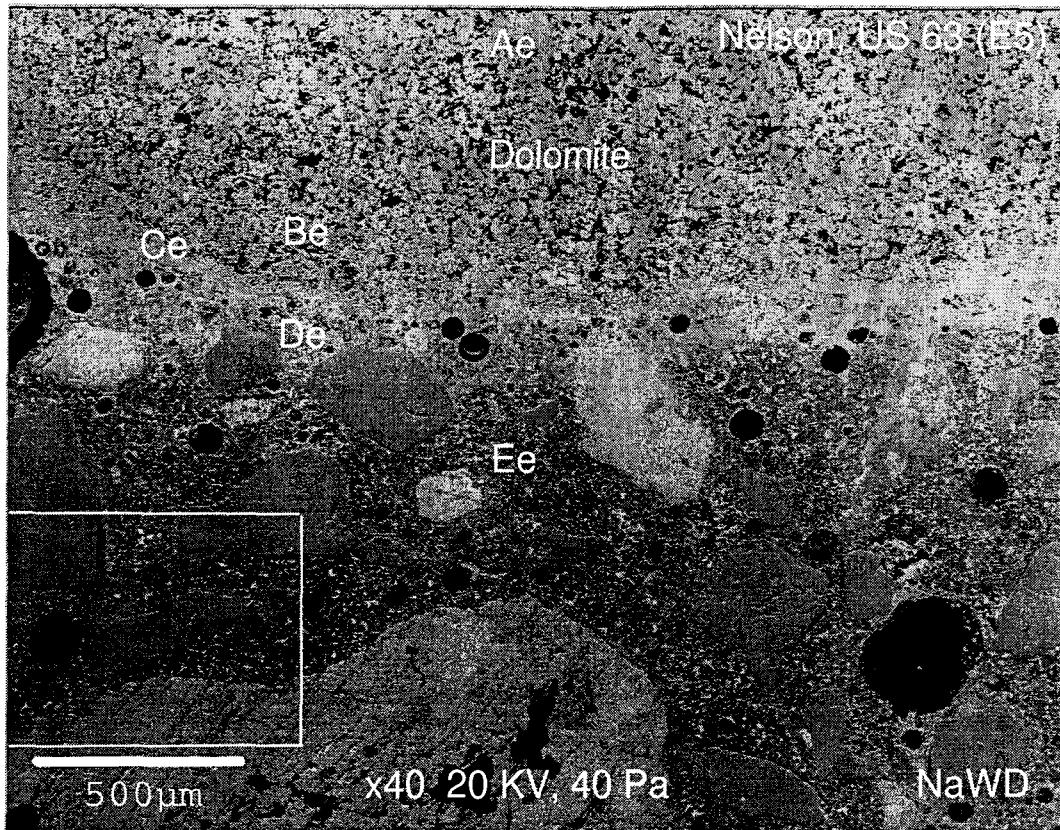


Fig. 29

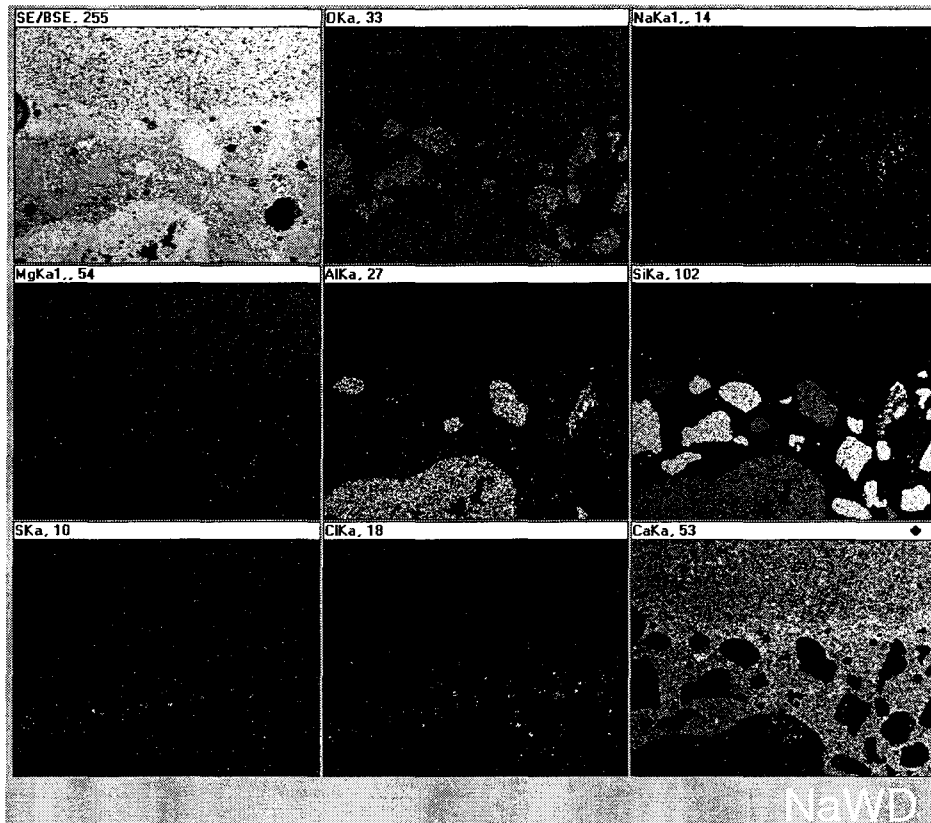


Fig. 30. High magnification SEM micrograph and EDAX area maps of area shown in

Fig. 29. Material rich in Ca, Al, S, and Cl with minor Si, occurs in air voids and has a morphology identical to that of ettringite in untreated samples. This material is ettringite with partial substitution of its Al by Si. The Ca-Al-Cl material is probably calcium chloroaluminate. Note that the Cl-rich material typically occurs at the outer margins of S-rich material.

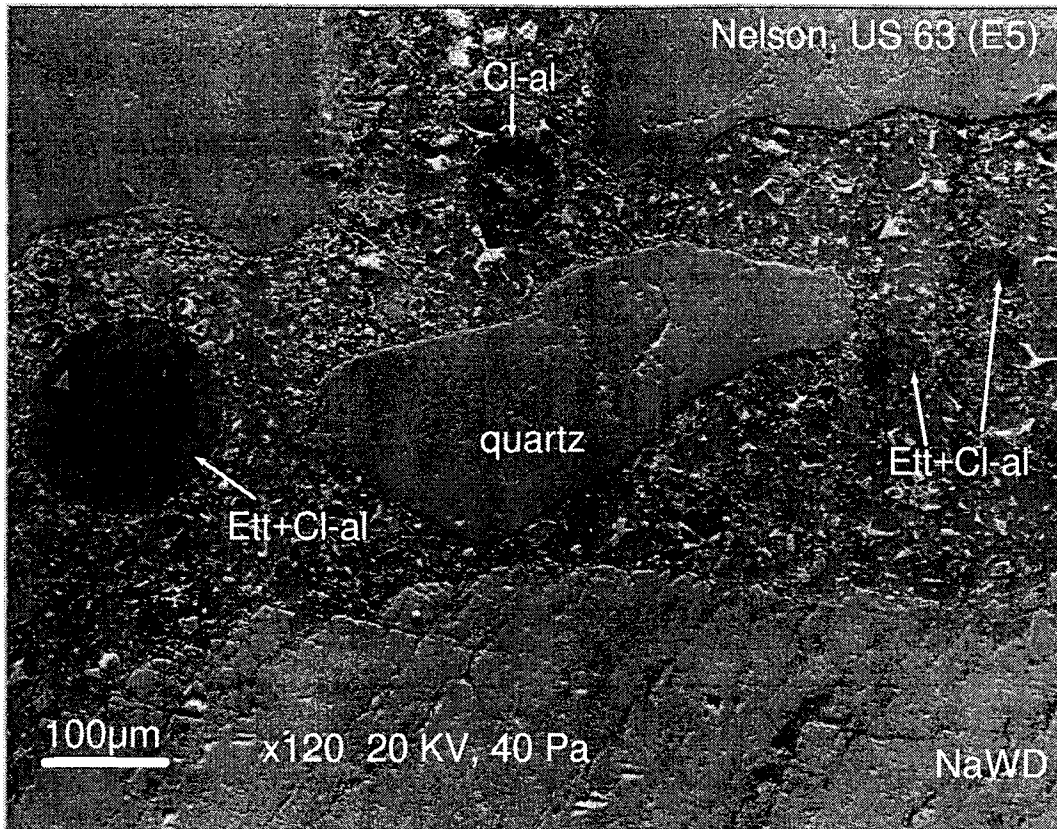


Fig. 30

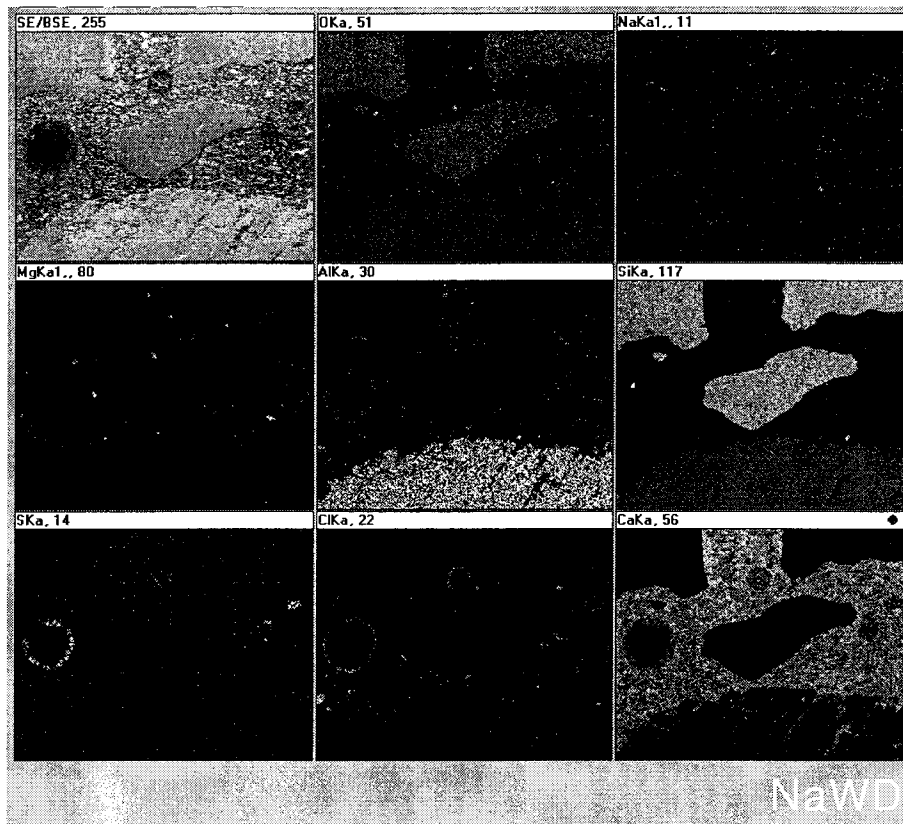


Fig. 31. EDAX point analyses of void-filling minerals shown in Fig. 30.

a. EDAX point analysis at the inner margin of void-fill mineral shows that this material contains both S and Cl strongly indicating that Cl ions substitute for S in the ettringite structure.

b. EDAX point analysis at the outer margin of void-fill mineral shows that it is enriched in Cl and depleted in S. This composition indicates that it is calcium trichloroaluminate which is structurally similar to ettringite. Note that it also contains a small amount of Si.

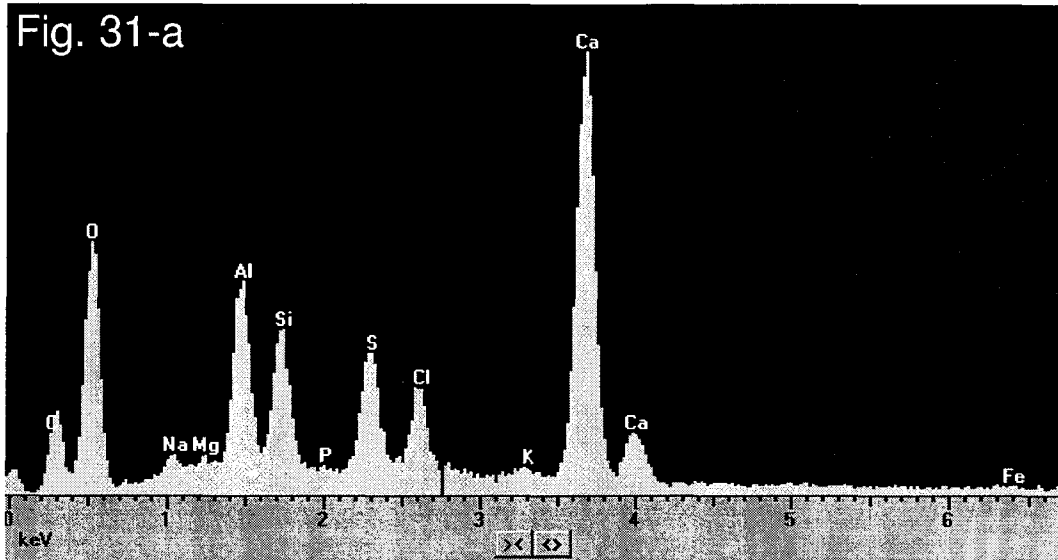


Fig. 31

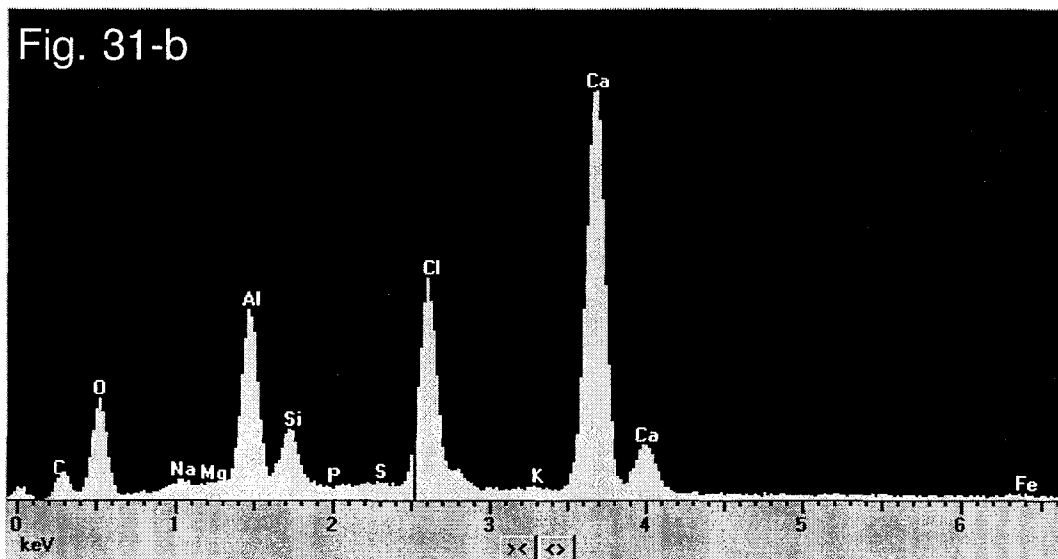


Fig. 32. SEM micrograph and EDAX area maps showing deterioration in Sundheim

quarry concrete from US 20 after wet/dry cycling in Na_2SO_4 . During cycling, both void-rim and void-fill ettringite precipitated in many air-entrainment voids compared with only very small quantities of ettringite present in untreated concrete samples. Ettringite did not form in the air voids located in the narrow light-colored cement paste Zone De.

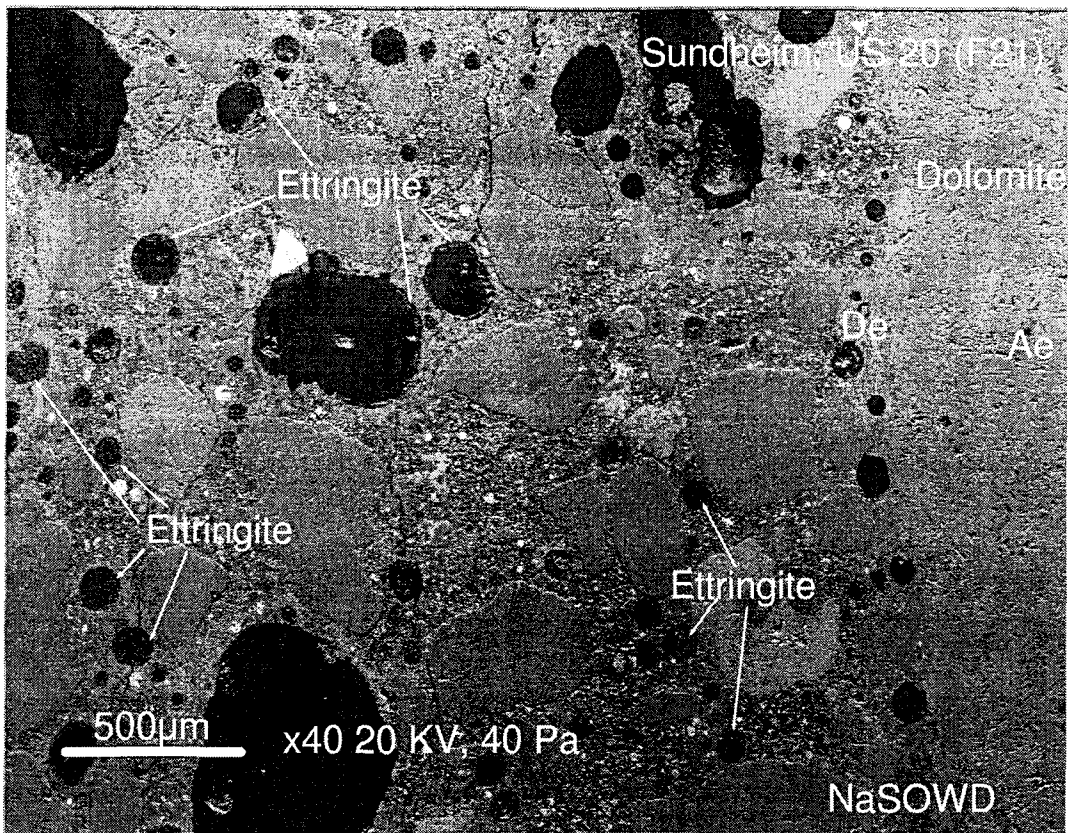


Fig. 32

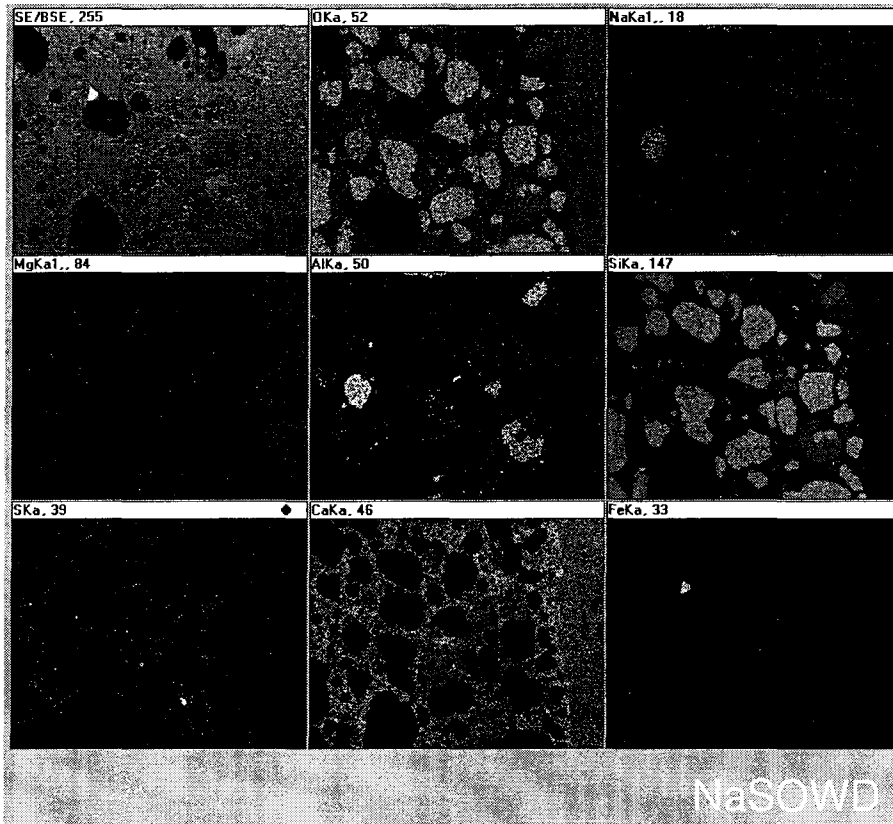


Fig. 33. SEM micrograph and EDAX area maps showing deterioration in Sundheim quarry concrete from US 20 after freeze/thaw cycling in Na_2SO_4 . Freeze/thaw cycling produced similar results as wet/dry conditions in that abundant newly-formed ettringite precipitated in air entrainment voids.

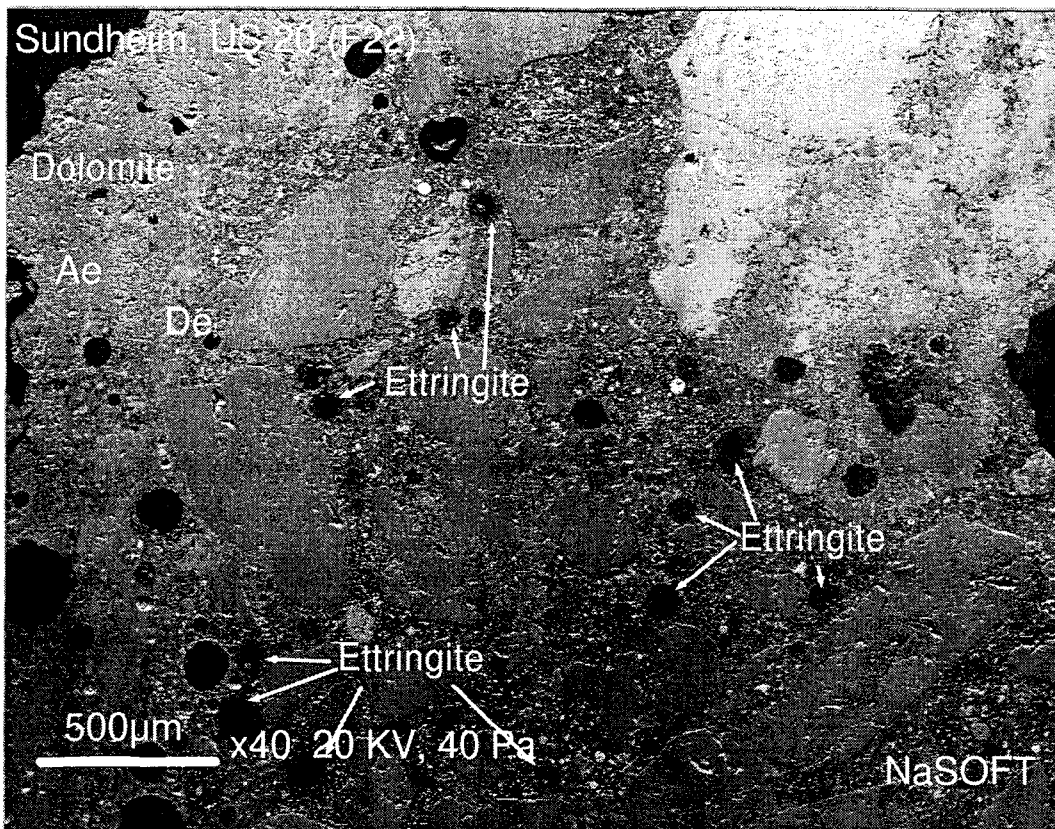


Fig. 33

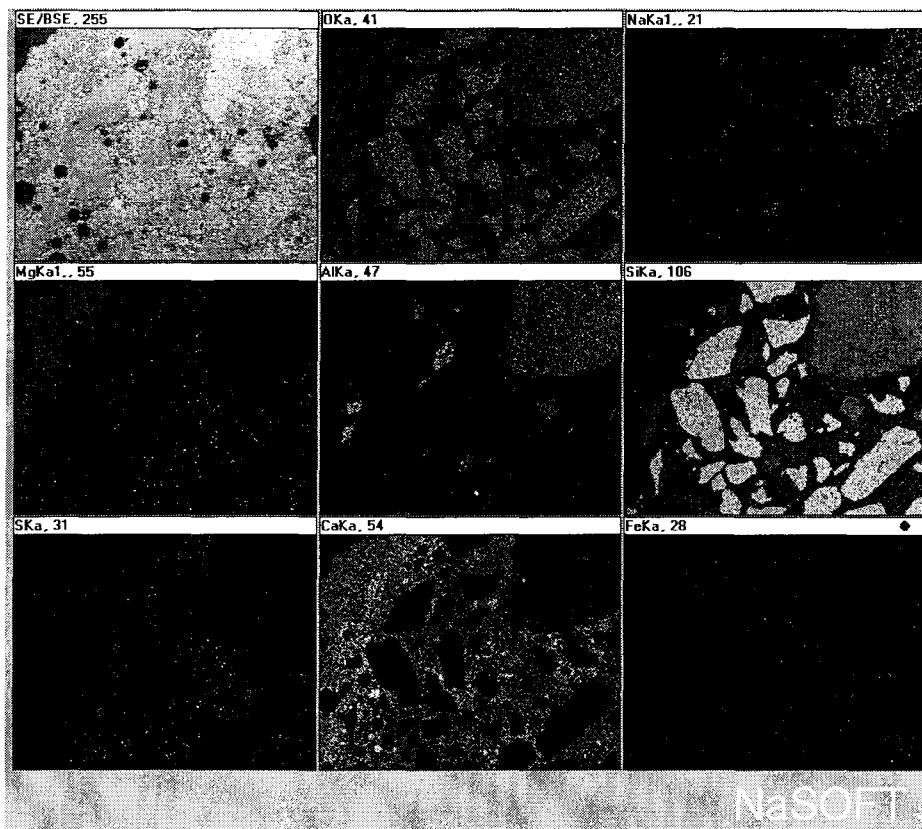


Fig. 34. High magnification SEM micrograph and EDAX area maps showing deterioration in Sundheim quarry concrete from US 20 after wet/dry cycling in Na_2SO_4 .

Ettringite frequently forms in the small interstitial voids and boundary spaces between fine aggregate and the cement paste through which solutions can easily migrate. Note the narrow cracks in the paste adjacent to quartz fine aggregate particles.

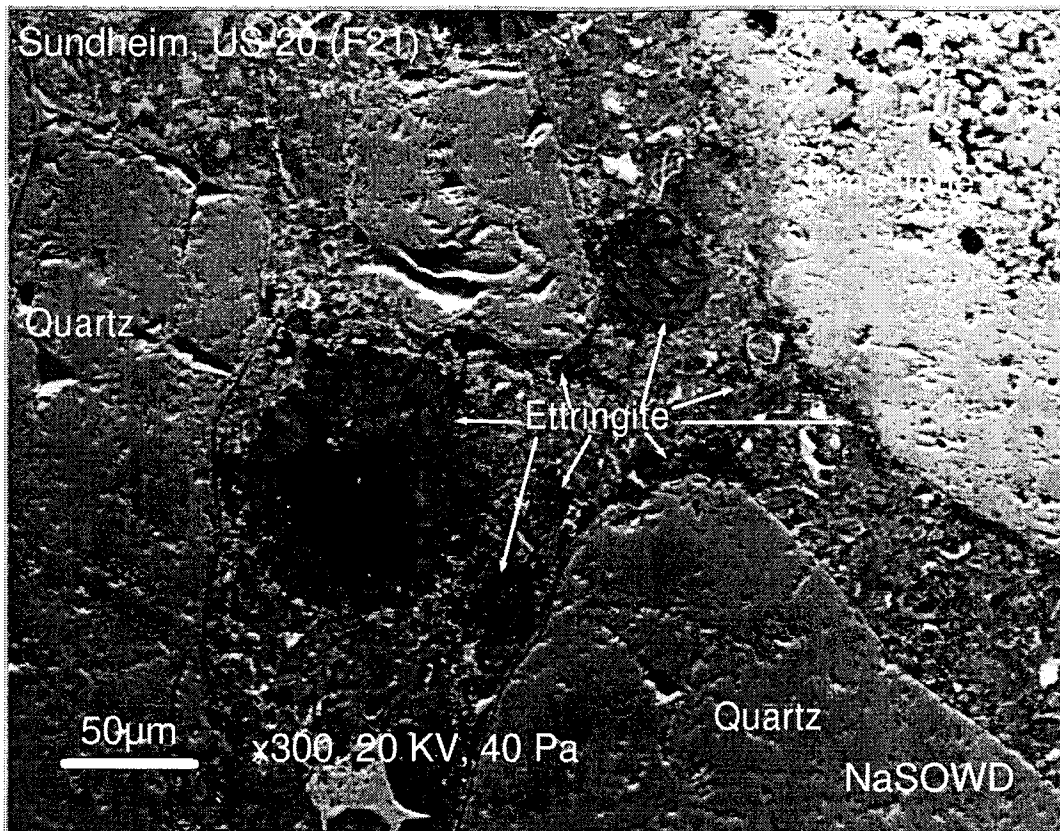


Fig. 34

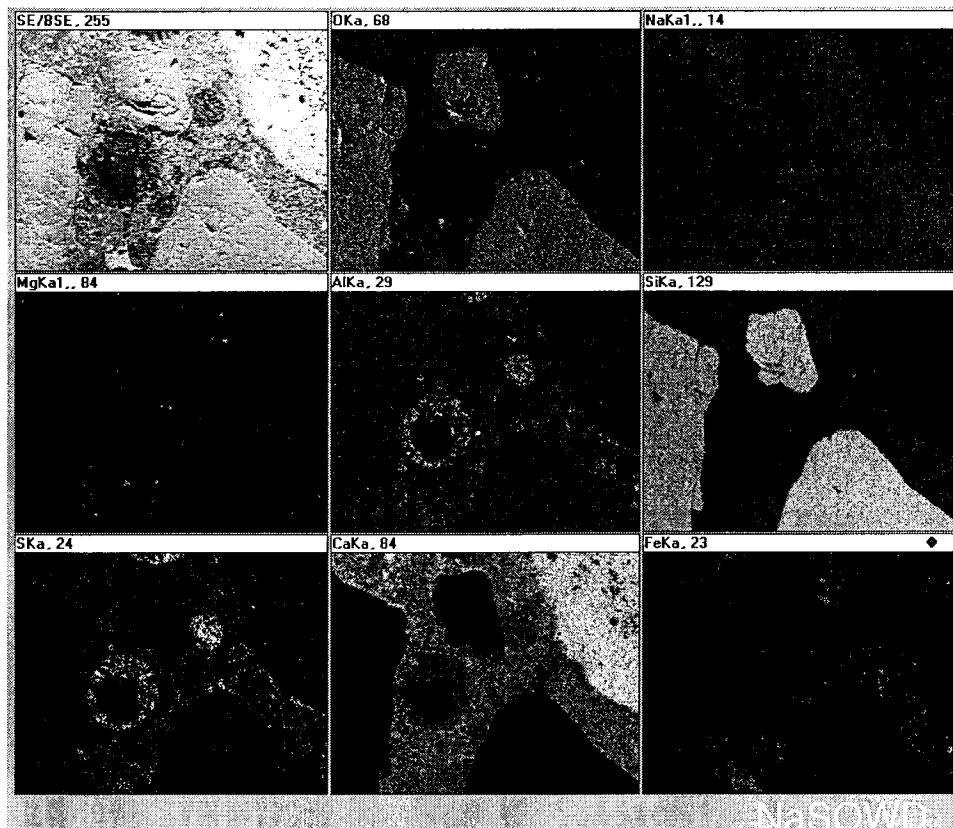


Fig. 35. EDAX area maps showing effects on Sundheim quarry concrete from US 20 after wet/dry cycling in Na_2SO_4 . Some ettringite which formed during Na_2SO_4 cycling contained Si indicating that some Si probably substitutes for Al in the ettringite.

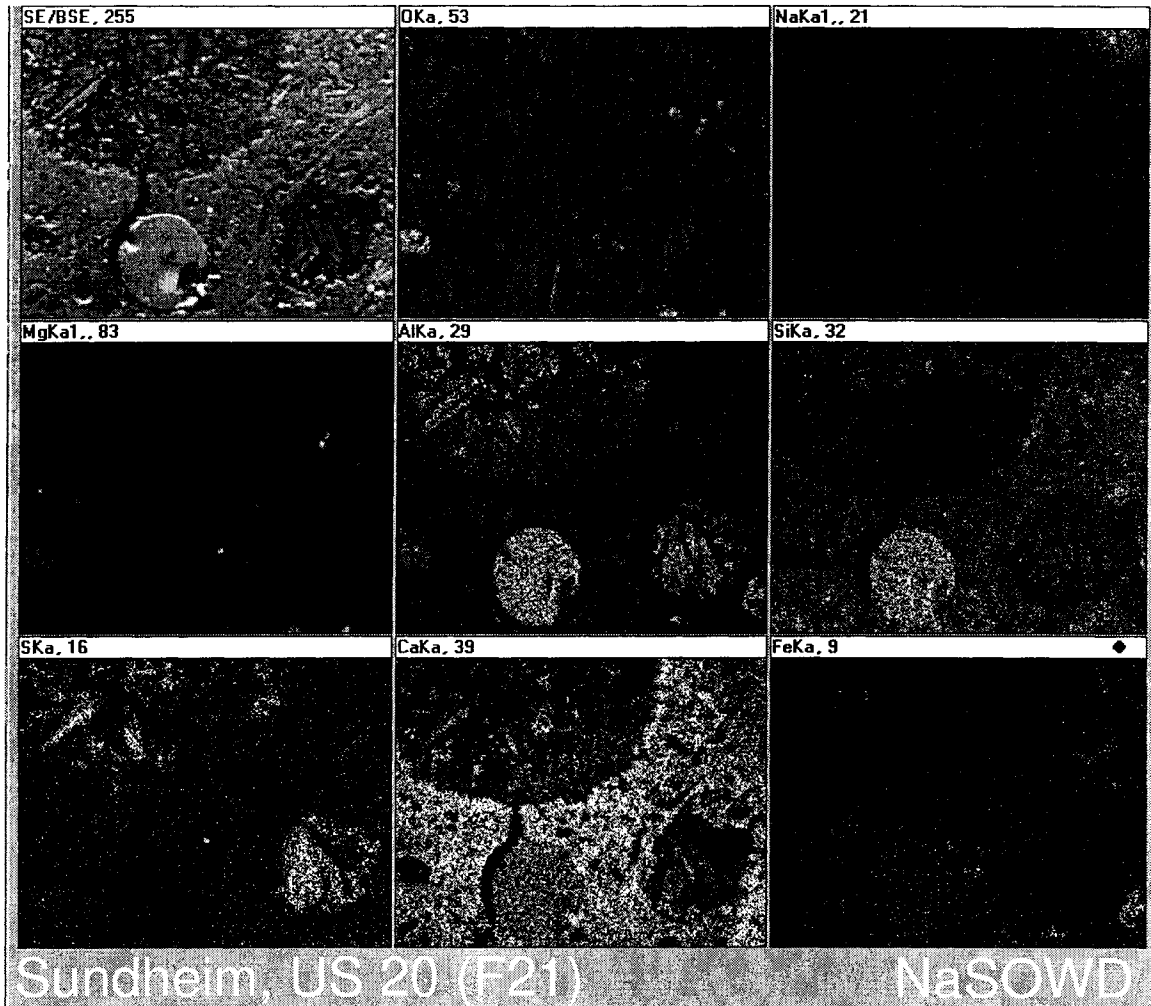


Fig. 35

Fig. 36. SEM micrograph and EDAX area maps showing experimentally-induced deterioration of Nelson quarry concrete from US63 after wet/dry cycling in CMA.

These images approximately correspond to the area shown in the petrographic thin-section of Plate V-A. Dark and light-colored dolomite rim zones Be and Ce are well-developed. EDAX element maps show that abundant interstitial brucite occurs in the light-colored dolomite rim, Zone Ce. Increased Mg concentrations in the cement paste are probably due to the formation of MSH as well as to brucite precipitation. Note that light-colored cement rim, Zone De, which is characterized as a dense calcite accumulation zone, is not altered to MSH. The white-outlined rectangle shows the area of Fig. 40.

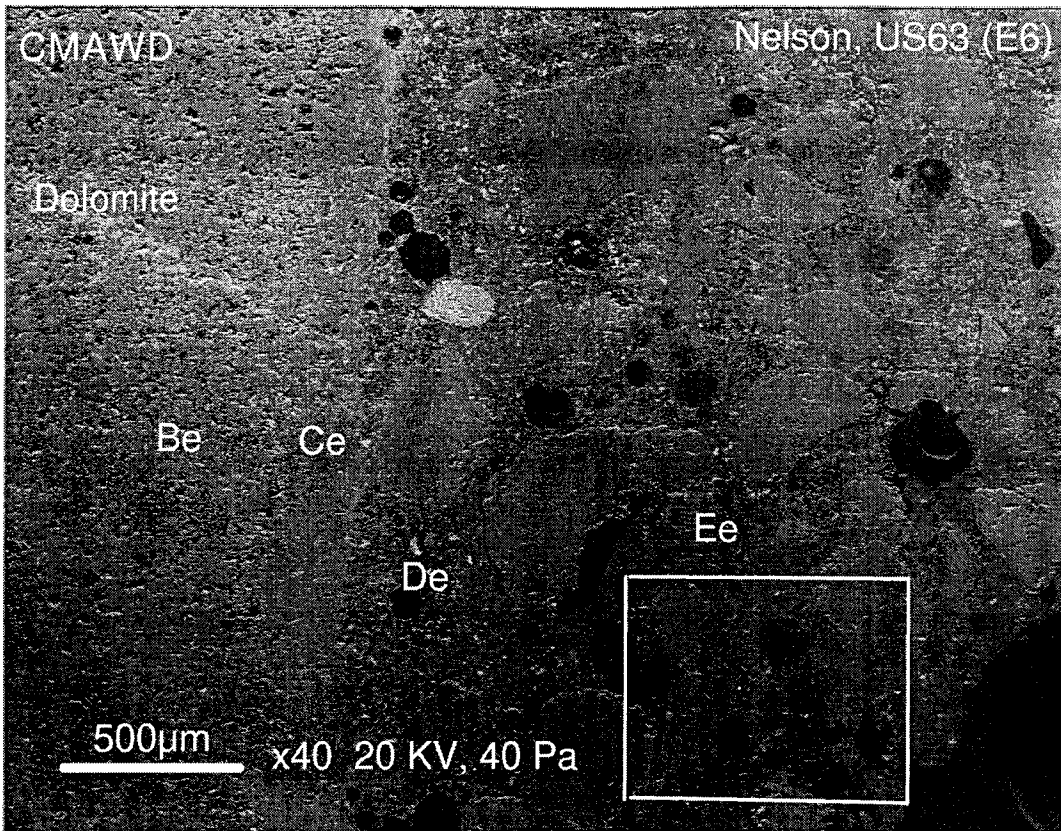


Fig. 36

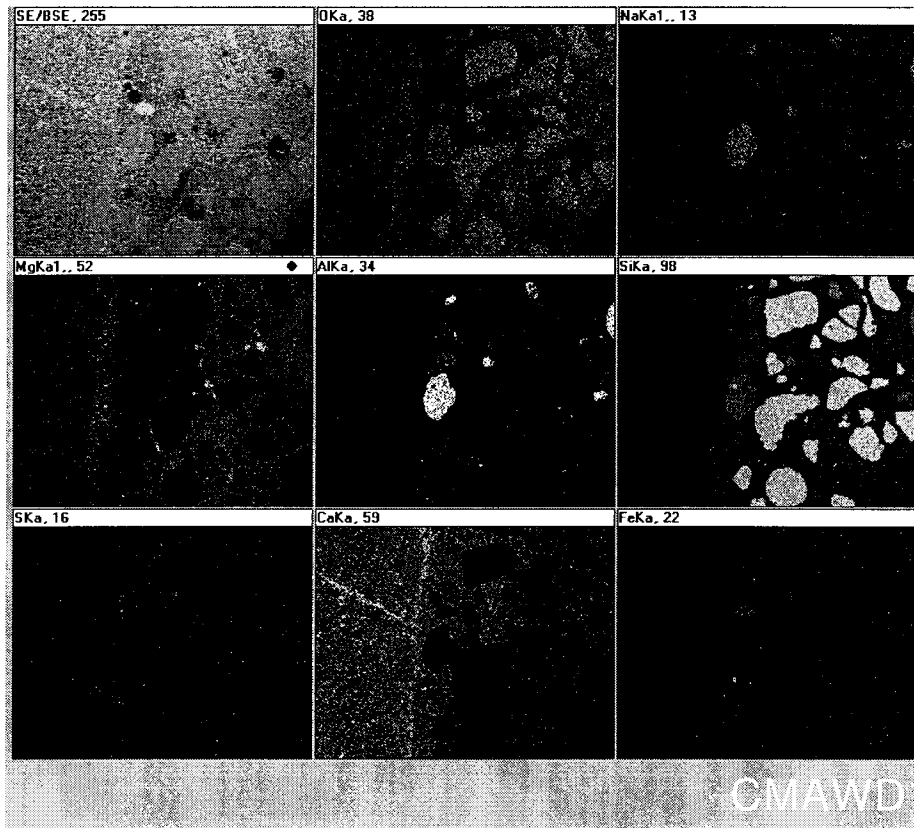


Fig. 37. SEM micrograph and EDAX maps showing secondary mineral growth in Sundheim quarry concrete from US20 after freeze/thaw cycling in CMA. The images show approximately the same area as Plate V-B. Brucite and magnesium silicate hydrate formed in voids after freeze/thaw cycling. Brucite crystals grow as a thin layer around open spaces, and MSH occurs between the brucite and cement paste. Microcrystalline Mg and C rich material (probably Mg acetate) largely occurs in open spaces. The large circular form near the center of the micrograph is an artifact of sectioning and has no significance. EDAX element maps show that calcite also occurs as a thin layer interior to the brucite layer and shows that the cement paste change was altered to MSH near the void rims.

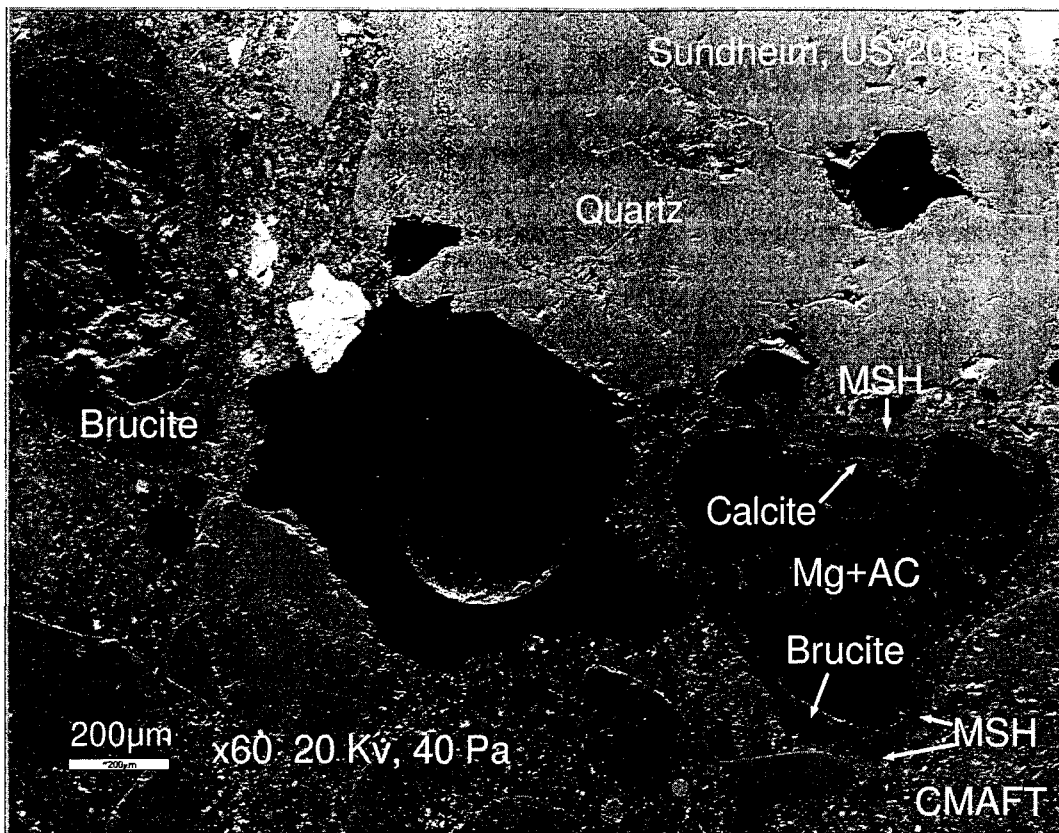


Fig. 37

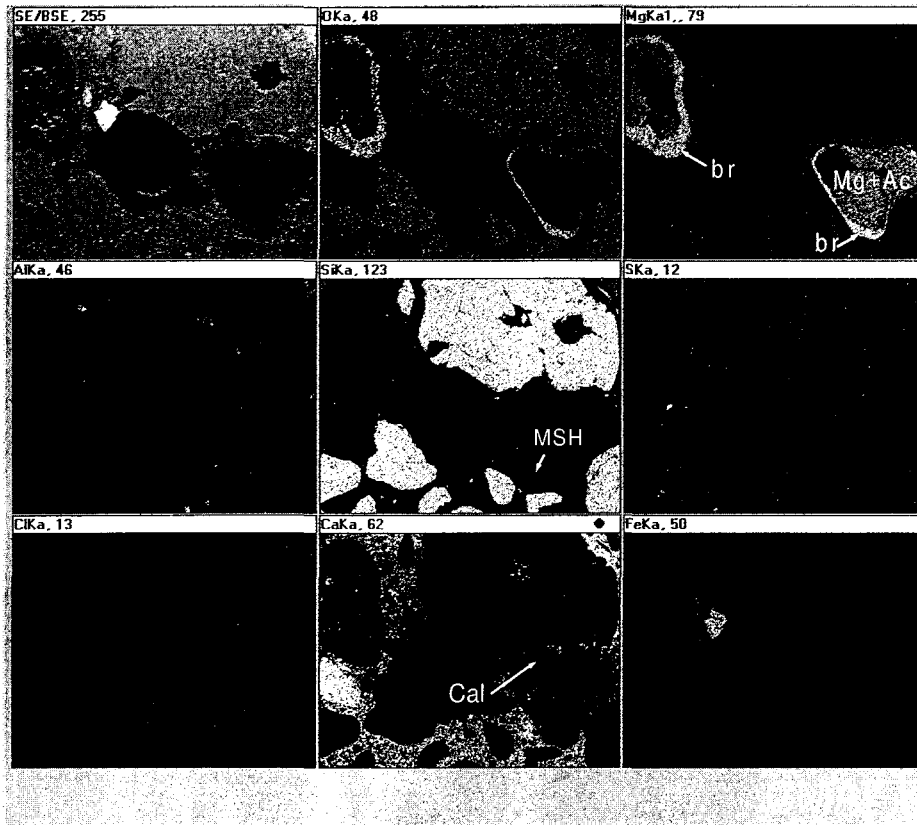


Fig. 38. SEM micrograph and EDAX element maps showing the growth of brucite and calcite in Nelson quarry concrete from US63 after wet/dry cycling in CMA.

Brucite (br) and calcite (Cal) grew in voids after cycling. Calcium silicate hydrate, CSH, in the cement has changed to magnesium silicate hydrate, MSH, with the development abundant cracks. A wide solution channel, which appears to develop because of paste dissolution by CMA, formed between a limestone coarse aggregate particle and the surrounding cement. Note that Si-rich crystals are silicon carbide grains (Gr) from grinding powder used during thin-section preparation.

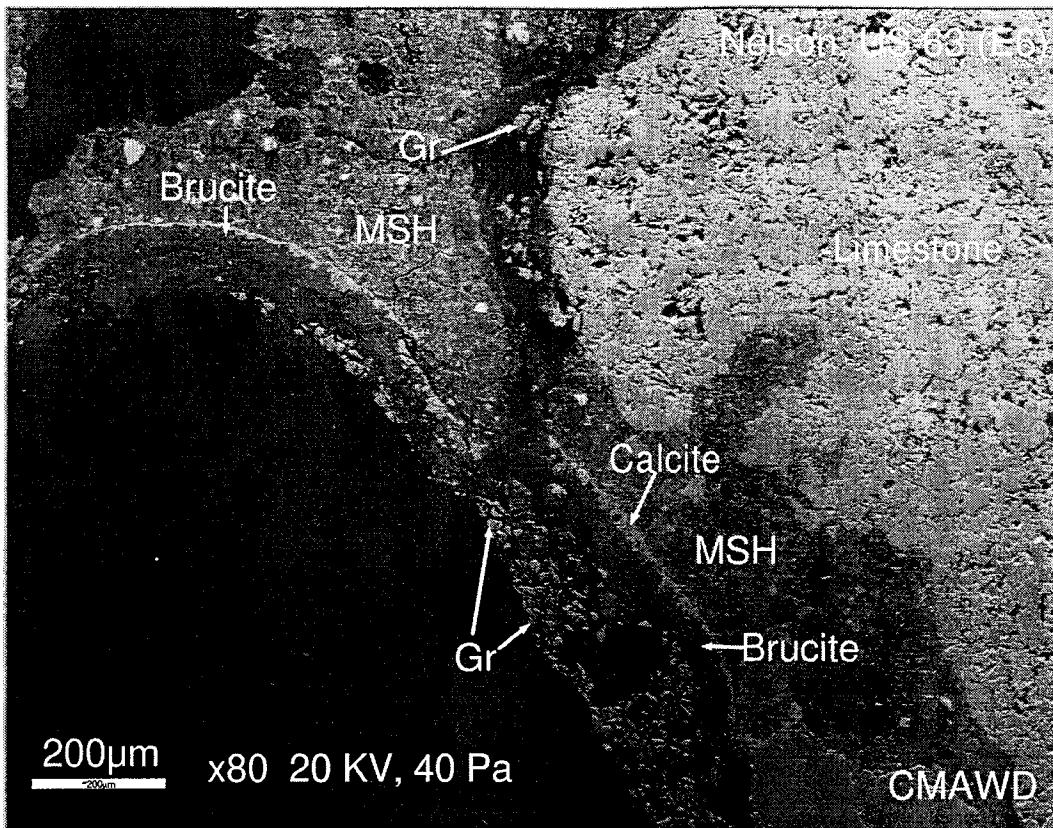


Fig. 38

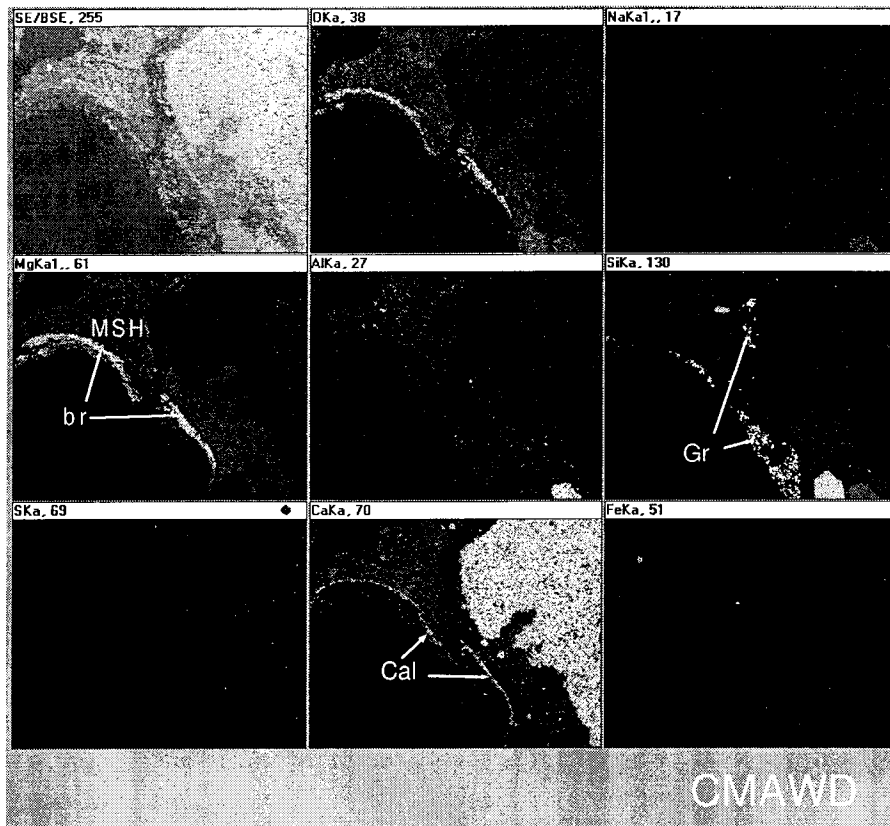


Fig. 39. EDAX element maps of the same area shown in Plate VI-A showing crack-filling minerals that formed after wet/dry cycling in CMA. Brucite (br) is a major crack-filling mineral and thin layers of calcite often occur. Silica-gel (Si), in rare instances, has formed at the margins of these cracks.

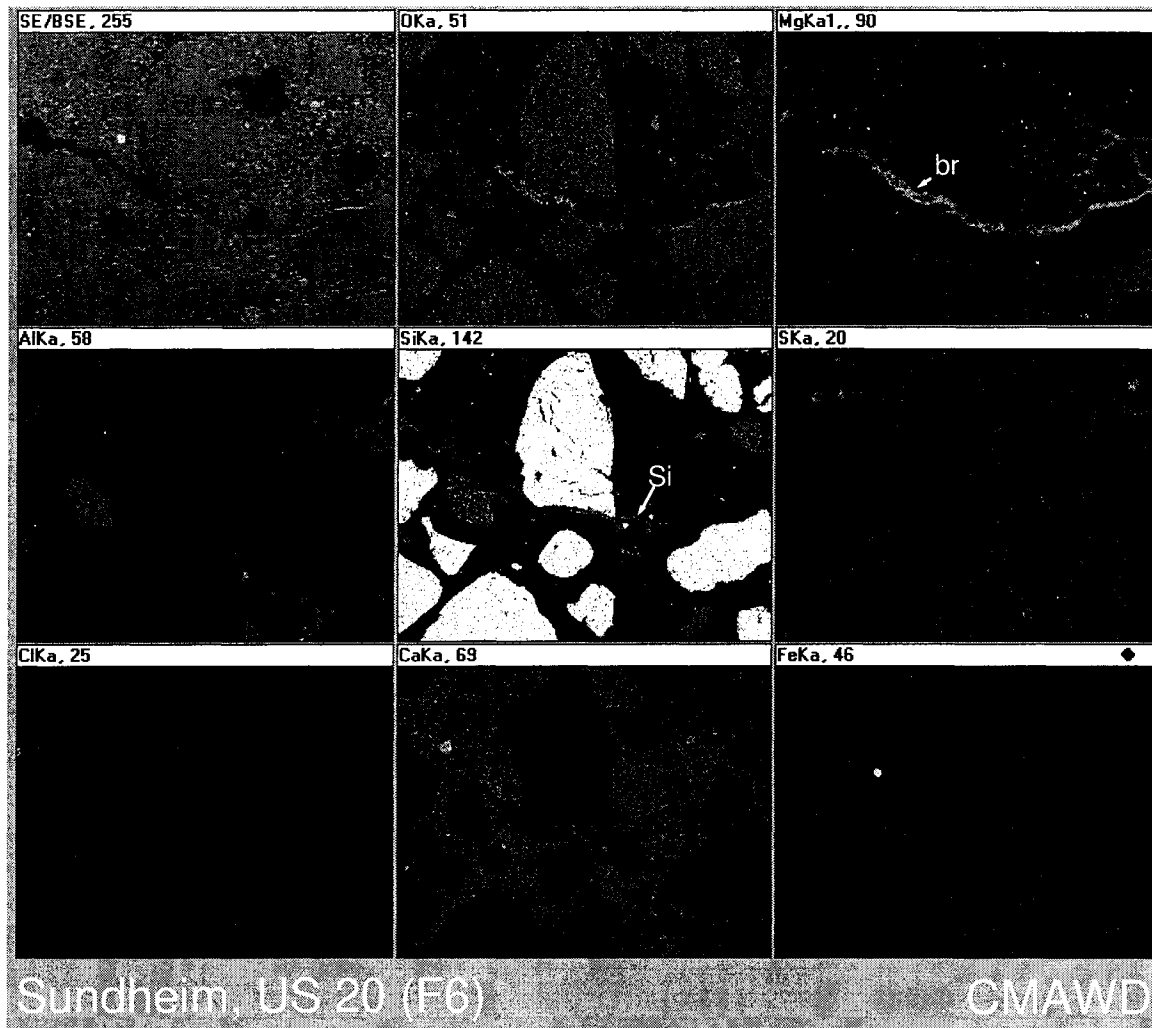


Fig. 39

Fig. 40. High magnification SEM and EDAX maps showing part of the area of Fig. 36.

The cement paste has altered to MSH and abundant shrinkage cracks have developed as a result of CMA treatment. Calcium released by MSH formation migrated to tiny open spaces where it precipitated as calcite. Void-filling minerals show various compositions.

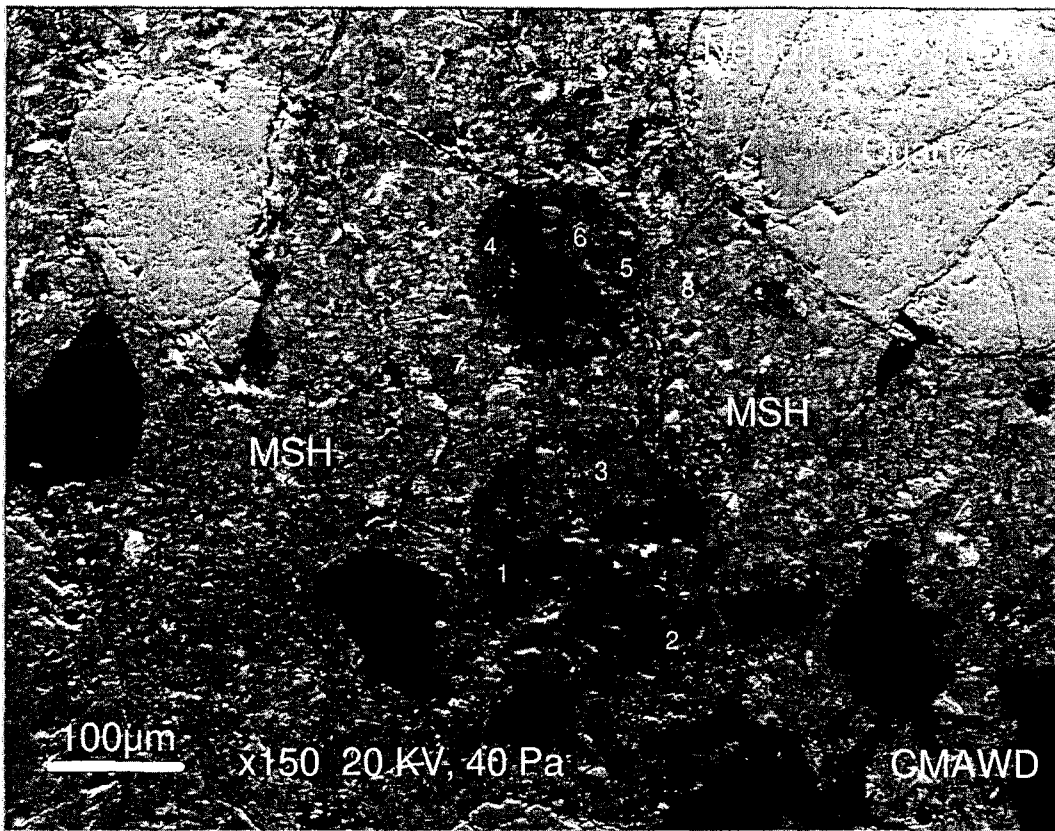


Fig. 40

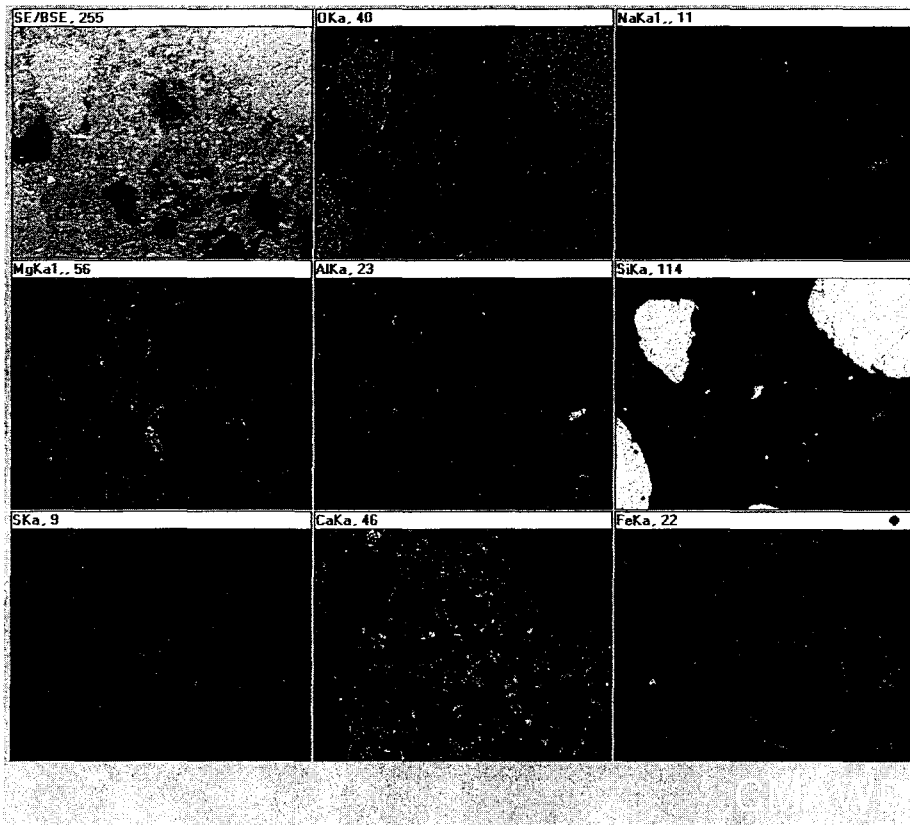


Fig. 41. EDAX point analysis of void-filling minerals shown in Fig. 40. For the locations of each point analysis refer to the numbers associated with the air-entrainment void of Fig. 40.

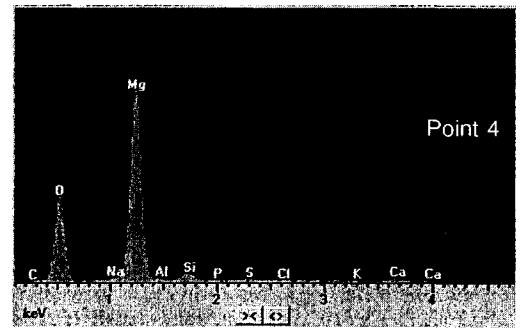
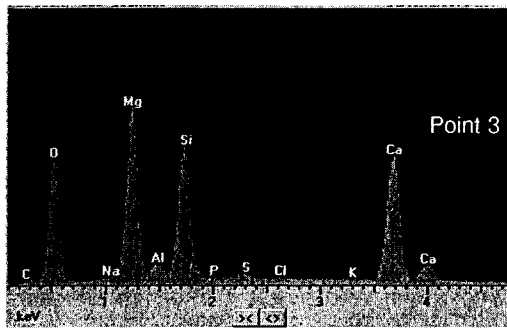
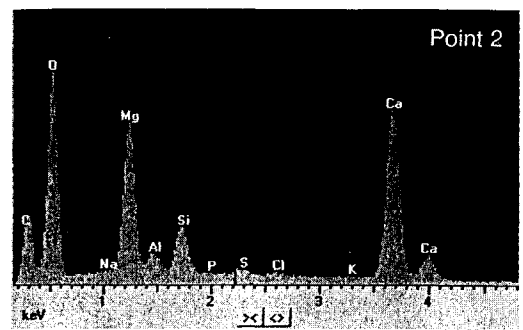
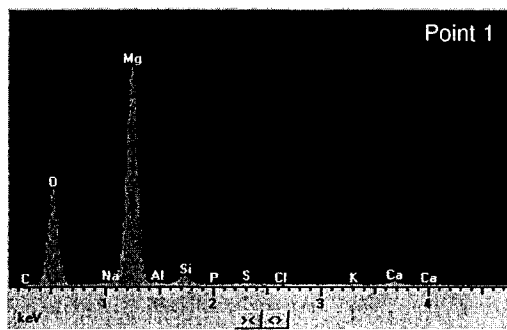


Fig. 41

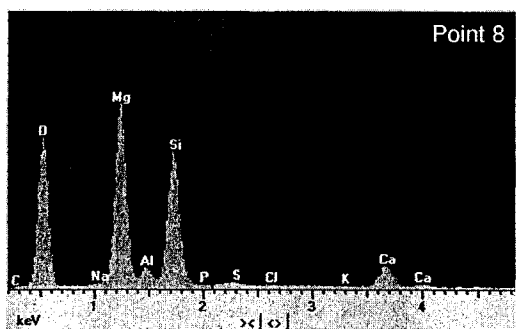
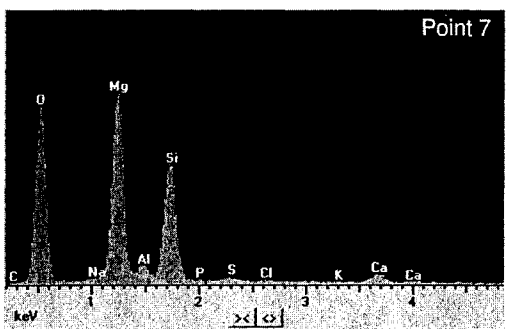
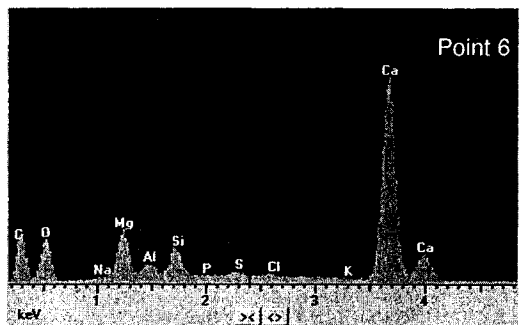
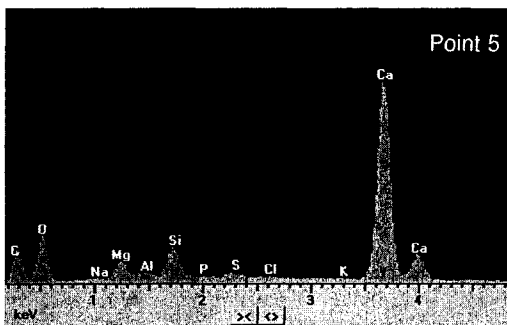


Fig. 42. SEM micrograph and EDAX area maps showing experimentally-induced deterioration of Sundheim quarry concrete from US 20 after wet/dry cycling in magnesium acetate. Abundant brucite grew as thin linings in air voids of the durable concrete during wet/dry cycling. EDAX element maps show cement paste has been enriched in magnesium and depleted in calcium, indicating that CSH altered to MSH.

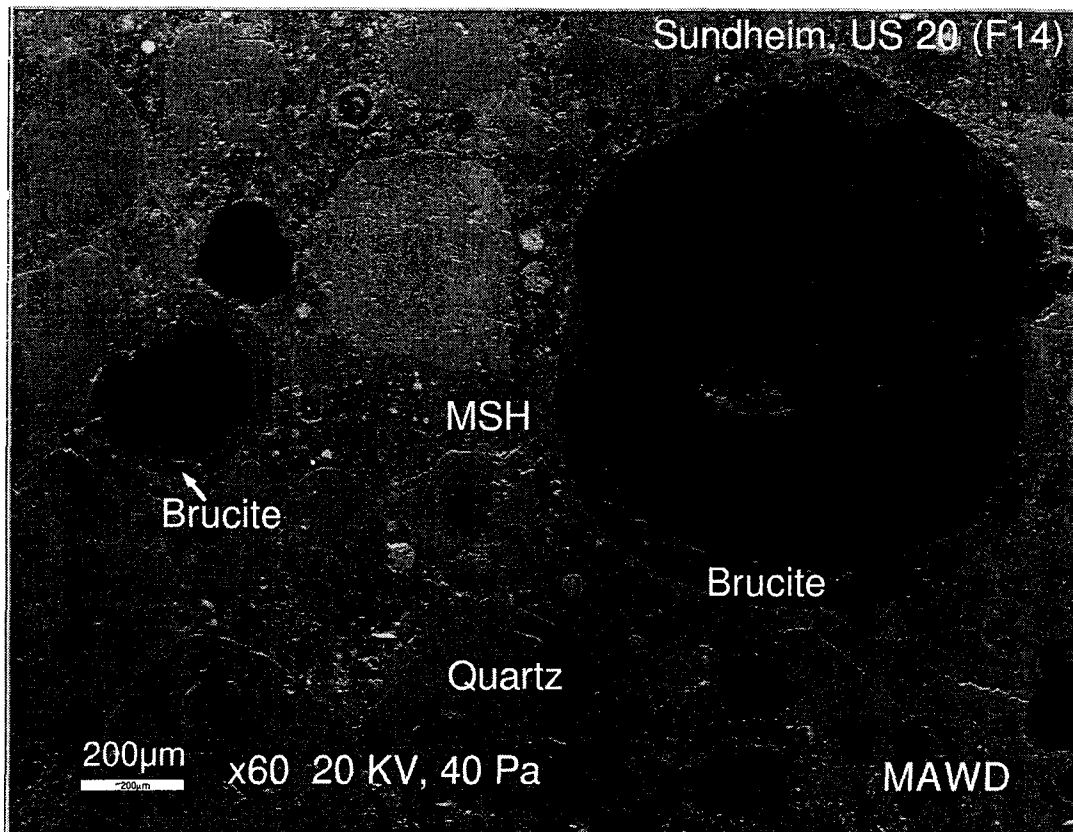


Fig. 42

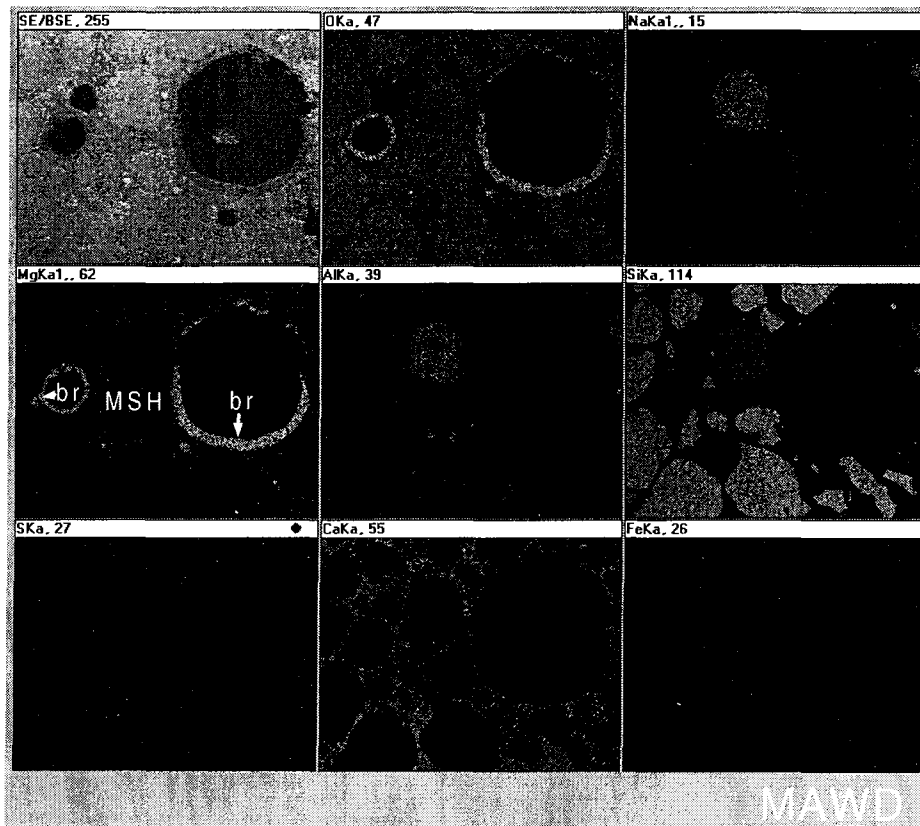


Fig. 43. SEM micrograph and EDAX area maps showing the growth of brucite in voids of durable Sundheim quarry concrete (US 20) after freeze/thaw cycling in magnesium acetate. Features shown are very similar to those of Fig. 37. Many of the voids in which brucite crystals occur are caused by removal of fine-aggregate debonded from the cement. Debonding results from alteration of CSH to non-cementitious MSH.

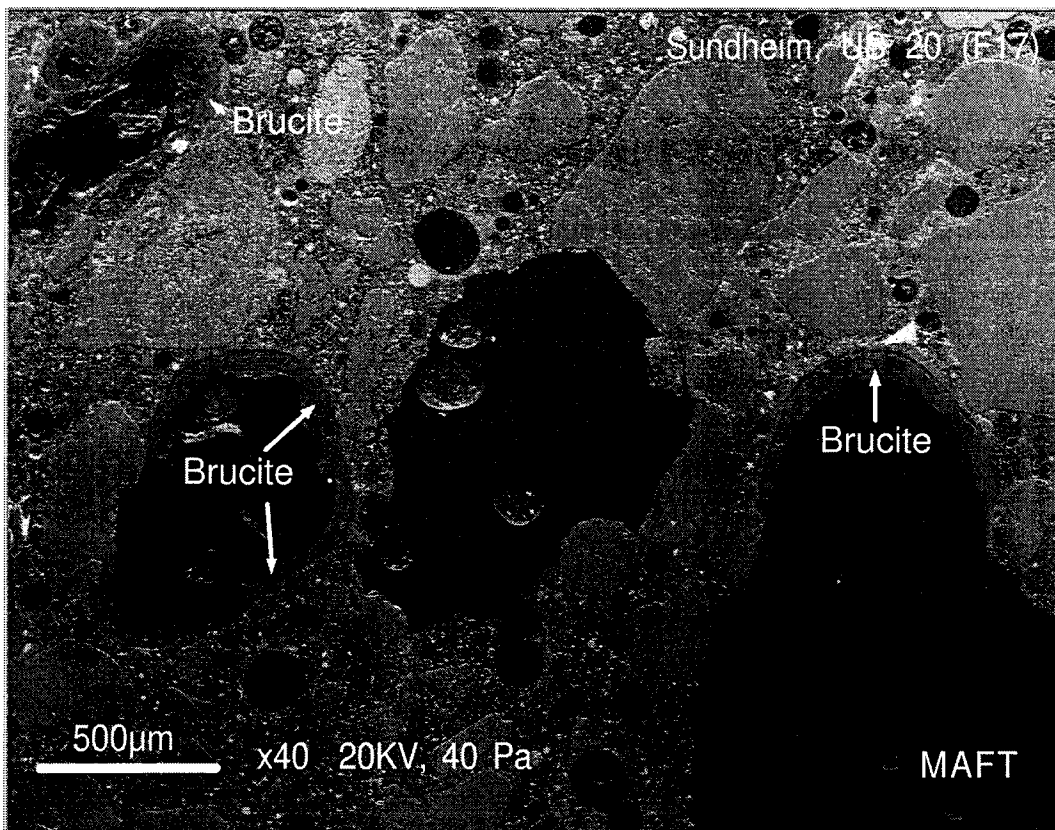


Fig. 43

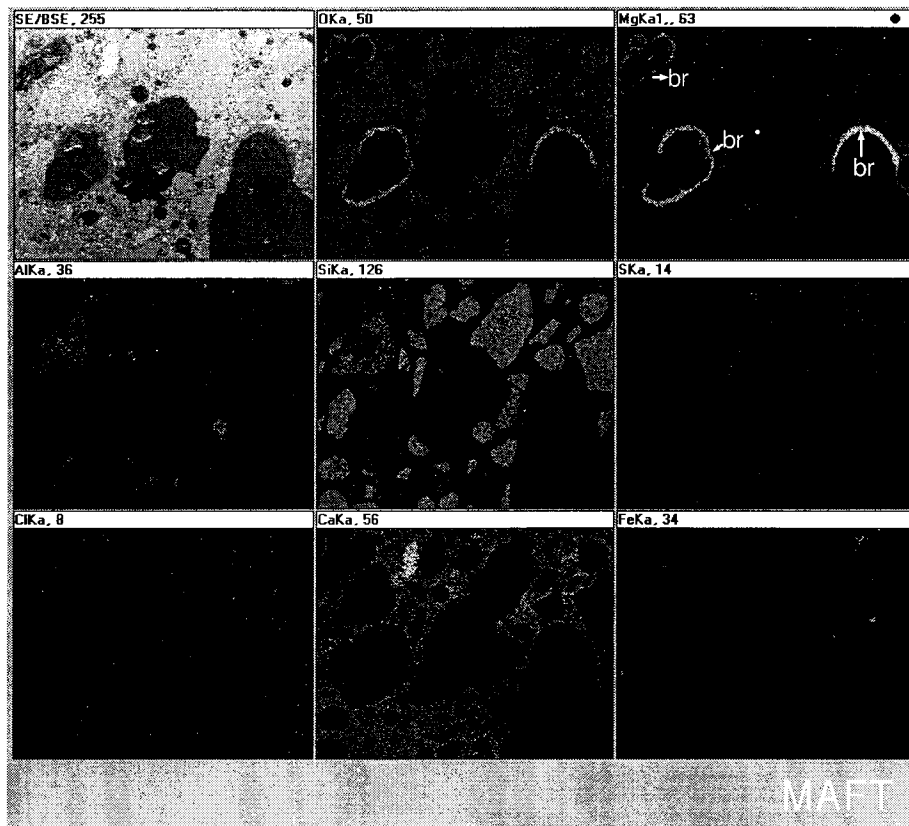


Fig. 44. SEM micrograph and EDAX area maps showing results of wet/dry cycling in calcium acetate, Sundheim quarry concrete from US 20. Ca concentration in the cement increases during cycling, especially near the dolomite aggregate-paste interface. Note that a wide Ca-rich zone, Zone De, has formed at the interface between non-reactive dolomite aggregate and cement paste. This zone is not present in untreated concrete containing dolomite coarse aggregate from the Sundheim quarry. Little brucite has formed in the cement paste. Ettingite, considered to be pre-treatment, is not significantly altered. Other than calcite in Zone De, no other newly-formed minerals were found. Neither paste dissolution nor fine aggregate debonding were observed.

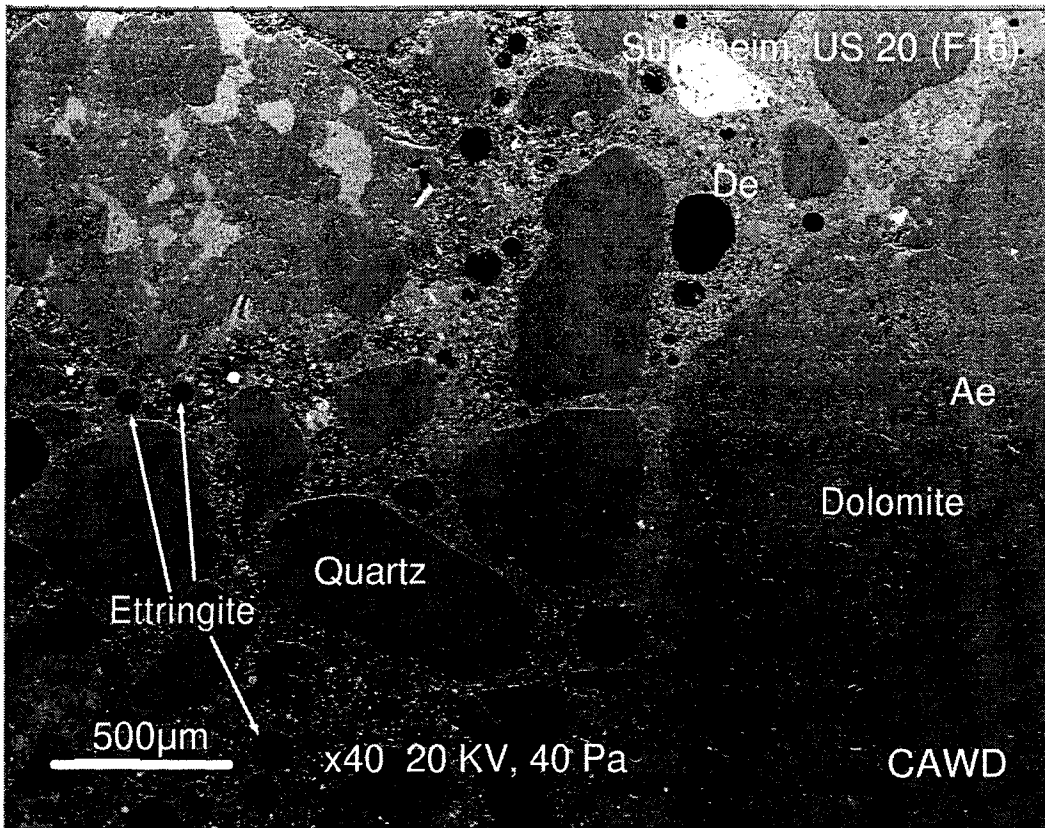


Fig. 44

